

# Model Predictive based Energy Efficient Control of an On-Grid PV Inverter

by

Amit Kumer Podder

A thesis submitted in partial fulfillment of the requirements for the degree of  
Master of Science in Engineering in Electrical and Electronic Engineering



Khulna University of Engineering & Technology

Khulna 9203, Bangladesh

March 2019

## Declaration

This is to certify that the thesis work entitled “*Model Predictive based Energy Efficient Control of an On-Grid PV Inverter*” has been carried out by *Amit Kumer Podder* in the Department of *Electrical and Electronic Engineering*, Khulna University of Engineering & Technology, Khulna, Bangladesh. The above thesis work or any part of this work has not been submitted anywhere for the award of any degree or diploma.



Signature of Supervisor




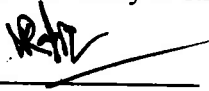



Signature of Candidate

## Approval

This is to certify that the thesis work submitted by *Amit Kumer Podder* entitled “*Model Predictive based Energy Efficient Control of an On-Grid PV Inverter*” has been approved by the board of examiners for the partial fulfillment of the requirements for the degree of *Master of Science in Engineering* in the Department of Electrical and Electronic Engineering, Khulna University of Engineering & Technology, Khulna, Bangladesh, in March, 2019.

### BOARD OF EXAMINERS

1.   
Dr. Md. Habibullah  
Associate Professor, Department of Electrical and Electronic Engineering  
Khulna University of Engineering & Technology  
Chairman  
(Supervisor)
2.   
Head of the Department  
Department of Electrical and Electronic Engineering  
Khulna University of Engineering & Technology  
Member
3.   
Dr. Bashudeb Chandra Ghosh  
Professor, Department of Electrical and Electronic Engineering  
Khulna University of Engineering & Technology  
Member
4.   
Dr. Md. Abdur Rafiq  
Professor, Department of Electrical and Electronic Engineering  
Khulna University of Engineering & Technology  
Member
5.   
Dr. Md. Ashrafal Hoque  
Professor, Department of Electrical and Electronic Engineering  
Islamic University of Technology (IUT), Gazipur  
Member  
(External)

## **Acknowledgement**

I wish to express my deep gratitude to my supervisor, Dr. Md. Habibullah for his substantial guidance, encouragement and support during my research work. It was a valuable learning experience for me to be one of his students. His innovative thinking, knowledge, and expertise on Model Predictive Control (MPC) help me to fulfill my research work properly. From him, I have gained not only extensive knowledge, but also a sincere research attitude. I express my gratitude and special thanks to Dr. Naruttam Kumar Roy for providing preliminary directions and valuable comments throughout my research work.

I would also thank to Dr. Md. Rafiqul Islam, Head of the Department of Electrical and Electronic Engineering for providing me all possible facilities without which I could not think of the completion of the research work. I would also like to acknowledge the entire teaching and non-teaching staff of Electrical and Electronic Engineering department of KUET for establishing a working condition and for constructive discussions.

Finally, I would like to thank my family for their endless support and love. I greatly appreciate the sacrifices they have made over the years, without which the completion of my study would not be possible.

## Abstract

Renewable energy is now one of the most interesting topics in the field of distributed energy generation. Among the renewable energy sources, the solar photovoltaic (PV) source has become the most popular and effective one. Generally, PV system is connected to an ac grid through an inverter. The inverter should be controlled in such a way that it can penetrate maximum power to the grid. However, designing a controller for the inverter is a difficult task due to the intermittent PV source. The traditional pulse width modulation (PWM) based inverters produce high total harmonic distortion (THD) in the output current. This causes a significant amount of power loss and thus less power penetration to the grid. It makes the on-grid PV systems inefficient. Therefore, model predictive control (MPC) based energy efficient conversion of PV power is proposed in this research work. In the proposed MPC, the control objectives (current and switching frequency) are predicted using a finite number of voltage vectors produced by the inverter. MPC selects an optimal control action (i.e. switching state) in every sampling instant for the inverter by minimizing a predefined cost function. The cost function includes current tracking error and number of switching transitions. These two control objectives are combined in the cost function with a weighting factor. The first control objective provides a smooth current tracking accuracy, which increases the r.m.s amplitude of the injected current and thus increases the power penetration to the grid. The second control objective reduces the average switching frequency, which actually reduces the switching loss. The value of weighting factor in the cost function is selected by making a tradeoff between the current THD and the average switching frequency. Simulation results show that the proposed controller tracks the reference current accurately with mean absolute error of 2.5% which is 30% for the PWM based controllers. The low current tracking error for MPC based inverter yields low current THD of 2.07%, whereas in traditional PWM based inverter the current THD is 7.26%. As a result, the proposed MPC based inverter penetrates 12.8% more active power to the grid than the PWM based inverter. The active power penetration is confirmed by load flow analysis using IEEE 13 bus test feeder. The energy efficient operation of the MPC based inverter is also verified by doing loss analysis. There are three types of loss considered in the research work: conduction, switching and harmonic losses. The conduction, switching, and harmonic losses of the inverter are reduced by 36.8%, 50%, and 91.9%, respectively, in comparison with the PWM control based inverter. The performance of the proposed controller is also analysed in terms of transient response, decoupling control, and fault tolerant ability. It is shown that the proposed MPC yields decoupled current control and fast transient response, and capable of handling the symmetrical and unsymmetrical faults in the grid. The research outcome from this comprehensive analysis proves that the proposed controller reduces the power loss to maximize the penetrated power and ensures the performance of the proposed controller as an energy efficient controller for an on-grid PV inverter.

# Contents

	<b>PAGE</b>
Title Page	i
Declaration	ii
Approval	iii
Acknowledgement	iv
Abstract	v
Contents	vi
List of Tables	x
List of Figures	xi
Nomenclature	xv
Abbreviation	xvii
<b>Chapter I</b>	
Introduction	1
1.1 Background	1
1.1.1 Demands Defined by the Grid	5
1.1.2 Demands Defined by the Photovoltaic Module(s)	6
1.1.3 Demands Defined by the Operator	6
1.2 Motivation Behind the Research work	6
1.3 Research Objectives	7
1.4 Dissertation Organization	8
<b>Chapter II</b>	
Literature Review	9
2.1 Introduction	9
2.2 Power Converter	9
2.3 Types of Control Strategies	10
2.3.1 Hysteresis Control	11
2.3.2 Linear Control	11
2.3.3 Sliding Mode Control Technique	13

2.3.4	Intelligent Control Techniques	13
2.3.5	Predictive Control	15
2.4	Model Predictive Control	17
2.4.1	Continuous Control-Set (CCS) MPC	19
2.4.2	Finite-Control Set (FCS) MPC	19
2.5	Existing Research on MPC	19
2.6	Conclusion	21
<b>Chapter III</b>	<b>System Modeling</b>	<b>22</b>
3.1	Introduction	22
3.2	Proposed System Model	22
3.3	Methodology	23
3.4	PV System Modeling	25
3.4.1	PV Array Modeling	25
3.4.2	Technical Data for System Design	28
3.5	Closed loop dc/dc Boost Converter Modeling	30
3.6	Proposed MPC Based On-grid Inverter Modeling	31
3.6.1	Three-Phase Two-Level VSI Model	31
3.6.2	Transformation of $abc$ to $\alpha\beta$ Co-ordinates	34
3.6.3	Three Phase Active Load Model	35
3.6.4	Discrete-Time Model for Prediction	36
3.6.5	Cost Function Flexibility	38
3.6.6	Cost function Design	39
3.6.7	Algorithm of Proposed Controller	40
3.6.8	Working Strategy of Proposed Controller	42
3.7	Existing Controller Modeling for Comparison	44
3.7.1	PI-PWM Controller	45
3.7.2	PR-PWM Controller	45
3.7.3	PR-SHEPWM Controller	47
3.8	Load Flow Analysis	48
3.9	Power Loss Analysis	51

3.10	Fault Analysis	53
3.11	Conclusion	54
<b>Chapter IV</b>	<b>Simulation Results</b>	<b>55</b>
4.1	Introduction	55
4.2	Performance Analysis of Proposed Controller	55
4.2.1	Steady-state Analysis	57
4.2.2	Current Tracking Accuracy	59
4.2.3	Effect of Switching Frequency Term in the Cost Function	59
4.2.4	Power Loss Analysis	62
4.2.5	Load Flow Analysis	64
4.2.6	Fault Handling Capacity Analysis	66
4.3	Comparison with the Existing Controllers	68
4.3.1	Transient Analysis	68
4.3.1.1	PI-PWM Controller	68
4.3.1.2	PR-PWM Controller	69
4.3.1.3	PR-SHEPWM Controller	70
4.3.1.4	Proposed MPC based Controller	71
4.3.2	Reference Current Tracking	72
4.3.2.1	PI-PWM Controller	73
4.3.2.2	PR-PWM Controller	75
4.3.2.3	PR-SHEPWM Controller	77
4.3.2.4	Proposed MPC based Controller	78
4.3.3	Load Flow Analysis	81
4.3.4	Loss Analysis	82
4.4	Conclusion	86
<b>Chapter V</b>	<b>Conclusions and Future Prospects</b>	<b>87</b>
5.1	Conclusion	87
5.2	Future Prospects	89



References  
Publications

a  
m

## List of Tables

<b>Table No.</b>	<b>Description</b>	<b>Page</b>
Table 1.1	Harmonic distortion limitation	5
Table 1.2	IEEE and IEC standards	6
Table 2.1	Advantages and disadvantages of numerous control strategies of on-grid inverter control	16
Table 3.1	Table for the specifications of the PV array	27
Table 3.2	Average daily solar radiation, clearness index and temperature	29
Table 3.3	Voltage vectors of the 2L-VSI	33
Table 3.4	Value of cost function for the eight individual voltage vectors	44
Table 3.5	Parametric value of in-line transformer	50
Table 3.6	Parametric value of shunt capacitor	51
Table 3.7	Table for the line segment, distributed load and spot load data for the IEEE 13 bus test feeder	51
Table 4.1	Parameter values for the simulated systems	55
Table 4.2	Variation of THD and Losses with varying the value of weighting factor $\lambda$	60
Table 4.3	With and without connecting the proposed PV system to the IEEE 13 bus	64
Table 4.4	Load flow analysis data for PWM and MPC based current controller	82
Table 4.5	Parameters used for the power loss analysis	82
Table 4.6	Average loss for MPC and PWM controllers	83

## List of Figures

<b>Figure No</b>	<b>Description</b>	<b>Page</b>
Fig 1.1	Various types of renewable energy sources	1
Fig 1.2	Global capacity of electricity generation from renewable and non-renewable energy sources in percentage	2
Fig 1.3	Year-wise growth of global solar energy from 2007 to 2017	3
Fig 1.4	The development of off-grid and on-grid solar system in Bangladesh from 2010 to 2018	3
Fig 1.5	Different applications of solar power	4
Fig 2.1	Key challenges and objectives of power electronic converters	10
Fig 2.2	Block diagram of three-phase hysteresis current controller	11
Fig 2.3	PI controller based linear current controller using PWM/SVM modulation	12
Fig 2.4	A sliding mode control strategy alongside the PWM/SVM	13
Fig 2.5	A FLC strategy utilizing the pulse width/ space vector modulation	14
Fig 2.6	An ANN based load current controller for a three-phase on-grid inverter	14
Fig 2.7	A Neuro-fuzzy controller for a three-phase on-grid inverter	14
Fig 2.8	A predictive controller for a three-phase on-grid inverter	15
Fig 2.9	Basic operating principle of model predictive control	18
Fig 2.10	Statistical data after literature review on different perspectives of MPC	21
Fig 3.1	Block diagram of the proposed MPC based on-grid PV inverter	23
Fig 3.2	Methodology of the overall research work	24
Fig 3.3	Equivalent circuit of a perfect PV cell	25
Fig 3.4	$I-V$ and $P-V$ characteristics curve of the solar cell	26
Fig 3.5	(a) $I-V$ , and (b) $P-V$ curve for the selected PV array at different irradiance conditions	28
Fig 3.6	Variation of irradiance during summer and winter days at Khulna	29
Fig 3.7	Block diagram of the dc/dc boost converter	30
Fig 3.8	Output voltage waveform generated by the closed loop dc/dc converter	31
Fig 3.9	Two level voltage source inverter (VSI) power circuit	31
Fig 3.10	Space distribution of all admissible voltage vectors of the 2L-VSI	33

Fig 3.11	(a) Graphical representation, and (b) MATLAB implementation of $\alpha\beta$ transformation	35
Fig 3.12	Control parameter flexibility of MPC	38
Fig 3.13	Flow chart of the proposed predictive controller	41
Fig 3.14	The representation of reference and predictive currents in vector plot	42
Fig 3.15	Graphical representation of selecting optimal voltage vectors of reference and predictive currents	43
Fig 3.16	Value of cost function for the eight individual voltage vectors	44
Fig 3.17	Block diagram of the closed loop PI-PWM controller	45
Fig 3.18	Block diagram of the PR-PWM controller with harmonic compensator	46
Fig 3.19	Bode plot of the PR controller along with harmonic compensator	46
Fig 3.20	Block diagram of the PR-SHEPWM controller for generating gate pulse of VSI	48
Fig 3.21	Single-line diagram of IEEE 13 bus system	50
Fig 3.22	Intentional fault injection in the IEEE 13 bus test feeder (a) A healthy three phase system and several types of fault in the system such as (b) single line to ground fault, (c) Double line to ground fault, and (d) three-phase balanced fault	53
Fig 4.1	MATLAB/SIMULINK representation of the proposed MPC based on-grid PV inverter	56
Fig 4.2	Steady-state phase voltage ( $V_a, V_b, V_c$ ) before LC filter using the proposed controller	57
Fig 4.3	Steady-state phase voltage ( $V_a, V_b, V_c$ ) after LC filter using the proposed controller	57
Fig 4.4	Steady-state phase currents ( $I_a, I_b, I_c$ ) using the proposed controller	58
Fig 4.5	Steady-state phase currents ( $I_\alpha, I_\beta$ ) in $\alpha\beta$ plane using the proposed controller	58
Fig 4.6	The current waveforms ( $I_\alpha, I_\beta$ ) for transient response	59
Fig 4.7	Current THD without switching frequency term in the cost function	60
Fig 4.8	Switching frequencies and current THDs with the variation of weighting factor values, $\lambda$	61

Fig 4.9	Steady-state phase currents ( $I_a, I_b, I_c$ ) using the proposed controller for $\lambda = 0.4$	61
Fig 4.10	Conduction loss with and without switching frequency reduction term in the proposed controller	62
Fig 4.11	Switching loss with and without switching frequency term in the proposed controller	62
Fig 4.12	Harmonic loss with and without switching frequency term in the proposed controller	63
Fig 4.13	The overall loss per phase with and without switching frequency term in the cost function	63
Fig 4.14	IEEE 13 bus system with the proposed controller based PV system for load flow analysis	65
Fig 4.15	Voltage and current profile during and after the LG fault for the proposed controller	66
Fig 4.16	Voltage and current profile during and after the LLG fault for the proposed controller	67
Fig 4.17	Voltage and current profile during and after the LLLG fault for the proposed controller	67
Fig 4.18	Transient phase currents for the PI-PWM controller	68
Fig 4.19	Transient phase voltage in phase a, and currents ( $I_\alpha, I_\beta$ ) in $\alpha\beta$ frame for PI-PWM controller	69
Fig 4.20	Transient phase currents for the PR-PWM controller	69
Fig 4.21	Transient phase voltage in phase a, and currents ( $I_\alpha, I_\beta$ ) in $\alpha\beta$ frame for PR-PWM controller	70
Fig 4.22	Transient phase currents for the PR-SHEPWM controller	70
Fig 4.23	Transient phase voltage in phase a, and currents ( $I_\alpha, I_\beta$ ) in $\alpha\beta$ frame for PR-SHEPWM controller	71
Fig 4.24	Transient phase currents across the load using proposed controller	71
Fig 4.25	Transient phase voltage in phase a, and currents ( $I_\alpha, I_\beta$ ) in $\alpha\beta$ frame using proposed controller	72

Fig 4.26	Decoupling nature of transient phase currents ( $I_\alpha, I_\beta$ ) in $\alpha\beta$ plane	72
Fig 4.27	Steady-state phase current waveforms in $abc$ and $\alpha\beta$ frame for the PI-PWM controller	73
Fig 4.28	Reference current tracking response for PI-PWM control	73
Fig 4.29	Current tracking error for the PI-PWM controller	74
Fig 4.30	Current THD response for the PI-PWM controller	74
Fig 4.31	Steady state phase current response in $abc$ and $\alpha\beta$ frame for the PR-PWM controller	75
Fig 4.32	Reference current tracking response for PR-PWM control	75
Fig 4.33	Current tracking error response for the PR-PWM controller	76
Fig 4.34	Current THD response for the PR-PWM controller	76
Fig 4.35	Steady state phase current response in $abc$ and $\alpha\beta$ frame for the PR-SHEPWM controller	77
Fig 4.36	Reference current tracking response for PR-SHEPWM control	77
Fig 4.37	Current tracking error response for the PR-SHEPWM controller	78
Fig 4.38	Current THD response for the PR-SHEPWM controller	78
Fig 4.39	The current ( $I_\alpha, I_\beta$ ) tracking performance under steady-state condition	79
Fig 4.40	Mean tracking absolute error between the reference and measured current.	79
Fig 4.41	Steady-state grid current THD response for the proposed predictive controller	80
Fig 4.42	Comparison of Current THD values for the PI-PWM, PR-PWM, PR-SHEPWM and the proposed controller	80
Fig 4.43	Comparison of individual harmonic component THD values for the PI-PWM, PR-PWM, PR-SHEPWM and the proposed controller	81
Fig 4.44	Instantaneous arm current in the upper IGBT for MPC	83
Fig 4.45	Instantaneous arm current in the upper IGBT for PWM	83
Fig 4.46	Instantaneous conduction and switching loss in MPC	84
Fig 4.47	Instantaneous conduction and switching loss in PWM	84
Fig 4.48	Comparison of conduction, and switching loss between MPC and PWM	85

## Nomenclature

$I_{ph}$	Produced Photocurrent
$N_p, N_s$	Quantity of PV cells in Parallel and Series Respectively
$I_o$	Saturation Current
$q$	Charge of Electron
$R_s$	Series Resistance
$R_p$	Parallel Resistance
$A$	Ideality Factor
$K$	Boltzmann's Constant
$T$	Temperature
$I_D$	Diode Current
$I_{SC-STC}$	Short Circuit Current at Standard Test Conditions
$T_{STC}$	Temperature at Standard Test Conditions
$G$	Irradiation on cell surface
$G_{STC}$	Irradiation at Standard Test Conditions
$K_i$	Short Circuit Current Coefficient
$V_{OCV-STC}$	Open Circuit Voltage at Standard Test Conditions
$K_V$	Open Circuit Voltage Coefficient
$V_{th}$	Thermal Voltage of Cell
$P_{max}$	Maximum Current
$I_{sc}$	Short Circuit Current
$V_{oc}$	Open Circuit Current
$D$	Duty Cycle
$V_{sys}$	System Voltage
$V_i$	Input Voltage
$V_o$	Output Voltage
$C_o$	Output Capacitance
$K_p, K_i$	Proportional Gain and Integral Gain
$w_c$	Cutt-off Frequency

$\omega$	Angular Frequency
$\alpha$	Switching Angle
$M$	Modulation Index
$f_{sw}$	Switching Frequency
$V_{ce0}$	Threshold Voltage of IGBT
$T_0$	Output Period
$I_x(t)$	IGBT Current in Arm
$R_{ce}$	IGBT Differential Resistance
$\tau(t)$	Duty Ratio
$I_{dc}$	DC Link Current
$I_{ccnom}, V_{ccnom}$	Nominal Current through IGBT and Nominal Voltage Across IGBT during Test
$P_{sw\ instantaneous}$	Instantaneous Switching Loss across IGBT
$P_{sw}$	Average Switching Loss across IGBT
$P_{con}$	Average Conduction Loss
$P_{con\ instantaneous}$	Instantaneous Conduction Loss
$f_0$	Output Frequency
$I_L$	Load Current
$R_L$	Load Resistance
$P_{harmonic}$	Loss Due to Harmonic
$I_{ah}, I_{bh}, I_{ch}$	Harmonic Current in a,b,c Phases
$I_R, I_Y, I_B$	Current of Phase R, Y, B
$Z_F$	Fault Impedance
$J$	Jacobian Matrix
$V_{ab}, V_{bc}, V_{ca}$	Line Voltage across the Load
$T$	Period of a Cycle
$A_n$	Amplitude of $n^{th}$ Harmonics
$I_{THD}$	Total harmonic Distortion Current
$V_{THD}$	Total Harmonic Distortion Voltage
$I_n, V_n$	Current and Voltage of $n^{th}$ harmonics



## Abbreviations

GW	Giga Watts
MW	Mega Watts
PV	Photovoltaic
USD	United States Dollar
MPPT	Maximum Power Point Tracking
CDV	Committee Draft for Vote
NEC	National Electrical Code
EN	European Standard
IGBT	Insulated Gate Bipolar Transistor
MOSFET	Metal-Oxide Semiconductor Field Effect Transistor
THD	Total Harmonic Distortion
PEC	Photo Electro Chemical
SVPWM	Space Vector Pulse Width Modulation
SRF	Synchronous Reference Frame
PI-PWM	Proportional Integral Pulse Width Modulation
PR-PWM	Proportional Resonant Pulse Width Modulation
FPGA	Field Programmable Gate Array
DC	Direct Current
EMC	Electromagnetic Compatibility
AC	Alternating Current
DPC	Direct-Coordinated Power Control
DTC	Direct Torque Control
SVM	Space Vector Modulation
SHE	Selective Harmonic Elimination
FOC	Field Oriented Control
VOC	Voltage Oriented Control
ANN	Artificial Neural Network
FLC	Fuzzy Logic Controller
FCS-MPC	Finite Control Set Model Predictive Control
MV	Medium Voltage
MPDTC	Model Predictive Direct Torque Control

IM	Induction Machine
IEEE	Institute of Electrical and Electronics Engineers
SCC	Short Circuit Current
STC	Standard Test Conditions
OCV	Open Circuit Voltage
PTC	PVUSA Test Condition
HOMER	Hybrid Optimization of Multiple Electric Renewables
NASA	National Aeronautics and Space Administration
BC	Boost Converter
P&O	Perturb and Observe
CCM	Continuous Conduction Mode
2L-VSI	Two Level Voltage Source Inverter
BJT	Bipolar Junction Transistor
DN	Distribution Network
LU	Lower Upper
NR	Newton-Raphson
DER	Distributed Energy Resources
NEV	Neutral Earth Voltage
LVN	Low Voltage Network

## Chapter I

### Introduction

#### 1.1 Background

For socio-economic advancement and growth, energy is an imperative component. Because of the quick advancement of human life, increase in population, swelling human demands, the interest for additional power generation is now a hot topic. The widely used sources of power generation, for example, nuclear and non-renewable energy sources (oil, coal and flammable gas) are unsustainable as the recharge rate of the assets may fail to meet the upcoming demands of electricity [1]. Also, the ample utilization of petroleum derivatives causes an irreparable loss to our living condition. With the exhaustion of petroleum products and soaring dimensions of CO<sub>2</sub> in the environment, renewable energy sources keep on picking up prominence as a long haul economical and sustainable source of electricity generation [2]. Of late, the world researcher put a lot of efforts of this promising renewable energy field which have been impelled compellingly by ecological, economic and political intentions [3].

Renewable energy sources are always recharged by the earth with the energy received from the sun either directly, or in a roundabout way (such as bioenergy, hydro and wind), just as from other common sensation, (for example, tidal and geothermal energy) [4]. Various types of renewable energy sources are presented in Fig. 1.1 [5-7].

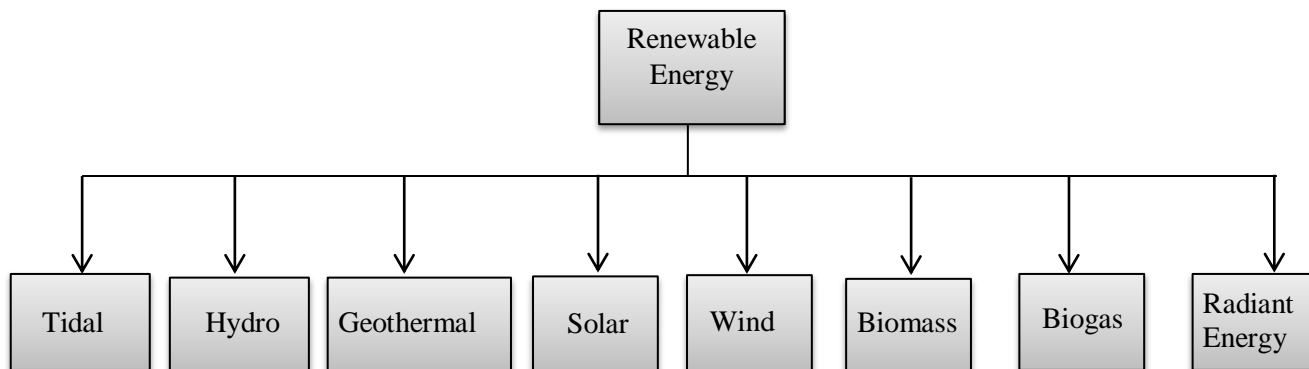


Figure 1.1: Various types of renewable energy sources.

The largest growth of electricity generation from the renewable energy source is seen in 2017, about 178GW energy with 9% more from the year 2016 [8]. As of 2017, the global capacity of electricity generation from the renewable energy sources have reached to 2,195 GW, which meets about 26.5% electricity demand of the whole world as shown in Fig.1.2 [8]. It is suggested that among the renewable energy sources, the most dominating one is the hydro-electric power source which contributes about 16.40% of the total 26.5% [8].

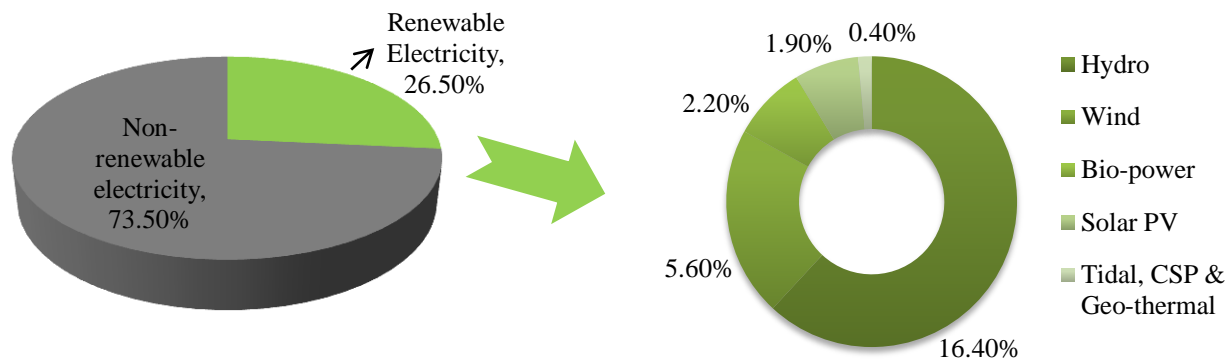


Figure 1.2: Global capacity of electricity generation from renewable and non-renewable energy sources in percentage [8].

In 2017, about 19 GW energy is added to the worldwide capacity of hydropower, which makes the overall capacity to nearly 1,114 GW [9]. China remained the perpetual pioneer in appointing new hydropower limit, representing about 40% of new establishments in 2017 [9]. The other pioneer countries are Brazil, Turkey, India, and Angola. Electricity generation from wind power is the second most contributing source among the other renewable energy sources. The total global energy came from this source is 539 GW (up to 2017), in which about 52 GW wind power is added to the total in 2017 [10]. China leads from the front for the developing and harvesting electricity from this source, while Europe and India also contribute significantly. Bio-power which includes bio-mass and bio-gas are also contributing to the world electricity generation significantly. Bio-power provides 2% energy demand and 3% transport demand of the total global electricity generation. This energy source also meets about 4% of heat demand in buildings and 6% in industry [11]. Although geothermal energy sources are not much popular across the whole world, it may be better sources of renewable energy due to its recent progress. As of 2017, the total capacity of geothermal energy reaches 12.8 GW in which nearly 0.7 GW came in 2017 alone [12]. Indonesia and Turkey represented three-fourths of new capacity. The other countries such as Chile, Iceland, Honduras, Mexico, the United States, Japan, Portugal, and Hungary also started harvesting electricity from this prominent source. Tidal energy or marine energy is another encouraging source of renewable energy. Approximately, 529 megawatts (MW) of tidal power is available in 2017, over 90% was provided by two tidal barrage facilities. Ocean energy (barring tidal flood) had a decent year, as tidal stream and wave energy saw new limit come on the web, quite a bit of it in the waters of Scotland [13]. Solar PV is now one the most promising and growing renewable energy sources. Although as of now, it contributes only 1.90% of the total global renewable capacity; its growth over the year is the most significant than other sources. Previously, the European countries contribute mostly by harvesting electricity from solar, but now China leading from the front. The total capacity of solar power reaches to 402GW<sub>p</sub> in 2017 [14-15].

In the last couple of decades, cost and efficiency were the two hardship elements for the development of PV panels. For example, the cost per watt of crystalline silicon PV modules was 101.05 USD in 1975 contrasted with 0.61 USD in 2017 [16]. Because of the large scale manufacturing, a further decrease has been found in the cost of PV modules. From an efficiency perspective, PV module efficiencies fluctuate from 6% to around 40% [17-18]. Due to the cost of production, it is not always wise to use a highly efficient PV cell. From an economic point of

view, most of the PV cell efficiency lies between 14 to 19% [17]. Apart from the issues, the growth of PV systems has shown a tremendous peak. From 2007-2017, the overall development of PV had been an exponential curve as appeared in Fig. 1.3 [8].

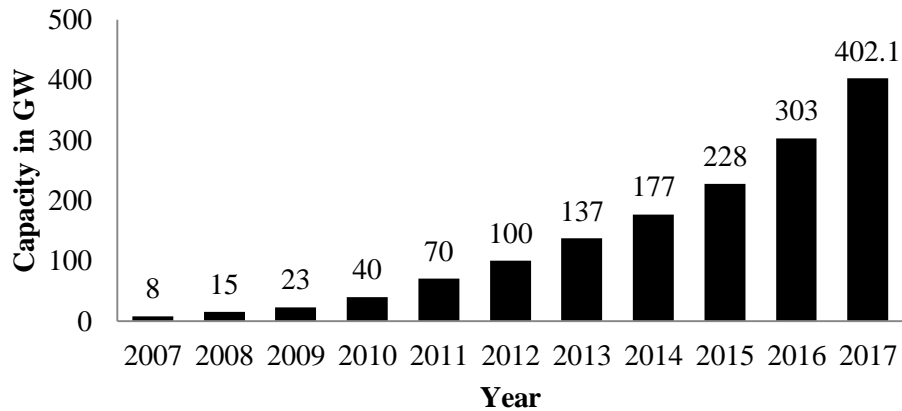


Figure 1.3: Year-wise growth of global solar energy from 2007 to 2017 [8].

The year 2017 was a landmark one for solar PV, the world added more capacity from solar PV than from any other type of power generating technology [8]. From Fig. 1.3, it is shown that the generation of solar PV in 2016 is 303 GW, which is increased by 32% in 2017. This led to a total global solar power capacity of over 400 GW in 2017, after solar exceeded the 300 GW mark in 2016 and the 200 GW level in 2015 [8].

Alongside the whole world, solar PV is also popular in Bangladesh. Due to the geographical location of Bangladesh, the solar PV can be a significant source for electricity generation. Therefore, the government of Bangladesh has taken several steps to raise the solar energy source and has set a target of 10% share of renewable energy sources by 2020 [19]. Solar PV system can be both off-grid and on-grid. Bangladesh contributes to the world energy generation by both this two ways. The development of off-grid and on-grid solar systems in Bangladesh from 2010 to 2018 is shown in Fig. 1.4 [19].

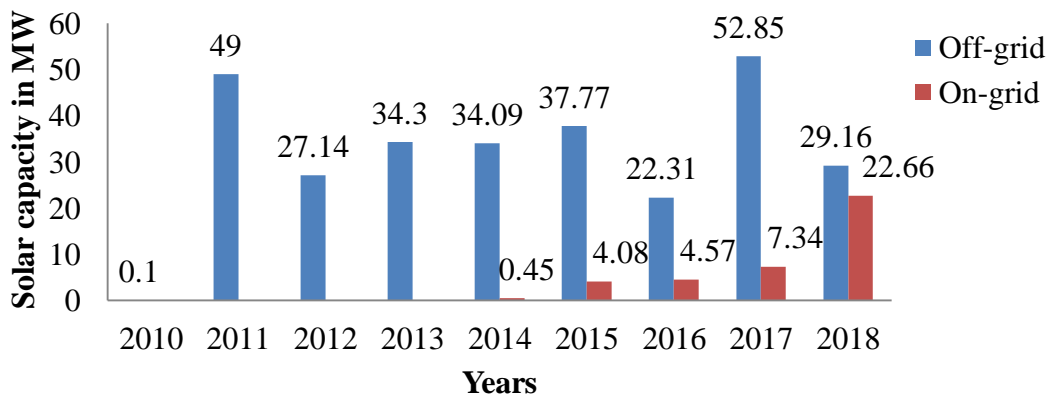


Figure 1.4: The development of off-grid and on-grid solar systems in Bangladesh from 2010 to 2018 [19].

Figure 1.4 suggests that Bangladesh started reaping solar energy by off-grid process only. However, years after it is also reaping solar energy by both the on-grid and off-grid processes. A rapid growth has been seen from 2011 to 2018, which promises a significant source of electricity generation for Bangladesh. Therefore, several agencies and power generating companies started utilizing this source for generating power through several projects. The agencies/companies contribute to this issue through different applications of solar power as shown in Fig. 1.5.



Figure 1.5: Different applications of solar power.

Figures 1.4 and 1.5 show an eye-catching improvement of solar energy in Bangladesh. However, the solar energy system is facing challenges when the off-grid system is connected to the grid. Therefore, the compatibility of the on-grid system with the utility grid for different output frequencies is an essential task. To understand this issue, the systems need to utilize a type of interface which makes them ready to change over their output frequency and injects synchronized power into the network. In case of an ac grid, a dc to ac on-grid inverter is the main part of the interfacing system. Harmonic free load current should be injected by the PV inverter.

As the PV system is now been a significant source of power generation, the effect of PV modules on the utility grid cannot be overlooked. On-grid PV system can cause a disturbance on the grid, for example, infusing more harmonics or diminishing the stability level of the power system [20]. This issue can be extreme when an expansive scale PV module is associated with the grid. Again, current and voltage distortions and undesirable operation of the system can be caused by harmonic content of the injected current [21]. Hence, the reduction of harmonics from the injected grid current is a concerning issue. To raise the capacity of solar power and keep up power quality, it is important to consent to a few necessities, for example, compensation of harmonics, power quality enhancement etc. [22]. The IEEE Standard [23], which was presented in 1981 and reconsidered in 2003, gives guidance on managing harmonics created by static power converters and nonlinear loads. This standard keeps harmonics from adversely influencing the utility grid. Therefore, for an on-grid PV system the following three categories of demands and standards are preferably needed.

- i. Demands defined by the grid,
- ii. Demands defined by the PV modules, and
- iii. Demands defined by customers.

The aforementioned three categories are described below.

### 1.1.1 Demands Defined by the Grid

As the utility grid is actually connected to the grid-tied inverter output, the utility company's standard has to be followed. In particular, the future international standard (still a Committee Draft for Vote (CDV)) IEC61727 [24] and the present standards EN61000-3-2 [25], IEEE1547 [23] and the U.S. National Electrical Code (NEC) 690 [26] are worth considering. Quality of the power, off-grid operation detection, grounding etc. is accorded with the standards. For instance, the PV panels' negative pole must have to be grounded.

The present EN standard (connected in Europe) is less demanding to adapt to, with respect to current harmonics, than the standards of IEEE and IEC. This is likewise reflected in the inverter topologies, which have changed from large thyristor-based grid-tied inverters to smaller on size IGBT/MOSFET. The standard of IEEE [23] and the IEC [24] put impediments on the maximum allowable injected dc current to the utility grid. To nullify the saturation of the distribution type transformer, the impediments of the injection is made [27]. Nonetheless, the cutoff points are fairly little (0.5% and 1.0% of the rated output current), and such little qualities can be hard to gauge exactly with the energizing circuits inside the inverters. This can be moderated with enhanced measuring circuits or by including a line-frequency transformer between the grid and the inverter. The checking of grounding the PV system and its related grounding issues are given importance in NEC 690 standard. For example, the system ground or negative terminal of the PV panels should be grounded and checked regularly if the PV output dc voltage reaches a specified voltage i.e. 50V [26, 28]. This can be troublesome for some high-control transformer-less systems, since a single stage inverter with line-to-neutral is system grounded already on the grid side.

In addition, if the frequency of the grid digresses outside of a predetermined range, the inverter must stop injecting power to the grid within a predefined time. As indicated by this standard, the operating frequency extent is between 59.3 and 60.5Hz, and the inverter needs to stop to empower the system inside 6 cycles (0.1s) on account of recognizing out of range frequencies on the utility matrix [29]. Other than the necessities, it is alluring to have a low dimension of injected current harmonics into the grid. The permissible amount of harmonics in the injected current to the grid is presented in Table 1.1 [17, 29]. While designing the control of inverter, the power factor of the system should also be considered. When the inverter output power is 10% and 50% greater than the rated power, the power factor of it should be greater than 0.85 and 0.9 respectively as shown in Table 1.2 [17, 29].

Table 1.1: Harmonic distortion limitation [17, 29]

Odd harmonic order	THD of odd harmonics	THD of even harmonics
THD	5%	25% of odd harmonic limit
3 <sup>rd</sup> – 9 <sup>th</sup>	< 4%	25% of odd harmonic limit
11 <sup>th</sup> – 15 <sup>th</sup>	< 2%	25% of odd harmonic limit
17 <sup>th</sup> - 21 <sup>st</sup>	< 1.5%	25% of odd harmonic limit
23 <sup>rd</sup> – 33 <sup>rd</sup>	< 0.6%	25% of odd harmonic limit
>33rd	< 0.3%	25% of odd harmonic limit

Table 1.2: IEEE and IEC standards [17, 29]

Issue	IEC61727	IEEE1547
Nominal Power	10kW	30kW
Maximum current THD	5%	5%
Power factor at 50% of rated power	0.90	0.90
Voltage range for nominal operation	85%-110% (196V-121V)	88%-110% (97V-121V)
Frequency range	$50 \pm 1.5$ Hz	59.3-60.5Hz
DC current injection	$< 1\% I_{out}$	$< 1\% I_{out}$

### 1.1.2 Demands Defined by the Photovoltaic Module(s)

The most well-known recent PV technologies are the multi-crystalline and mono-crystalline-silicon modules, which depend on conventional, and costly, microelectronic assembling procedure [30]. Nonetheless, new advances like thin-layer silicon, indistinct silicon, and Photo Electro Chemical (PEC) are being developed [30-31]. These kind of PV modules can be made self-assertively vast by a modest “roll-on– move off” process. The operating condition in which the PV modules capture the maximum solar energy is known as the MPPT condition. The MPP voltage extend for the PV modules is regularly characterized in the range from 23 to 38 V at an output dc power of roughly 160W, and their open-circuit voltage is underneath 45V. This MPPT voltage may be extended by around 0.5 to 1.0V at several hundred amperes for each square meter cell [32-33].

### 1.1.3 Demands Defined by the Operator

As mentioned previously, output PV voltage and current are impacted by the insolation of the sun and encompassing temperature. Since the two parameters change in a wide range, from the manufacturer's perspective, a grid-tied PV system is required to have highly efficient over a wide scope of output power and voltage. Conveying a high-effectiveness transformation in such a wide scope of variation is exceedingly attractive in the on-grid PV system. Besides, a grid-connected PV system must be very dependable and have a long operational lifetime [34].

## 1.2 Motivation behind the Research Work

Availability, ease of maintenance, cost declination and eco-friendly nature of renewable energy source supplants the fossil fuel based energy production techniques [35]. Among the popular renewable energy sources, the photovoltaic (PV) energy has gained more attention than the other sources such as wind, fuel cell, hydro-energy, etc. The worldwide growth of PV energy has increased tremendously in recent years. In 2016, the worldwide capacity of the solar PV system is 303GWp. After one year, this capacity has become 402.1GWp which is 32% more than the growth of 2016. Now, in 2018, this PV growth is expected to increase by 27% from the growth of 2017 and have the worldwide capacity of 508GWp [36-37]. This PV system either is a dc micro-grid or an ac micro-grid. In a dc grid, the energy generated from the PV array and dc-dc converter is directly delivered to the load or battery, whereas dc-ac converter or an inverter is required to supply the energy to the ac load in the ac grid. This inverter section may be of a



single phase or three-phase, which is the heart of a grid-connected system. Producing a proper switching signal for the inverter is an important task to achieve lower current total harmonic distortion (THD), lower power loss, and improve reliability and safety of the grid [38]. The presence of harmonics in the injected currents leads to an additional loss of power, decaying the quality of the power and lifetime of the system equipment [39]. Therefore, this has been a hot topic in power electronics.

A lot of control strategies have been found in the literature for controlling the operation of the inverters. The pulse width modulation (PWM), space vector PWM (SVPWM), deadbeat control, repetitive control, sliding mode control, synchronous reference frame (SRF), model predictive control (MPC) etc. are the various control strategies [40]. To reduce the periodic disturbances, repetitive control is an excellent one, however, this one does not provide good tracking accuracy and has the inability to reject non-periodic disturbance [41]. The usual use of conventional PI regulator is allowed by SRF control but similarly suffers from poor disturbance rejection ability due to the limited gain of PI regulator [42]. The sinusoidal PI-PWM and SVPWM are the commonly used control strategies, but they suffer from poor total harmonic distortion (THD) and poor de-coupled nature. The deadbeat and the sliding mode control have parameter variation sensitivity, complexity and loading condition problems. However, the controllers yield good dynamic performance in control of the instantaneous inverter output voltage. To compensate the selected harmonics of line currents, a closed loop selective harmonic compensation method is utilized in [43]. To suppress the selected harmonics and compensate the reactive power, a hybrid active power filter utilizing proportional-resonant (PR) controller has been developed in [44]. Among these control strategies, MPC has gained widespread popularity due to its faster dynamic response, easily understandable, and having the ability to handle various systems constraints and non-linearities [45]. In MPC, the control objectives are predicted using the model of the system and an optimal switching sequence is selected by minimizing a predefined cost function. Then the selected switching states are applied to the inverter. There are different MPC algorithms, such as predictive current and power control, for on-grid PV inverters [46]. The losses in the inverters can be minimized by including a switching frequency term in the cost function of the predictive controller. Then more power from a PV source can be penetrated to the grid. The effectiveness of the MPC in terms of this active power penetration to the grid for a specified PV system has not been reported yet. Therefore, the main motivation of this research is to develop an energy efficient control of an on-grid inverter which presents better performance in terms of current THD, steady-state and dynamic responses, reference tracking accuracy, de-coupling capability, penetrated power to the grid, and switching loss. The performance of MPC will also be compared with the traditional controllers such as PI-PWM, proportional-resonant, and proportional-resonant selective harmonic elimination controller.

### **1.3 Research Objectives**

In an on-grid PV system, the inverter is treated as the heart of the system. To achieve a lower current THD, lower power loss, and reliability and safety of the grid, the controlling of the inverter is an important task. The presence of harmonics in the injected currents leads to an additional loss of power, decaying the quality of the power and lifetime of the system. Therefore, the proper controlling of the on-grid inverter is necessary. The specific objectives of the proposed research work are:

- i. To develop an MPC based on-grid PV inverter controller that reduces the harmonics of the injected grid current and also complies the IEEE and IEC current THD standards;
- ii. To design, develop, and evaluate the on-grid PV system utilizing the proposed controller in MATLAB/SIMULINK platform;
- iii. To analyze the performance of the controller in terms of current tracking accuracy, steady-state and transient responses, THD, inverter switching loss and fault tolerant ability;
- iv. To ensure maximum power penetration to the ac grid from a specified PV source by minimizing current THD;
- v. Finally, to validate the proposed controller, the results will be compared with the existing related controllers for on-grid PV inverters.

#### **1.4 Dissertation Organization**

This dissertation deals with the design and analysis of a model predictive based energy efficient controller for an on-grid PV inverter system. The controller ensures more power penetration to the ac grid derived from the PV source. The research work presented in the dissertation is subdivided into five chapters. The work that is carried out in each chapter is summarized below.

Chapter I presents the background study of performing the research work on on-grid PV system and its importance for the future power generation. The motivation behind the research work and the research objectives are also presented in this chapter.

Chapter II presents the background study of the research work which includes the characteristics and key challenging issues of the power converter, existing control strategies for the converter, suitability of the proposed controller, and its basic operating strategy along with pros and cons. This chapter also presents a key statistics of existing research works to show why the research work is chosen and the importance of it in the field of power and energy technology.

Chapter III presents the methodology of the research work and the system modeling part. In this chapter, the PV system modeling, dc/dc converter design and the proposed controller modeling with grid interconnection are presented in detail. The mathematical expressions of the load flow, and power loss analysis for the proposed controller are presented. The fault tolerant ability testing technique of controller is also discussed in the end of this chapter.

Chapter IV provides the simulation results for the model presenting in Chapter III, which includes the performance analysis of the proposed controller, comprehensive comparison of it with the existing controllers, results from the load flow, power loss and fault analyses to validate the proposed controller as an efficient controller.

Chapter V presents the conclusions of the work along with the future scopes followed by the references.

## Chapter II

### Literature Review

#### 2.1 Introduction

The goal of the research work is to design an energy efficient controller for the inverter using model predictive control (MPC) which is utilized in the on-grid PV system. In an on-grid PV system, the power electronic converter and its control strategy is an important issue. Therefore, the characteristics and challenging issues of the power converter, overview of existing control strategies, and the operation of MPC are discussed in this chapter. Comparison with the existing controllers is also done in order to discuss the pros and cons of the MPC. It is expected that MPC would fulfill the modern industrial demand. Different research papers and articles have been studied to understand the current scenario of the controllers and find the research gap and scope of the research work. In short, the purpose of this chapter is to provide an overview for readers who are interested on the recently developed MPC for the power converter utilized in the on-grid PV system.

#### 2.2 Power Converter

For an efficient energy conversion, three things are most significant in the research areas of the power converter. They are (i) type or nature of the semiconductor device, (ii) the control configuration or strategy of the devices, and (iii) the appropriate switching of the devices [47]. Therefore, the control of power converters is an exceptionally dynamic research theme and is always advancing as per the electrical improvements in semiconductor devices and control stages, control prerequisites, control quality measures, and grid code necessities, and so forth [48-49]. Although, the research work in the field of power converter is enhancing day by day, this work is also facing several key challenges as shown in Fig. 2.1 [7]. Hence, converter control methods have been an exceptionally dynamic research point in the field of power electronics, covering numerous topologies for low, medium, and high-control applications. Several classical controllers including linear and non-linear controllers have developed for enhancing the performance of power converter. The classical controllers normally deal with dynamic execution and system stability. Due to the expanding demand of industry, the research works in this field demanding further development of these control methods. Advanced control platform, for example, FPGA and dSpaces are generally acknowledged by the industrial norms and standards for computerized executions of the controllers.

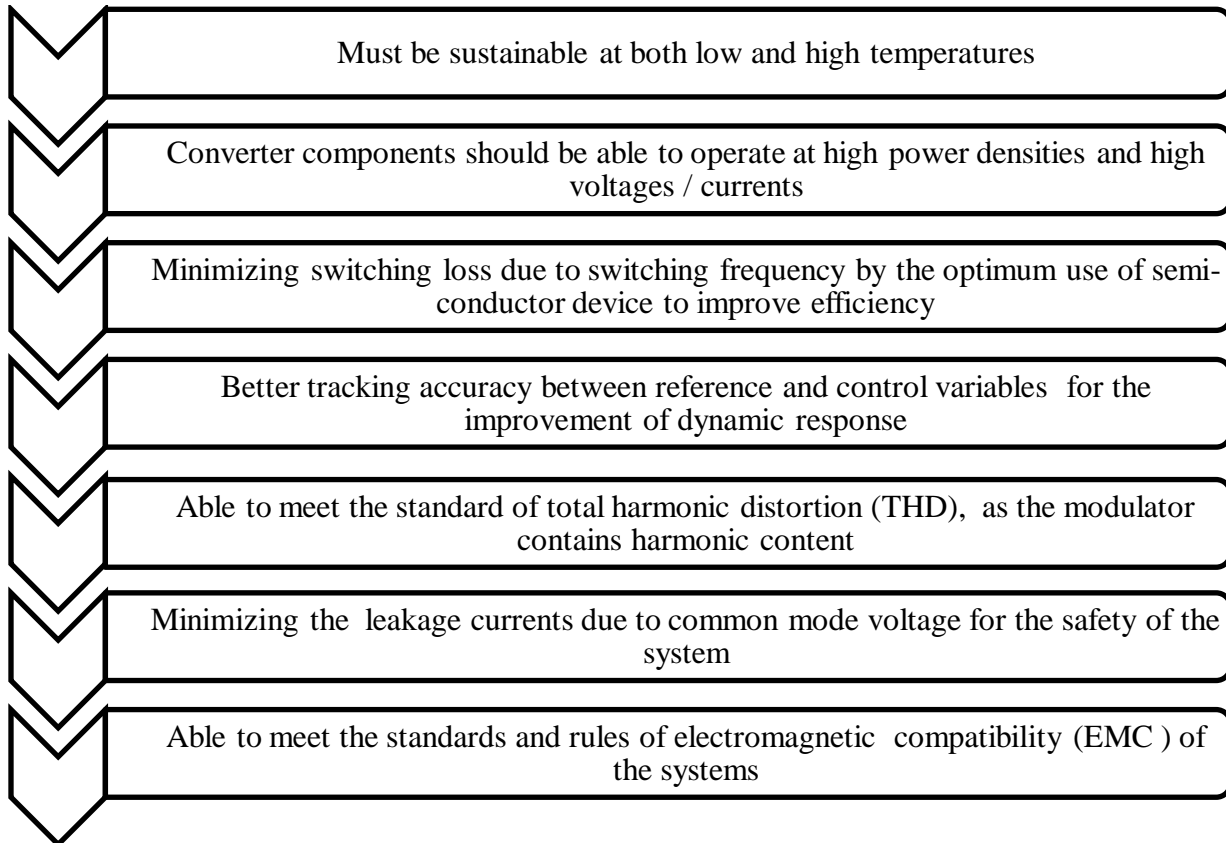


Figure 2.1: Key challenges and objectives of power electronic converters.

The advanced control platforms dependent on floating point processor are generally acknowledged by the scholarly world. However, platforms dependent on fixed point processor in view of the minimal amount of cost and satisfactory calculation are also welcomed by the industry world [50]. Power converters are utilized for different applications and in numerous ventures, for example, transportation, industrial control system, domestic usage, and sustainable power source. In a solar based PV system, the power derived from the solar panel is fed to the dc/dc converter where the optimal output is drawn through various MPP tracking techniques. From there on, the dc power is changed over to ac by an inverter for injecting sinusoidal current to the grid. Power converters for sustainable power generation offer the optimal power extraction, execution, and nature of the power injected [51-52]. Therefore, the various types of control techniques including the linear and non-linear techniques are discussed in the next subsection.

### 2.3 Types of control strategies

For efficient operation of the power converter, the control technique of it is an important factor. Therefore, extensive research is going on the efficient control strategy of the power converters and new strategies are developed in every year. Some of these control strategies are described below.

### 2.3.1 Hysteresis Control

In hysteresis control, a hysteresis error limit is utilized for determining the switching states by comparing the measured variable to the reference [53-54] as shown in Fig. 2.2. The switching state is changed when the controlled current achieves the limit.

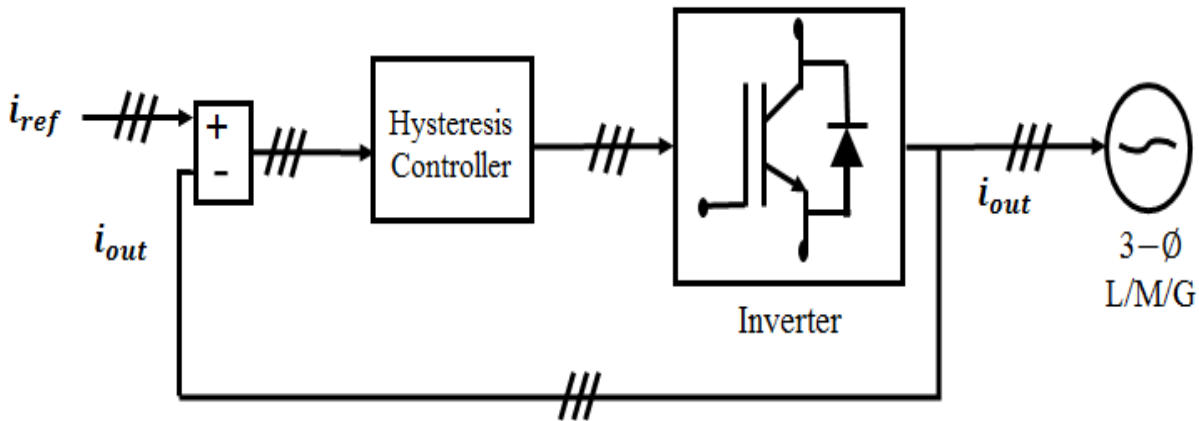


Figure 2.2: Block diagram of three-phase hysteresis current controller.

The application of the strategy is simple like the current control, however, can likewise be connected to higher multifaceted nature applications like direct torque control (DTC) [55] and coordinate power control (DPC) [56]. Hysteresis control is settled [57] and started with simple devices. If the control is implemented in digitally, it requires a high inspecting recurrence to consistently keep the controlled factors inside the hysteresis band.

### 2.3.2 Linear Control

The linear controllers of the power converter always consist of a modulating stage. By producing the control signals for the control switches, this modulating device actually linearizes the non-linear converter control strategy. The linear control techniques are actually developed for solving the drawbacks of the previously described hysteresis controller. Proportional-integral (PI) controller is the most widely recognized linear controller. In this methodology, a reference sinusoidal signal is compared with a triangular carrier signal to produce a PWM signal for the switching device. For instance, when the prompt value of the carrier is not as much as that of the reference signals, the switch state is changed with the goal that the output signal increments, and vice-versa [49]. Apart from this modulation method, some other techniques are available in the literature such as space vector modulation (SVM) and selective harmonic elimination (SHE) [58-63]. Using the SVM/PWM, a linear controller has been presented in Fig. 2.3, for the current control of the system, where the reference load currents are compared with the measured ones and the error found between those is processed by the traditional PI modulators.

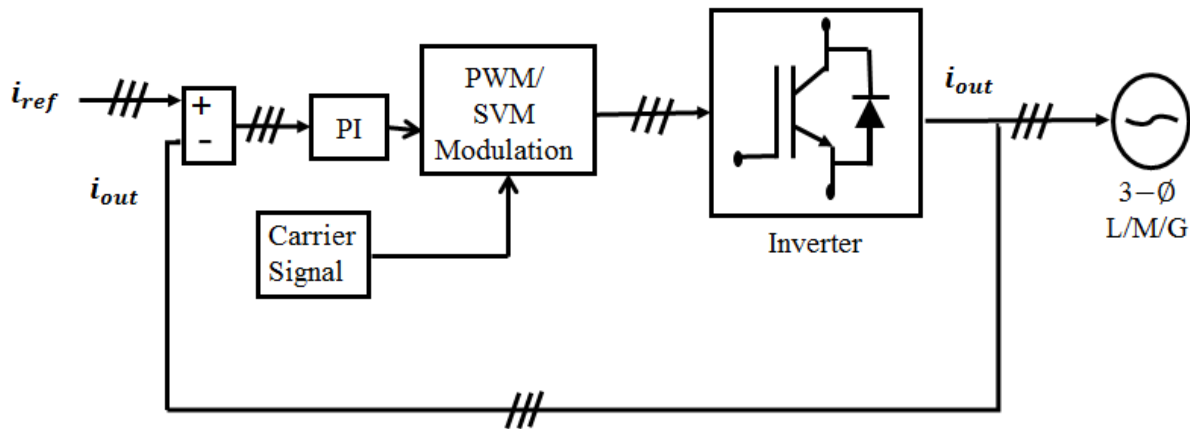


Figure 2.3: PI controller based linear current controller using PWM/SVM.

The SVM is perceived as an effective strategy as it offers lower total harmonic distortion (THD) and improved dc-link voltage usage in contrast with the PWM [64]. With the SVM, the nearest vectors to the reference voltage vector are chosen dependent on dwell time figuring and switching structure [65-66]. On the other hand, the SVM includes several steps of designing the model and the model is a little bit complex, which prompts a higher computational burden in contrast with the PWM. The SHE is mostly dependent on the calculation of switching angles to such an extent that particular lower order harmonics can be eliminated [67-69] and reduce the drawbacks of the previous SVM controller [70]. The switching frequency of the linear controllers utilizing these PWM/SHE/SVM modulating techniques is fixed and the value of error is minimal if the Park's transformation or dq co-ordinate system is utilized in contrast to the  $\alpha\beta$  transformations co-ordinates. The PI parameters are intended for one working condition, and if the converter works at different working conditions, the performance of the control crumbles and the stability of the system is being questioned [71]. Since this linear controller is applied to the power converter which is nonlinear in nature, the execution acquired is unsymmetrical and it fluctuates by the working condition. The presumption of the linear model gives good execution just if a high bandwidth modulation is utilized. This situation prompts a high switching frequency operation which subsequently causes higher switching losses.

In the area of industrial drive and energy producing system, these linear controllers are extensively utilized. For controlling the flux and torque of the widely used induction motor in a decoupled manner, field oriented control (FOC) is utilized [72]. This control methodology consists of transforming the reference frame, utilization of PI controllers, filtering of output variable and the modulation stage as the previous control has. Similar to this, for controlling the on-grid inverter, voltage oriented control (VOC) is utilized [72]. This control strategy provides the decoupled feature of grid reactive power and dc-bus voltage.

### 2.3.3 Sliding Mode Control Technique

The sliding mode control is a propelled power converter control strategy and has a place with the group of variable structure control and versatile adaptive control [73-74]. This control method is nonlinear in nature and well connected to linear or nonlinear frameworks. A sliding mode control strategy alongside the PWM/SVM appears in Fig. 2.4. The sliding controller is utilized to produce the load voltage references. As the name infers, the control variable is compelled to track or slide along the predefined direction [74]. With this technique, the structure of the controller is purposefully changed to accomplish a powerful and stable operation in case of the variation of the parameters and load aggravations [75]. This control strategy gives a strong response contrasts with the established controllers talked about before.

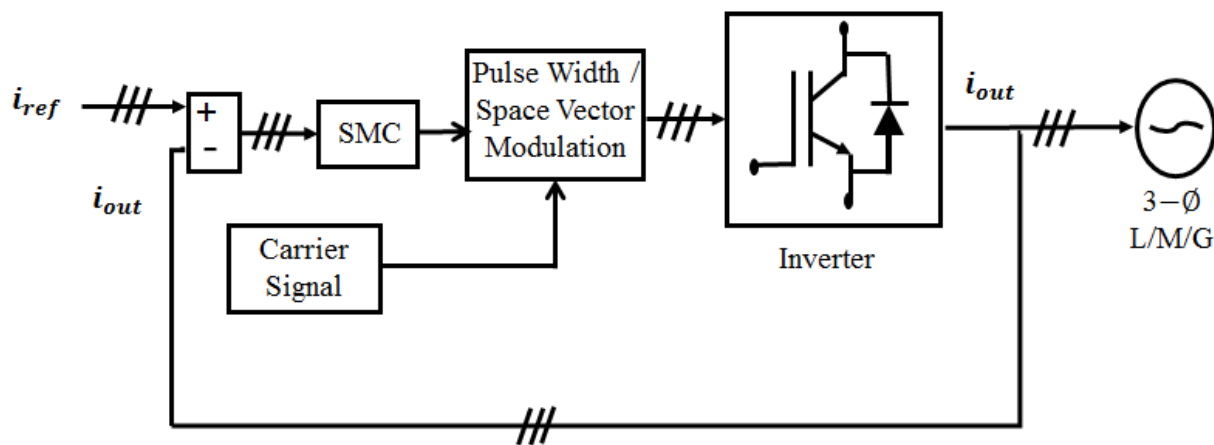


Figure 2.4: A sliding mode control strategy alongside the PWM/SVM.

### 2.3.4 Intelligent Control Techniques

The artificial neural network (ANN), genetic algorithms, and fuzzy logic controller (FLC) have found a place with the group of intelligent control methods [76-78]. An FLC method is showed in Fig. 2.5, where the PI controller is supplanted by the FLC. The FLC input is the error of the reference load current and the derivate of it. This controller inserts the experience, learning, and instinct of the converter administrator/planner as membership functions. Since the power converters are non-linear in nature, the strength of the system amid parameter varieties can be enhanced by utilizing the FLC without realizing the appropriate converter model. It is additionally a class of nonlinear control methods, and decidedly the best among the versatile controllers [76, 77]. The ANN speaks to the most nonexclusive type of the human reasoning procedure contrasted with the other insightful controllers [76]. The ANN-based load current direction appears in Fig. 2.6 [77]. The load current tracking error are given as inputs to the ANN through a reasonable gain or scaling factor ( $K$ ), and the ANN controller produces changing signs to the power converter. With this methodology, a consistent switching frequency can be achieved. The upsides of FLC and ANN can be consolidated as appeared in Fig. 2.7 to

accomplish better control execution [78]. Despite the fact that the intelligent controllers need not bother with a converter model, they require exact information about the converter operation.

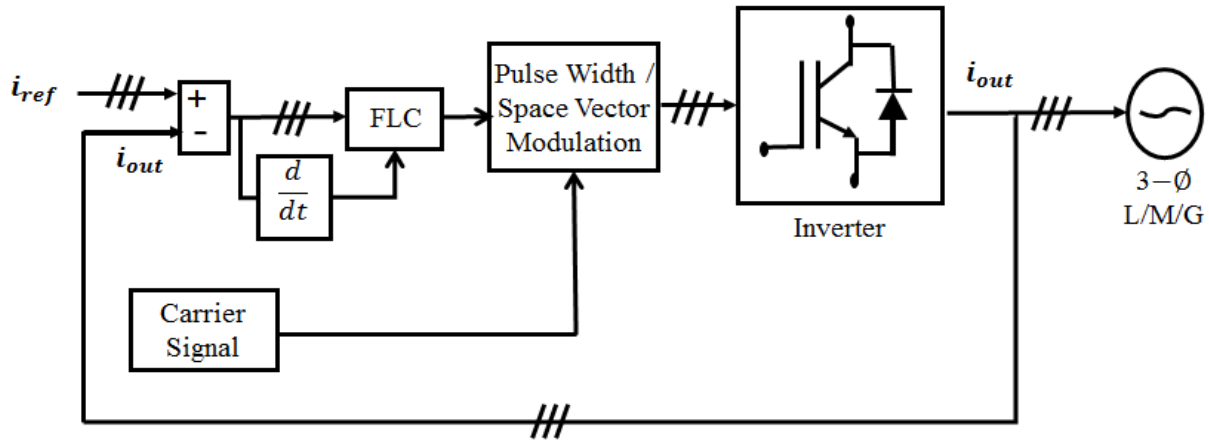


Figure 2.5: A FLC strategy utilizing the pulse width/ space vector modulation.

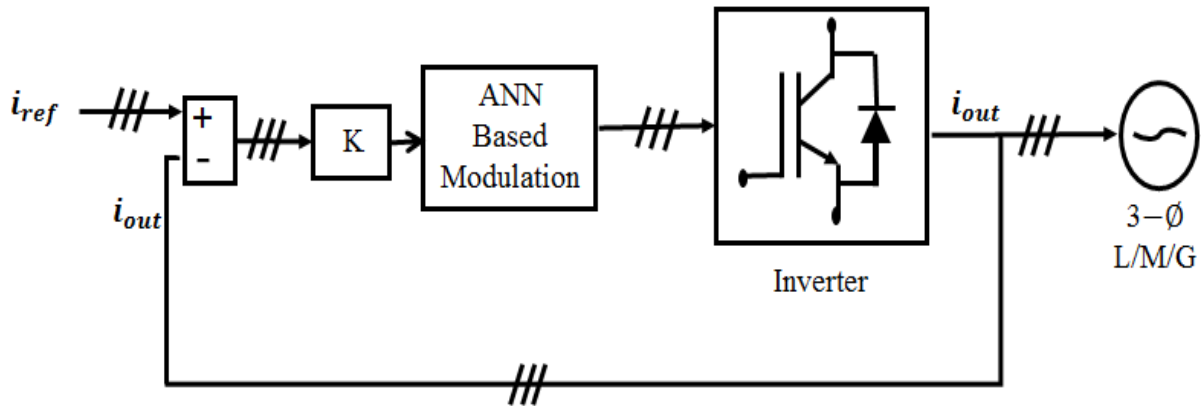


Figure 2.6: An ANN based load current controller for a three-phase on-grid inverter.

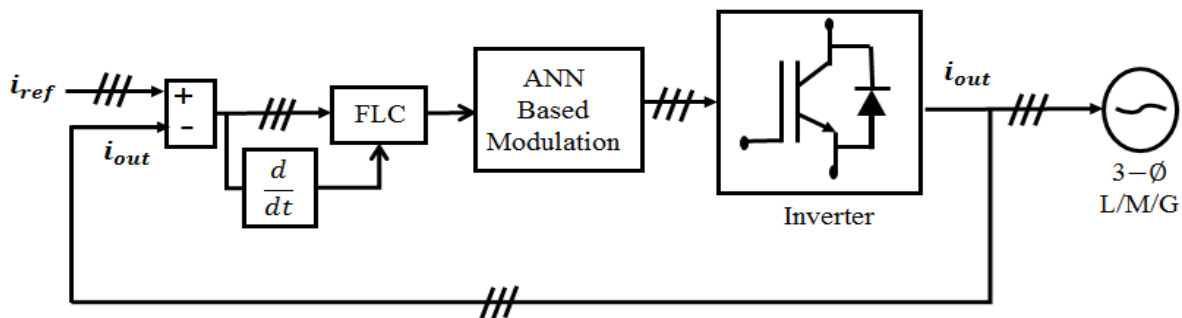


Figure 2.7: A Neuro-fuzzy controller for a three-phase on-grid inverter.



### 2.3.5 Predictive control

Predictive controller as shown in Fig. 2.8 provides flexibility of using any kind of algorithm that utilizes a model of the system to foresee its future behavior and chooses the most suitable control activity dependent on the cost function of the optimization [79]. However, the predictive control requires a high number of calculations than the classical controller. Thanks to the high speed microprocessors, that can handle this high number of calculations in a specified time frame [48].

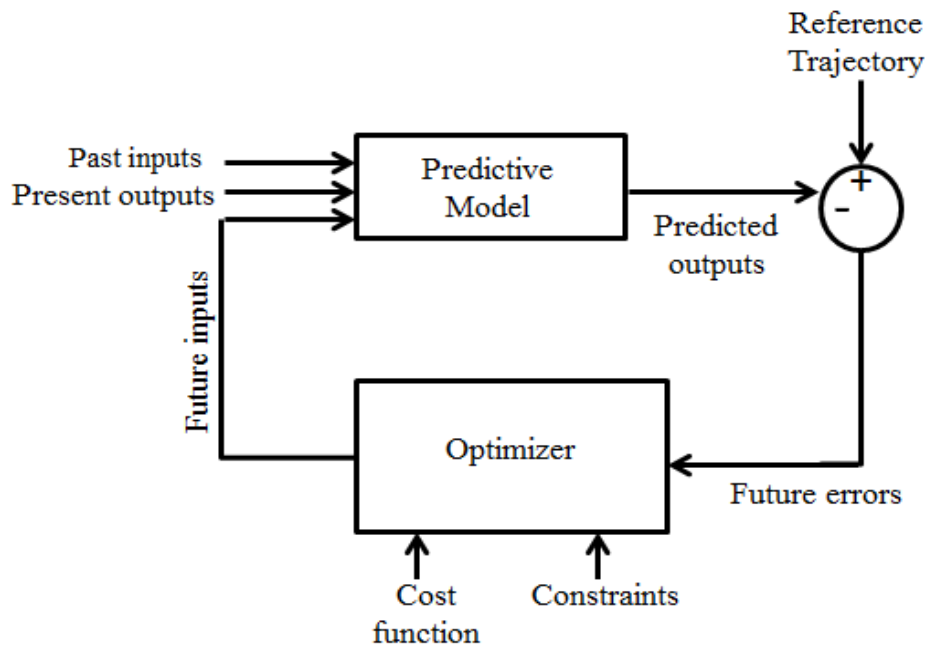


Figure 2.8: Fundamental concept of predictive control [80].

An alternate methodology is taken for the predictive controller in [81-83], where the system model is considered so as to anticipate the future behavior of the factors over a time period; the time allotment is an integer multiple of sample time. These expectations are assessed, in light of a cost function, and the sequence that provides a minimized cost function is then picked; along these lines the future control activities are determined.

After discussing the above control methods, it is seen that every controller has its own pros and cons. One controller may be simple but may not be accurate, again the other is accurate controllers but have some complexities. The advantages and disadvantages of the described methods are presented in Table 2.1.

Table 2.1: Advantages and disadvantages of numerous control strategies of on-grid inverter control

Control Strategies	Advantages	Disadvantages
Hysteresis control	<ul style="list-style-type: none"> <li>▪ Easily implementable</li> <li>▪ No need of highly sophisticated technology</li> <li>▪ No need of modulator</li> </ul>	<ul style="list-style-type: none"> <li>▪ Less effective for low power applications because of the switching losses</li> <li>▪ Switching frequency is variable as it depends on the width of the hysteresis, load parameters, non-linearity and operating conditions</li> <li>▪ Requires expensive filters to remove spectral components of it</li> </ul>
Linear control	<ul style="list-style-type: none"> <li>▪ Less costly</li> <li>▪ Simple and easily implementable</li> <li>▪ Less complex</li> </ul>	<ul style="list-style-type: none"> <li>▪ Higher switching losses</li> <li>▪ Contains lower order harmonics</li> <li>▪ Poor power quality</li> <li>▪ Less stable</li> <li>▪ Higher steady-state error</li> </ul>
Sliding Mode Control	<ul style="list-style-type: none"> <li>▪ Provides robust response</li> <li>▪ Remains stable during load disturbance and parameters variation</li> </ul>	<ul style="list-style-type: none"> <li>▪ Hard to implement</li> <li>▪ Produces high frequency oscillations</li> <li>▪ Cannot cope up with unmatched uncertainties</li> <li>▪ Performance depends on the sliding surface selection</li> </ul>
Intelligent controller	<ul style="list-style-type: none"> <li>▪ Provides better performance compared to the linear controller</li> <li>▪ Simplified controller with intelligent approach</li> <li>▪ Provides real-time operation</li> </ul>	<ul style="list-style-type: none"> <li>▪ Precise knowledge about the behavior of the converter is required</li> <li>▪ Sufficient training data is required</li> <li>▪ Solution results are hard to interpreted</li> </ul>
Predictive Control	<ul style="list-style-type: none"> <li>▪ Provides faster dynamics response</li> <li>▪ Simpler in design</li> <li>▪ Higher tracking accuracy</li> <li>▪ Inclusion of non-linearity and constraint is possible</li> <li>▪ Less sensitive to the system model</li> </ul>	<ul style="list-style-type: none"> <li>▪ Computational complexity</li> <li>▪ Switching frequency is variable</li> </ul>

From Table 2.1, it can be readily said that the predictive controller provides better performance than the other controllers and this predictive controller is the main focus of this research work.

## 2.4 Model Predictive Control

MPC is an optimization method in which a cost function is minimized for a pre-defined time horizon, subject to the system constraints and model [7]. The outcome is a succession of optimizing the cost function. Among each sampling instant, when the optimization is settled, again the controller will apply just the primary component of the succession utilizing the new estimated information and getting another sequence of optimal actuation each time. The prediction model utilized in this method is a discrete-time model, which can be expressed as a state-space model as pursues below [7, 51].

$$\begin{aligned}x(k+1) &= Ax(k) + Bu(k) & k \in \{0, 1, 2, \dots\} \\y(k) &= Cx(k) + Du(k) & k \in \{0, 1, 2, \dots\}\end{aligned}$$

where,  $x(k)$  and  $u(k)$  represent the state and control input at time,  $k$  and the future predicted value is indicated by  $x(k+1)$ . For representing the required behavior of the system, a cost function is designed. The future states, actuations, and the reference are accounted by the following cost function,  $g$ .

$$g = f(x(k), u(k), \dots, u(k+N)) \quad k \in \{0, 1, 2, \dots\}$$

For a predefined time horizon  $N$ , the defined cost function  $g$ , is minimized and the result can be presented as a sequence of optimized  $N$  actuations.

$$u(k) = [1 \ 0 \ 0 \ \dots \ \dots \ \dots \ 0] \arg \min g$$

Although  $u(k)$  contains achievable plants contributions over the whole time horizon only the main component is utilized in regular MPC. At each executing time, with a newer measured value, the optimization is further done to determine another sequence of optimized actuation. The basic operation of MPC is represented graphically in Fig. 2.9. As it is appeared by utilizing the deliberate data and model of the system until time  $k$ , the future estimation of the system state is anticipated until the time  $(k+N)$  in the horizon. At that point, the optimized value is determined by optimizing the cost function [84].

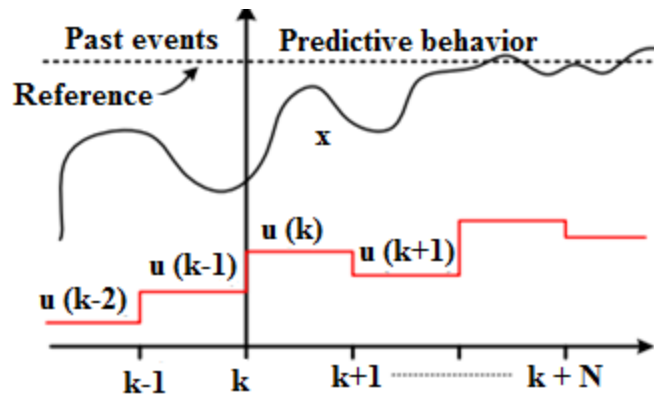


Figure 2.9: Basic operating principle of model predictive control.

The non-linear model is allowed in MPC and it can deal with general system constraints, which are required to secure component against over-voltages or over-currents. MPC provides several excellent features than the existing linear and non-linear controllers. The features that separate it from others are,

- i. Easily understandable and simple concept
- ii. Inclusion of multiple variables problem is possible and easier
- iii. Easy Inclusion of non-linearities in the model
- iv. Compensation for dead time is easier than others
- v. Provides easier and simpler accommodation of constraints
- vi. Easy implementation
- vii. Inherent discrete nature of the power converters are utilized
- viii. Many technical and control requirements can be fulfilled at the same time
- ix. Treats the power converter as a discontinuous and non-linear model which is the closest approximation to the real-time scenario
- x. Modification of the control schemes based on the specific applications can be easily done
- xi. Provides good dynamic response
- xii. Superior tracking accuracy
- xiii. Less sensitive to the system

Apart from these superior features, MPC also faces some challenges as below [51].

- i. For selecting and estimating the proper switching state, the computational burden is higher than the other existing controllers. This complexity of the computation may be solved or mitigated by using intelligent optimization techniques.
- ii. Dependency of the controller on the system architecture may decrease the quality and performance of the controller, as the controller is generally designed depending on the quality of the system model [57].

- iii. Difficult to tune the parameters in the presence of constraints, sometimes much concentration should be invested on the simulation to ensure the closed loop stability.
- iv. High speed processor is needed to speed up the solution time. This limitation can somehow be mitigated as high speed micro-processors are available nowadays.

MPC can be partitioned into two subsets: continuous and finite control set MPC. These two strategies are described below.

#### **2.4.1 Continuous control-set (CCS) MPC**

In CCS-MPC, a PWM based modulator is utilized to transmit the output from the controller. The modulator provides the switching signal to the converter. Hence, the achievable reference set exchanged to the modulator must be determined and a cost function is used to choose the most appropriate reference set.

#### **2.4.2 Finite-control-set (FCS) MPC**

FCS-MPC does not require a modulator to obtain the switching signals for the converter. When demonstrating a power electronic converter, the switches can be demonstrated as a perfect switch with just two states: “on” and “off”. Since power converters have a finite number of switching states, the optimization of MPC can be improved and simplified to the expectation of the behavior of the system for those allowed switching states. Every expectation is then used to assess a cost function, and in this way, the state with the least cost is chosen and produced. This control technique is known as FCS-MPC approach since the conceivable control activities (switching states) are finite. It has been effectively applied to a lot of power converters and drive applications as a current controller for two-level inverters [85-86], three-level inverters [87-88] and four-level inverters [89].

### **2.5 Existing Research on MPC**

The basic idea of MPC firstly came to light during the 1960s and pulled in enthusiasm from industry during the 1970s [90]. From then, MPC has been utilized in the synthetic and process enterprises. The time constants were adequately long for computations to be finished. During the 1980s, MPC was presented in the power industry in control applications with low switching frequency [91]. The control calculation required long estimation times; in this manner applications with high switching frequencies were unrealistic at the time. The rapid technological advancement in the field of microprocessors brings light to solve the computational problem of MPC. As a result, MPC received more responses from the industry and became popular [92]. MPC is a strategy that is utilized for handling the dynamics of non-linear components of the system as well as various system constraints. MPC presents a sensational development in the hypothesis of recent automation technology [93]. Presently, it is being considered in different regions, for example, power electronics and drives [51, 94-95]. The explanation behind the

developing enthusiasm for the utilization of MPC in this field is the presence of good numerical models to foresee the behavior of the system variables. It is now widely utilized for on-grid applications as the replacement to the traditional PWM technique. Traditional PWM controller generates a significant amount of harmonic component, and a filter is utilized to remove the effect of the harmonic component [96]. An LCL-filter is the most well-known for this application as it offers preferable features of reducing harmonic component over the conventional series inductors and provides a switching frequency reduction for medium-voltage (MV) while maintaining the standard limit of harmonic content [97]. However, the capacitance of LCL-filter causes a deferral between the grid and converter making it hard to perform control on grid-side quantities [98]. A control technique for the grid-connected converter (three-phase) with a reduced order LCL filter model is presented in [99]. In this model, the state-space expression is designed by approximating the L-filter and taking an extra term of disturbance to express the LCL-filter resonance. The state feedback and distortion rejection are calculated offline and the MPC is executed online through the proposed model. The main goal of the model is to track the reference active and reactive component smoothly and also reduce the resonance of the LCL filter. Utilizing space-vector PWM and LCL filter, an unconstrained MPC technique is proposed in [96]. The proposed method is utilized to control the grid-current of a single-phase grid-connected converter. To reduce the 3rd, 5th and 7th fundamental components of the grid-voltage harmonics, multiple numbers of resonant controllers are utilized. Again for a three-level neutral point clamped converter, a finite control set-MPC is proposed in [100]. In the controller, the reactive and active power that is injected into the grid is controlled. Furthermore, the FCS-MPC technique is also utilized in motor drives. FCS-MPC based model predictive direct torque control (MPDTC) is presented in [101]. An extension of the research work is also applied to the induction machine (IM) [101-103], where the stator currents of IM is modified by model predictive direct current control. Recently MPC is widely used for the on-grid PV inverter. For critically controlling the dc voltage of an on-grid PV inverter, a predictive control strategy is proposed in [104] based on the relationship of energy balance during the control period. For ameliorating the on-grid PV current, an exact transient analytic model is proposed in [105]. For a PV on-grid inverter, a model predictive direct power control technique is designed in [106], which can efficiently track the insolation change and the output power with better steady-state and dynamic response. Based on the mathematical model of three phase on-grid inverter, a predictive current control technique in static  $\alpha\beta$  frame is presented in [107]. It is shown that the controller can easily tracks the change of maximum power point of PV and penetrates active power to the grid with low distortion. To improve the stability of the power system, an MPC based low voltage ride through method is proposed in [108] for the on-grid PV inverter, where a detail analyses of the power imbalance problem during the symmetrical grid voltage drop is presented.

After reviewing the literatures, further literature review is done to know the recent works on this MPC based controller. The published research works somewhere in the range of 2007 and 2018 in IEEE Xplore has been investigated by playing out an inquiry utilizing the catchphrases “model

predictive control” and “power converter”. This hunt produced in excess of 1600 papers on MPC applied to the traditional PWM control converters in published journals and conference proceedings. The applications secured by these exploration works can be ordered into three primary categories: model predictive control of grid-connected PV, model predictive control with output LC filter and model predictive control of the motor drive as, shown in Fig. 2.10.

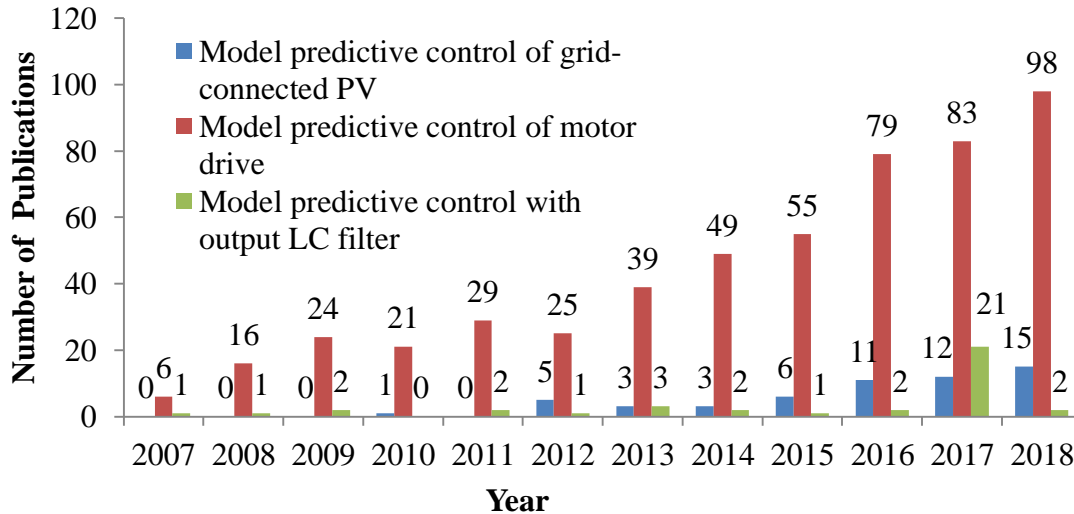


Figure 2.10: Statistical data after literature review on different perspectives of MPC.

Figure 2.10 demonstrates how the research works are circulated among the aforementioned three categories. It can be seen that a lot of research works have been published in the field of motor drive and LC filter or LCL filters utilizing MPC. However, utilizing this technique to the on-grid PV system is not quite common. Load flow, power loss and fault current analyses are not done yet to prove MPC as an efficient controller. Therefore, an MPC based energy efficient control for the on-grid PV inverter is selected as the topic of this research work and expected to solve the ongoing problems for the recently growing PV system.

## 2.6 Conclusion

The state-of-the-art control strategies for the converter are reviewed in this chapter. The implementation of various control methods for the output current control is introduced alongside their pros and cons. The literature review is done on the evolution, challenges, and development of power converters. Predictive control techniques along with their advantages, disadvantages and working procedure are also presented. The point of this study is to explore the reasonableness of such a system to guarantee the nature of the injected grid current, while also minimizing power losses related to switching frequency and harmonics. The analysis displayed in this part supports the FCS-MPC technique as an efficient tool to accomplish high-performance operation for the on-grid inverters.

## Chapter III

### System Modeling

#### 3.1 Introduction

The power industry is continually looking toward the development and redesigned advancements. Researchers are continually endeavoring to discover a perfect solution of various issues which takes the power industry in a new era. For a similar reason, this research work has been done to expel the scourge of harmonics from the power system especially from the power converter. In this chapter, the block diagram of the proposed model predictive control (MPC), the ways how these research work are done, the mathematical model, load flow, power loss and fault current analysis of the proposed controller in order to verify the performance of it are presented one by one. It is anticipated that the power industry could easily construct the proposed model and find a sustainable solution to reduce the drawbacks of existing controllers.

#### 3.2 Proposed System Model

A finite-set model predictive current control based two level three phase on-grid PV inverter is proposed in this research work. The proposed controller simultaneously controls the inverter side current by means of reference tracking. The controller generates optimal switching state for the IGBT based inverter according to a predefined cost function. The cost function is designed in order to reduce the tracking error and the number of switching commutation. The proposed model is designed and analysed in MATLAB/SIMULINK environment. The system parameters are initialized properly and the simulation work of the controller has been performed. The block diagram of the proposed system is presented in Fig. 3.1.



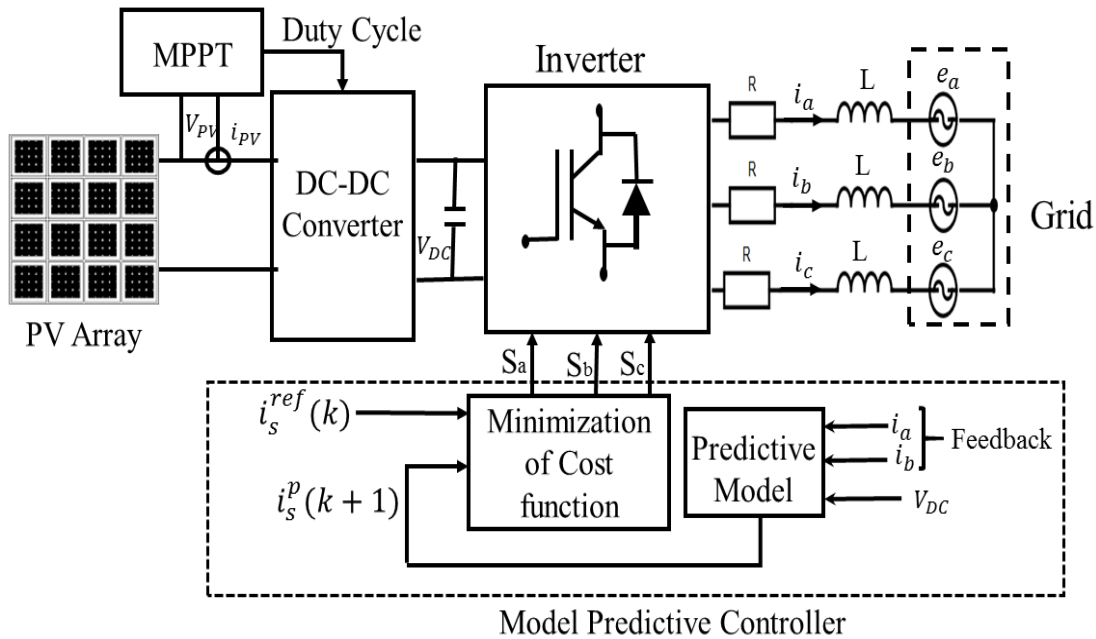


Figure 3.1: Block diagram of the proposed MPC based on-grid PV inverter.

### 3.3. Methodology

Every single piece of work needs to follow some steps for completing the total work. In this research work, the following steps are followed in order to design and simulate the proposed system.

**Step 1:** Designing a mono-crystalline based PV system along with the data of daily irradiance and mean temperature of a specified location which will provide the desired dc voltage level for the dc/dc boost converter.

**Step 2:** Designing a dc/dc Boost converter along with an MPPT controller to stabilize the output of PV system which will be used as the input of the inverter, as the output of PV varies with the value of insolation and temperatures.

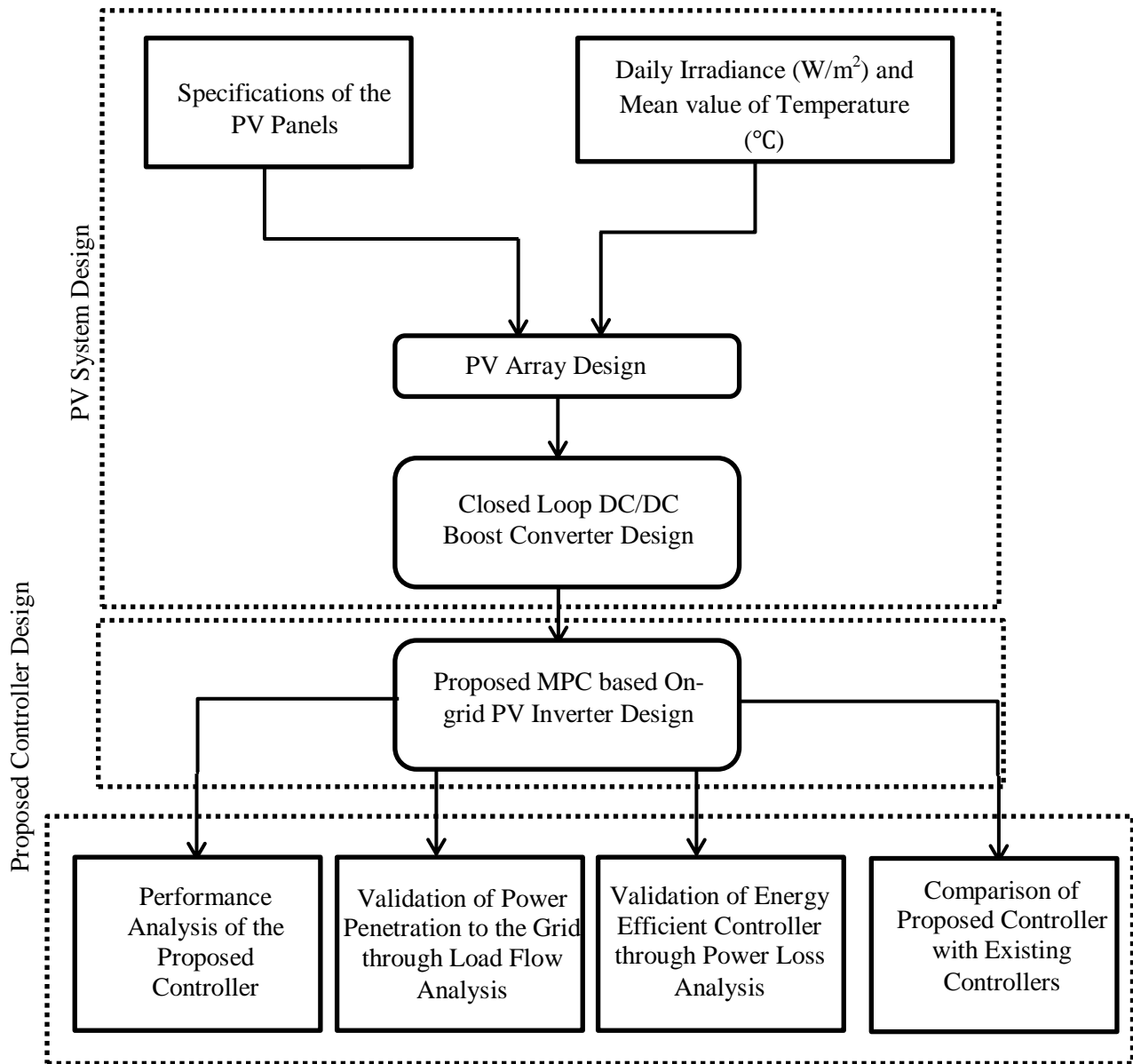
**Step 3:** Designing the proposed MPC based controller which is utilized for selecting the proper switching signals for the inverter.

**Step 4:** Establishing the connection of the proposed controller based inverter to the grid through in-line filters and running the system for determining the performance of it.

**Step 5:** Testing the performance of the proposed MPC based on-grid PV system through steady-state and transient analysis, tracking accuracy, and harmonic analysis and also comparing it with the existing controllers.

**Step 6:** Ensuring the penetration of PV power from the proposed system to the grid by utilizing IEEE test feeder through load flow analysis and also validating the controller as an efficient one through power loss and fault current stability analyses.

The aforementioned six steps of this research work are also shown by a flow chart in Fig. 3.2.



Testing the effectiveness of the proposed MPC based on-grid PV Inverter

Figure 3.2: Methodology of the overall research work.

### 3.4 PV System Modeling

Solar PV system, as a renewable energy source, is utilized in this work as the input of the proposed MPC based dc/ac inverter. The input PV system modeling includes the modeling of PV array and technical data required for the PV array. The PV system modeling is described below.

#### 3.4.1 PV Array Modeling

A PV array comprised of several combinations of PV modules, where every module is comprised of various solar cells [109]. Figure 3.3 displays the equivalent circuit of a perfect PV cell [110]. This ideal structure is sufficiently precise to comprehend the PV attributes and the reliance of PV cell on varying climatic conditions [111].

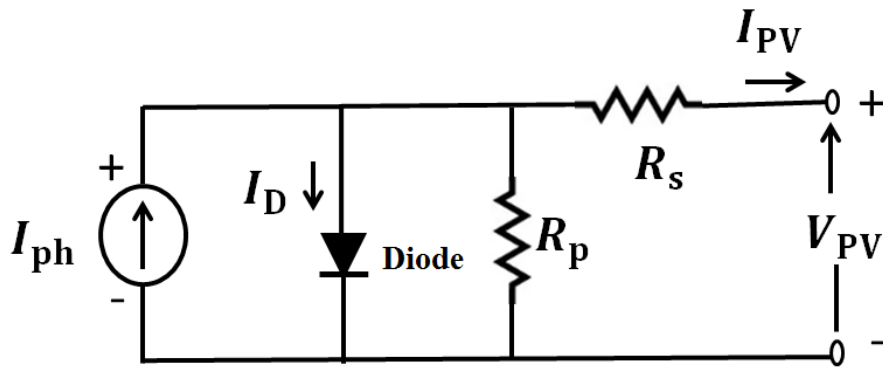


Figure 3.3: Equivalent circuit of a perfect PV cell.

In a PV system, the solar energy is converted to electrical energy by using one or more PV modules. Mainly, the system consists of panels and various mechanical electrical connectors in order to produce the desired output. The panels are connected in series-parallel connection to provide the desired amount of voltage and current. The aggregate output current of the parallel and series connected PV modules is expressed in Eqn. 3.1 [112]

$$I_{PV} = N_p \left( I_{ph} - I_o \left[ \exp \left( \frac{q(V_{PV} + R_s I_{PV})}{N_s A K T} \right) - 1 \right] - \frac{V_{PV} + R_s I_{PV}}{N_s R_p} \right) \quad (3.1)$$

where,  $I_{PV}$  is the output current and  $V_{PV}$  is the output voltage,  $R_s$  is the series and  $R_p$  is the parallel resistances,  $N_p$  and  $N_s$  are the number of PV cells in a PV module which are connected in parallel and in series, respectively,  $A$  is the ideality factor of p-n junction,  $K$  is the Boltzmann's constant,  $T$  is the temperature in Kelvin,  $q$  is the charge of electron [112], and  $I_{ph}$  is the produced photocurrent. The photocurrent depends fundamentally on the radiation and cell's temperature, which is expressed as,

$$I_{ph} = [I_{SCC-STC} + K_i(T - T_{STC})] \frac{G}{G_{STC}} \quad (3.2)$$

where,  $I_{SC-STC}$  refers to the short-circuit current (SCC) at standard test conditions (STC) in ampere,  $T_{STC}$  ( $25^{\circ}\text{C}$ ) is the cell temperature at STC,  $G$  (in watts per square meters,  $\text{W}/\text{m}^2$ ) is the irradiation on the cell surface,  $G_{STC}$  ( $1000\text{W}/\text{m}^2$ ) is the irradiation at STC and  $K_i$  is the SCC coefficient, as a rule, gave by the cell producer. In addition, the saturation current,  $I_o$  is impacted by the temperature as indicated by the accompanying equation [113-114].

$$I_o = \frac{I_{SC-STC} + K_i(T - T_{STC})}{\exp[V_{OCV-STC} + K_V(T - T_{STC})/AV_{th}]} \quad (3.3)$$

where,  $V_{OCV-STC}$  (in volt, V) is the open circuit voltage (OCV) at STC,  $K_V$  is the open circuit voltage coefficient,  $V_{th}$  refers to the thermal voltage of the cell, these values are available on the data sheet provided by module's manufacturer. With  $V_{PV}$  and the simplified  $I_{PV}$ , the power produced by the PV module is represented as [112],

$$P_{PV} = V_{PV} \times N_p (I_{ph} - I_o \exp\left(\frac{qV_{PV}}{N_s AKT}\right) - \frac{V_{PV}}{N_s}) \quad (3.4)$$

The  $I-V$  and  $P-V$  characteristics curve of the solar cell are shown in Fig. 3.4 [115]. The curves indicate that the operating point of the PV does not remain at a stable point; it actually varies from zero to open-circuit voltage. There is only one point which enables maximum power for a given set of solar insolation and temperature level. That particular point is indicated as MPP and at that point, the current and voltage are shown as  $I_{MPP}$  and  $V_{MPP}$ . The electronic device that is used to locate the MPP of the curve in order to make the best use of the solar array is termed as MPPT.

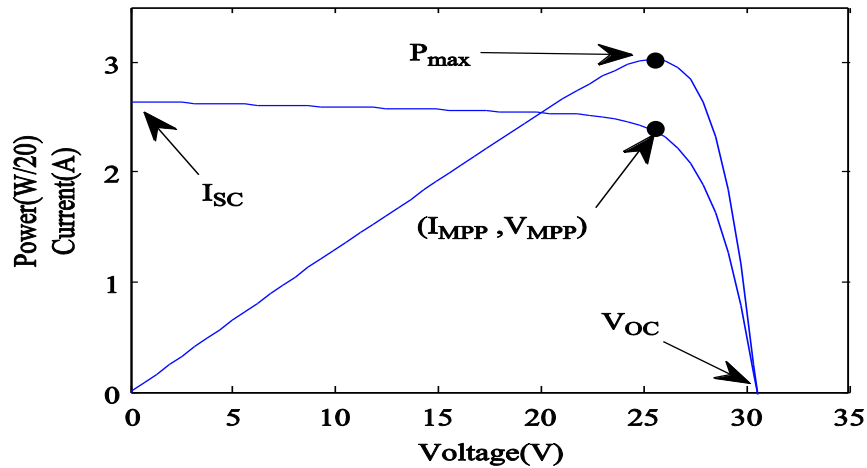


Figure 3.4:  $I-V$  and  $P-V$  characteristics curve of the solar cell [115].

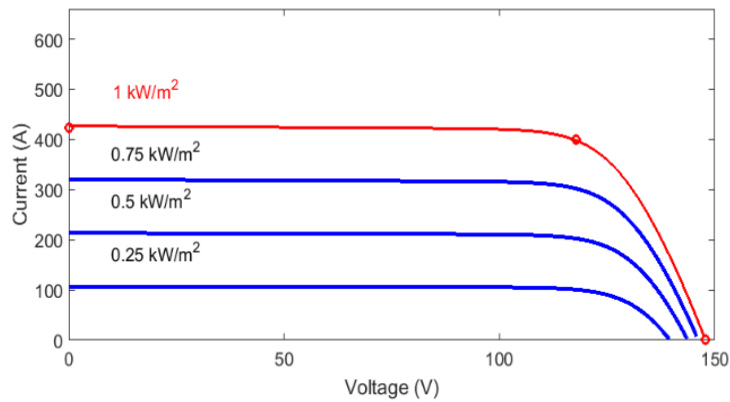
The  $I-V$  curve of a  $P-V$  cell firmly relies upon the solar radiation and temperature [116-117]. The output of PV will vary with the changing climatic conditions. Since the irradiance of the solar cell relies upon the incidence angle of the sunbeams, this parameter straightforwardly influences the output adjusting the  $P-V$  and the  $I-V$  characteristics [112]. The output current  $I_{PV}$  of a PV

module is broadly impacted by the variety of sun oriented irradiance,  $G$ , though the output voltage  $V_{PV}$  remains practically constant. On the other hand, for a changing temperature, it is found that the voltage shifts generally while the current remains practically unaltered [6]. The temperature of the PV cell increases because of three reasons: (i) its own heat amid photovoltaic activity, (ii) the energy emanated at the infrared wavelength which has a warming impact on the cell and (iii) an increase in sunlight based insolation [118].

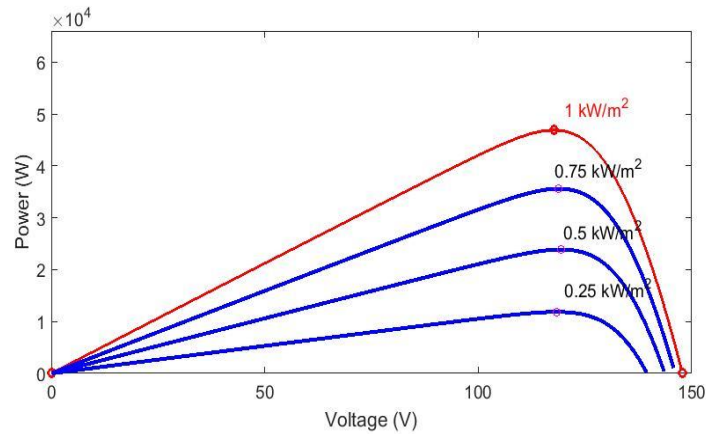
In this research work, Samsung SDI LPC235SM-02 module is selected as the PV panel which is of mono-crystalline type. The specification of the selected panel is demonstrated in Table 3.1 [119]. The  $I$ - $V$  and  $P$ - $V$  curves at different irradiance conditions are shown in Fig. 3.5 (a) and 3.5 (b), respectively.

Table 3.1: Table for the specifications of the PV array [119]

<b>Electrical Characteristics</b>	
<b>Parameters</b>	<b>Values</b>
Power at Standard Test Condition (STC)	235 W
Power at PVUSA Test Condition (PTC)	207.8 W
Voltage at maximum power	29.97 V
Current at maximum power	7.84 A
Open circuit voltage	37.24 V
Short circuit current	8.43 A
Nominal Operating Cell Temperature	48.8°C
Open circuit voltage Temp Co-efficient	-0.348 %/°C
Short circuit current Temp Co-efficient	0.053 %/°C
Maximum Power Temp Co-efficient	-0.46 %/°C
Number of modules	168
Number of modules in Series	8
Number of modules in Parallel	21
<b>Mechanical Characteristics</b>	
Length	1630.0 mm
Width	982.0 mm
Module area	1.6 m <sup>2</sup>
PV area	14 m <sup>2</sup>



(a)



(b)

Figure 3.5: (a)  $I$ - $V$  and (b)  $P$ - $V$  curves for the selected PV array at different irradiance conditions.

### 3.4.2 Technical Data for System Design

The first and the essential thing of the design is the geological area of the establishment, site review and radiation investigation. It decides if a solitary PV system is reasonable or not. The site review included the field visits to the sites in Khulna close to the campus of Khulna University of Engineering & Technology. The geographic area of the chosen site is at  $22^{\circ}55.6825'$  latitude and  $89^{\circ}30.996'$  longitude, a sun-rich district with a sunlight based irradiance of around  $600 \text{ W-h/m}^2$  every day [120]. The average surrounding temperature of around  $25.66^{\circ}\text{C}$ , though most extreme and least encompassing temperatures are  $28.25^{\circ}\text{C}$  and  $20.01^{\circ}\text{C}$ , respectively [120]. The variation of irradiance throughout the day during summer and winter in the selected site is shown in Fig. 3.6.

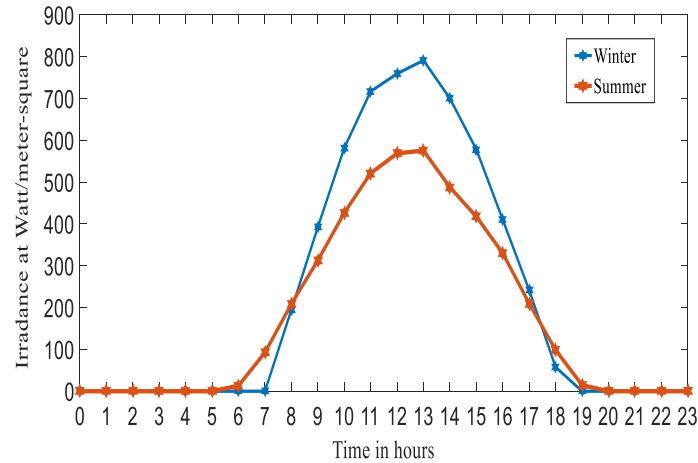


Figure 3.6: Variation of irradiance during summer and winter days at Khulna.

HOMER Pro (Hybrid optimization of Multiple Electric Renewables) software and NASA Surface meteorology and Solar Energy database are utilized to obtain the technical data for the PV system design. Monthly average daily temperature, clearness index and irradiation on the horizontal plane of the PV array for the chosen area are presented in Table 3.2.

Table 3.2: Average daily solar radiation, clearness index and temperature

Month	Monthly average daily radiation (kWh/m <sup>2</sup> /day)	Clearness Index	Daily Temperature (°C)
January	4.290	0.609	20.44
February	4.880	0.602	23.79
March	5.580	0.593	27.05
April	5.830	0.557	27.64
May	5.530	0.503	28.02
June	4.200	0.377	28.25
July	3.890	0.353	27.87
August	3.900	0.367	27.74
September	3.830	0.393	27.26
October	4.290	0.506	25.82
November	4.230	0.582	23.05
December	4.210	0.629	21.01

Here, the clearness index indicates the clearness of the atmosphere. It is the ratio of surface radiation and extraterrestrial radiation and a unit less parameter, ranging from 0 to 1. During sunny and clear weather, it has a higher value (like 0.75 in the month of June at Phoenix) and has a lower value (like 0.25 in the month of December at London) under cloudy weather condition.

### 3.5 Closed loop dc/dc Boost Converter Modeling

A dc/dc converter plays an important role in PV system application. PV array output parameters vary with the changes in irradiance and temperature. PV current is directly proportional to the irradiance (light) and PV voltage is inversely proportional to temperature. The major function of a dc/dc converter is to convert the unregulated dc voltage into regulated dc voltage. Without dc/dc converter, designing an inverter control will be complicated and the PV system will not be practical. The dc voltage input to the inverter will not be constant and will vary with the switching of the inverter. It will be difficult to control the power flow. The mathematical expression regarding the modeling of the closed loop dc/dc converter is described below.

Boost converter (BC) is used to ensure the required fixed voltage of equal to or greater than  $\sqrt{2}V_{sys}$ , given by Eqn. (3.5), for all irradiance and temperature conditions. The output voltage of BC is calculated by Eqn. (3.6) with duty cycle  $D$ , obtained by the output of an MPPT using Perturb and Observe (P & O) method [121]. Capacitor  $C_o$  for BC is sized according to the acceptable output voltage ripple using Eqn. (3.7) and BC is operated in continuous current mode (CCM) by  $L > L_{min}$  using Eqn. (3.8) [121].

$$V_{DC} \geq \sqrt{2}V_{sys} \quad (3.5)$$

$$V_o = \frac{1}{1-D}V_i \quad (3.6)$$

$$C_o = \frac{I_o}{\Delta v_o}DT \quad (3.7)$$

$$L \geq L_{min} = \frac{T}{2I_{LB}}D(1-D)V_o \quad (3.8)$$

The performance of the dc/dc converter is improved by incorporating closed loop control for providing the constant dc voltage to the inverter. The block diagram of the dc/dc boost converter is shown in Fig. 3.7.

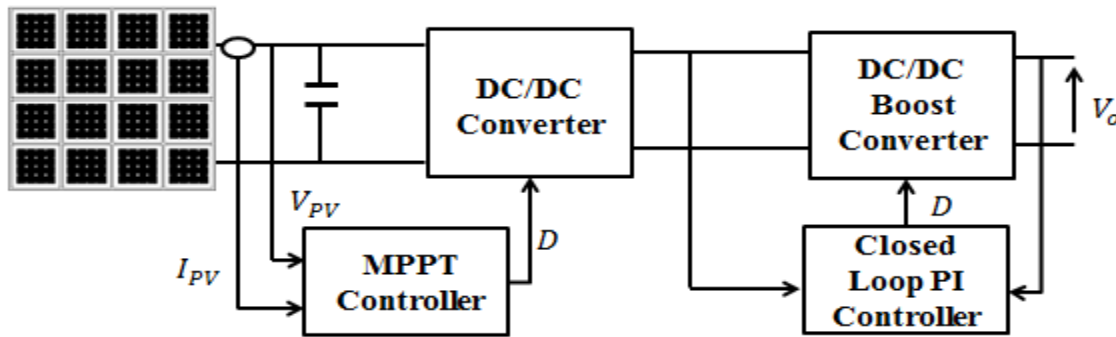


Figure 3.7: Block diagram of the dc/dc boost converter.



In this work, an 850V closed loop dc/dc boost converter is designed to provide a constant dc voltage to the inverter. The output voltage waveform generated by the closed loop dc/dc boost converter is shown Fig. 3.8.

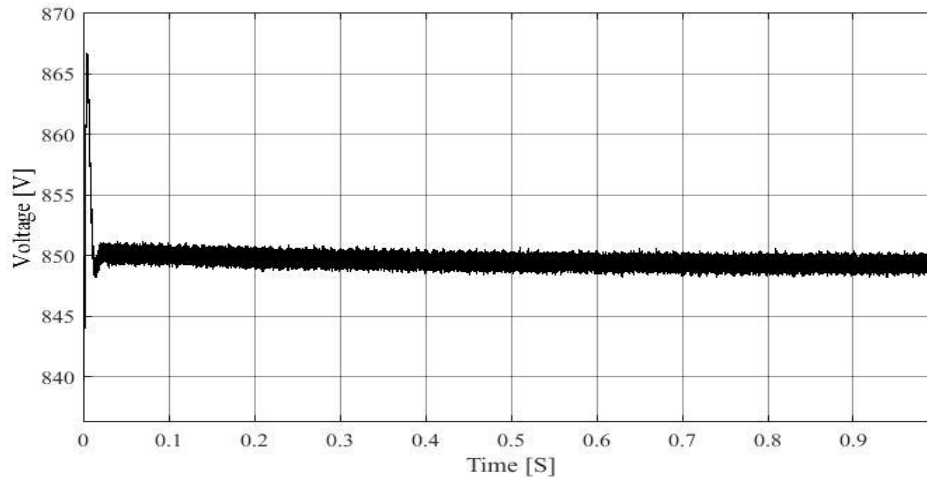


Figure 3.8: Output voltage waveform generated by the closed loop dc/dc converter.

### 3.6 Proposed MPC Based On-grid Inverter Modeling

For designing an MPC based on-grid inverter, several parameters and criteria have been initialized. The steps involving the design of the proposed MPC based on-grid inverter are presented in the following sub-section.

#### 3.6.1 Three-Phase Two-Level VSI Model

The two-level VSI has been chosen since it is a standout amongst the most utilized converter topologies in the industrial sectors. The structure and working principle of the inverter can be effectively stretched out to other converter topologies. The power circuit diagram for the three-phase two level converters for converting the input dc from the PV system to ac form is presented in Fig. 3.9.

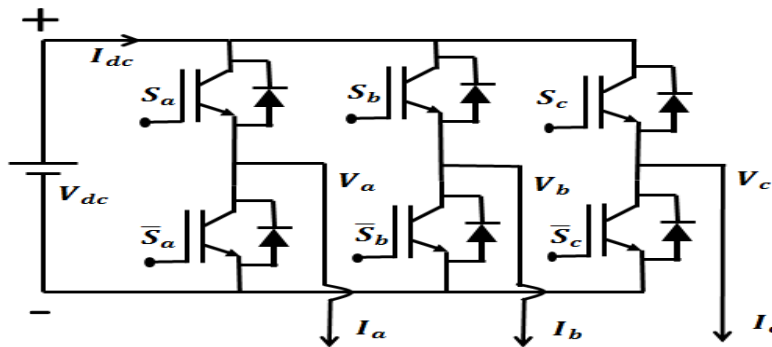


Figure 3.9: Two level voltage source inverter (VSI) power circuit [80].

Insulated Gate Bipolar Transistor (IGBT) switches are used in the inverter. By switching properly, the load terminal can be connected either to the positive (P) or the negative (N) bus bar of the converter. Taking into account that the two switches in every inverter phase work in complementary mode so as to keep away from short-circuiting the dc source. The switching condition of the power switches  $S_x$ , with  $x = 1, \dots, 6$ , by the switching states  $S_a, S_b$ , and  $S_c$  can be expressed as below [51].

$$S_a = \begin{cases} 1 & \text{if } S_1 \text{ on and } S_4 \text{ off} \\ 0 & \text{if } S_1 \text{ off and } S_4 \text{ on} \end{cases} \quad (3.9)$$

$$S_b = \begin{cases} 1 & \text{if } S_2 \text{ on and } S_5 \text{ off} \\ 0 & \text{if } S_2 \text{ off and } S_5 \text{ on} \end{cases} \quad (3.10)$$

$$S_c = \begin{cases} 1 & \text{if } S_3 \text{ on and } S_6 \text{ off} \\ 0 & \text{if } S_3 \text{ off and } S_6 \text{ on} \end{cases} \quad (3.11)$$

Now, the vector form of  $S$  can be expressed as [51]

$$S = \frac{2}{3}(S_a + aS_b + a^2S_c) \quad (3.12)$$

These switching signals define the value of the output voltages

$$V_{aN} = S_a V_{dc} \quad (3.13)$$

$$V_{bN} = S_b V_{dc} \quad (3.14)$$

$$V_{cN} = S_c V_{dc} \quad (3.15)$$

where,  $V_{dc}$  is the dc source voltage. Considering the unitary vector  $a, = e^{j2\pi/3} = -\frac{1}{2} + j\frac{\sqrt{3}}{2}$ , which represents the  $120^\circ$  phase displacement between the phases, the output voltage vector can be defined as [46]

$$v = \frac{2}{3}(V_{aN} + aV_{bN} + a^2V_{cN}) \quad (3.16)$$

where,  $V_{aN}, V_{bN}$  and  $V_{cN}$  are the phase-to-neutral ( $N$ ) voltages of the inverter. Now, the number of switching states has to be determined. The total number of switching states will be the resultant of the different switching state combination minus the impossible state. Here, the switching state that may be the reason of short-circuit is defined as the impossible states. In general, the switching states number,  $N_s$  can be obtained as

$$N_s = S^{NP} \quad (3.17)$$

where, the possible numbers of states are presented by  $S$  of each leg and  $NP$  presents the number of phases. For instance, a four phase, three level converter has  $3^4 = 81$  switching states. If all the possible combinations are considered for the following switching state for two level three

phase converter, eight possible voltage vectors are available as presented in Table 3.3. From the table, it is seen that  $v_0 = v_7$  which results in seven different voltage vectors in the complex plane and the states will generate different configurations of the three-phase load connected to the dc source. The voltage vectors can be represented in a two-dimensional  $\alpha\beta$  plane as shown in Fig. 3.10. The detail description of the transformation of  $abc$  to  $\alpha\beta$  plane is presented in the next sub-section.

Table 3.3: Voltage vectors of the 2L-VSI.

$v_n$	$S = [S_a S_b S_c]$	$v = v_\alpha + jv_\beta$
$V_0$	0 0 0	0
$V_1$	1 0 0	$2/3 V_{dc}$
$V_2$	1 1 0	$1/3 V_{dc} + j\sqrt{3}/3 V_{dc}$
$V_3$	0 1 0	$-1/3 V_{dc} + j\sqrt{3}/3 V_{dc}$
$V_4$	0 1 1	$-2/3 V_{dc}$
$V_5$	0 0 1	$-1/3 V_{dc} - j\sqrt{3}/3 V_{dc}$
$V_6$	1 0 1	$1/3 V_{dc} - j\sqrt{3}/3 V_{dc}$
$V_7$	1 1 1	0

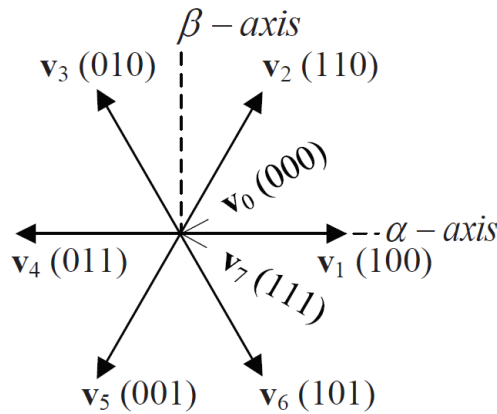


Figure 3.10: Space distribution of all admissible voltage vectors of the 2L-VSI [80].

Considering modulation methods, as PWM, the inverter can be approximated as a continuous system. However, in this work the inverter will be considered as a non-linear discrete system with just seven unique states as conceivable outputs.

### 3.6.2 Transformation of $abc$ to $\alpha\beta$ Co-ordinate

To make easy the control configuration procedure of a three-phase on-grid system, two fundamental transformations are utilized to decrease the elements of the numerical model of the system and the associated differential equations are decoupled [17]. These two transformation are the Clarke transformation or  $abc$  to  $\alpha\beta$  and Park transformation or  $abc$  to  $dq$  transformation. The difference between these two coordinate systems is that stationary resultant is produced in  $\alpha\beta$  transformation, while a rotating resultant with a fixed frequency is produced in  $dq$  transformation. Here, the details of  $\alpha\beta$  transformation are presented.

In  $\alpha\beta$  transformations, the dimension of the state-space representation of the three phase system is reduced. The expressions related to this transformation is [122]

$$\begin{bmatrix} x_\alpha \\ x_\beta \\ x_\gamma \end{bmatrix} = \sqrt{\frac{2}{3}} \begin{bmatrix} 1 & -\frac{1}{2} & -\frac{1}{2} \\ 0 & \frac{\sqrt{3}}{2} & -\frac{\sqrt{3}}{2} \\ \frac{1}{\sqrt{2}} & \frac{1}{\sqrt{2}} & \frac{1}{\sqrt{2}} \end{bmatrix} \begin{bmatrix} x_a \\ x_b \\ x_c \end{bmatrix} \quad (3.18)$$

where, the three-phase output current, voltage or power can be represented by the  $x_a$ ,  $x_b$  and  $x_c$ . In a three-phase symmetrical system, where  $x_a + x_b + x_c = 0$  and  $x_\gamma = 0$ , which shows only two vectors  $x_\alpha$  and  $x_\beta$  can represent the three-phase system. In another sense,  $\gamma$  axis is basically orthogonal to  $\alpha\beta$  plane and no projection exists due to  $\gamma$  axis on the  $\alpha\beta$  plane. Therefore, the transformations of  $\alpha\beta\gamma$  can be called as  $\alpha\beta$  transformations and can be expressed as [122]

$$\begin{bmatrix} x_\alpha \\ x_\beta \end{bmatrix} = \sqrt{\frac{2}{3}} \begin{bmatrix} 1 & -\frac{1}{2} & -\frac{1}{2} \\ 0 & \frac{\sqrt{3}}{2} & -\frac{\sqrt{3}}{2} \end{bmatrix} \begin{bmatrix} x_a \\ x_b \\ x_c \end{bmatrix} \quad (3.19)$$

Again, the inverse transformation of  $\alpha\beta$  transformations can be expressed as [17, 122]

$$\begin{bmatrix} x_a \\ x_b \\ x_c \end{bmatrix} = \sqrt{\frac{2}{3}} \begin{bmatrix} 1 & 0 \\ -\frac{1}{2} & \frac{\sqrt{3}}{2} \\ -\frac{1}{2} & -\frac{\sqrt{3}}{2} \end{bmatrix} \begin{bmatrix} x_\alpha \\ x_\beta \end{bmatrix} \quad (3.20)$$

Therefore, under symmetrical condition, this transformation can convert the three phase symmetrical system to two phase stationary system.

Since the measured current and the reference current both are the three-phase variables, these transformations are applied to both of these two variables in order to transform them. The graphical representation and the MATLAB implementation of the  $\alpha\beta$  transformation are shown in Fig. 3.11.

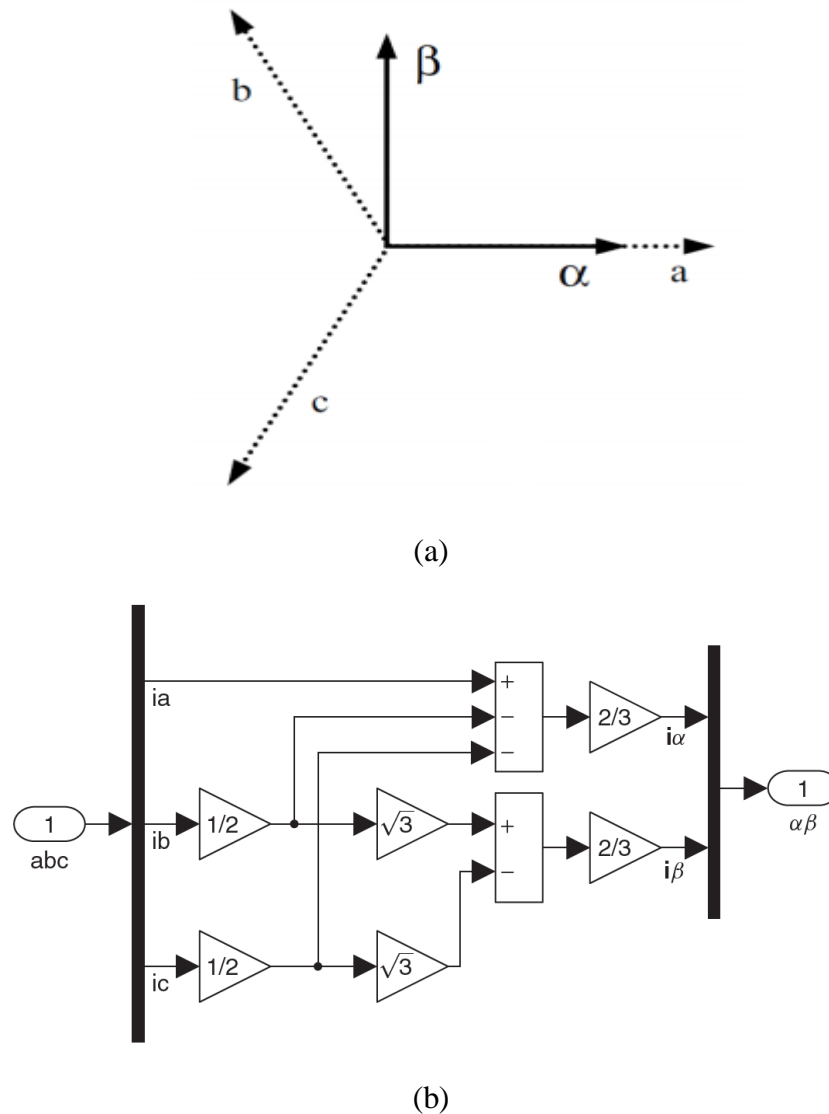


Figure 3.11: (a) Graphical representation and (b) MATLAB implementation of  $\alpha\beta$  transformation.

### 3.6.3 Three Phase Active Load Model

Taking into account the definitions of variables from the circuit shown in Fig. 3.9, the equations for load current dynamics for each phase can be written as [45, 86]

$$v_{aN} = L \frac{di_a}{dt} + Ri_a + e_a + v_{nN} \quad (3.21)$$

$$v_{bN} = L \frac{di_b}{dt} + Ri_b + e_b + v_{nN} \quad (3.22)$$

$$v_{cN} = L \frac{di_c}{dt} + Ri_c + e_c + v_{nN} \quad (3.23)$$

where,  $R$  is the load resistance and  $L$  the load inductance.

Considering the space vector definition for the inverter voltage, the load current and grid voltage space vectors can be expressed as [45]

$$i = \frac{2}{3}(i_a + ai_b + a^2i_c) \quad (3.24)$$

$$e_g = \frac{2}{3}(e_a + ae_b + a^2e_c) \quad (3.25)$$

and assuming the last term of (3.21-3.23) equal to zero

$$\frac{2}{3}(v_{nN} + av_{nN} + a^2v_{nN}) = \frac{2}{3}v_{nN}(1 + a + a^2) = 0 \quad (3.26)$$

then the load current dynamics can be described by the vector differential equation [45]

$$v = Ri + L \frac{di}{dt} + e_g \quad (3.27)$$

By substituting (3.24)-(3.25) into (3.27) a vector equation for the load current dynamics can be obtained as [45, 57]

$$v = L \frac{d}{dt} \left( \frac{2}{3}(i_a + ai_b + a^2i_c) \right) + R \left( \frac{2}{3}(i_a + ai_b + a^2i_c) \right) + \frac{2}{3}(e_a + ae_b + a^2e_c) \quad (3.28)$$

where,  $v$  is the voltage vector generated by the inverter,  $i$  is the load current vector, and  $e_g$  is the grid voltage vector. Note that for simulation and experimental results, the grid voltage is assumed to be sinusoidal with constant amplitude and constant frequency.

### 3.6.4 Discrete-Time Model for Prediction

The proposed model predictive control is actually an optimization algorithm. To actualize this procedure on digital platform of control, the continuous time model ought to be changed over to discrete time. In the control hypothesis, numerous discretization strategies are accessible, for example, forward difference, backward difference, bilinear transformations, impulse-invariant and zero-order hold. Because of the first order nature of the state equations that depicts in Eqn. (3.29), a first-order approximation for the derivative can be obtained by forward or backward Euler technique [86].

$$\frac{dx}{dt} = Ax + Bu \quad (3.29)$$

Now considering the present and future sample  $k$  and  $(k+1)$ , the forward Euler technique can be expressed as [86]

$$\frac{dx}{dt} = \frac{x(k+1)-x(k)}{T_s} \quad (3.30)$$

where,  $T_s$  presents the discrete sampling time. Now by replacing (3.30) into (3.29), the discrete-time model for the control variable can be expressed as [86]

$$\frac{x(k+1)-x(k)}{T_s} = Ax + Bu \quad (3.31)$$

$$x(k+1) = (1 + AT_s)x(k) + BT_s u(k) \quad (3.32)$$

Now, if considering the present and future samples  $k$  and  $k-1$ , the approximation for the derivative using backward Euler method can be expressed as

$$\frac{dx}{dt} = \frac{x(k)-x(k-1)}{T_s} \quad (3.33)$$

Similarly as Eqn. (3.31), the expression from Eqn. (3.33) can be replaced to Eqn. (3.29) and can be expressed as below

$$\frac{x(k)-x(k-1)}{T_s} = Ax + Bu \quad (3.34)$$

$$x(k) = \frac{1}{(1-AT_s)}x(k-1) + \frac{BT_s}{(1-AT_s)}u(k) \quad (3.35)$$

Between the described two Euler methods i.e. forward and backward Euler methods, the forward Euler method is simpler and easier to apply for the conversion of discrete time model. Therefore, in this research work, the forward Euler method is utilized for the discretization of load current.

Hence, the load current derivative  $di/dt$  is replaced by a forward Euler approximation can be expressed as [57, 86]

$$\frac{di}{dt} \approx \frac{i(k+1)-i(k)}{T_s} \quad (3.36)$$

Now placing the Eqn. (3.36) in Eqn. (3.27) to obtain the following expression that allows prediction of the future load current at time  $(k+1)$ , for each one of the seven values of voltage vector  $\mathbf{v}(k)$  generated by the inverter.

$$\mathbf{i}^p(k+1) = \left(1 - \frac{RT_s}{L}\right) \mathbf{i}(k) + \frac{T_s}{L} (\mathbf{v}(k) - \widehat{\mathbf{e}}_g(k)) \quad (3.37)$$

where,  $\widehat{\mathbf{e}}_g(k)$  denotes the grid voltage. The superscript  $\mathbf{p}$  denotes the predicted variables. The grid voltage can be calculated from (3.37) considering measurements of the load voltage and current with the following expression [51]

$$\widehat{e}_g(k-1) = \mathbf{v}(k-1) - \frac{L}{T_s} \mathbf{i}(k) - \left(R - \frac{L}{T_s}\right) \mathbf{i}(k-1) \quad (3.38)$$

where,  $\widehat{e}_g(k-1)$  is the estimated value of  $e_g(k-1)$ . The present grid voltage  $e_g(k)$ , needed in (3.38), can be estimated using an extrapolation of the past values of the estimated grid voltage. Alternatively, as the frequency of the grid voltage is much less than the sampling frequency, we will suppose that it does not change considerably in one sampling interval and, thus, assume  $\widehat{e}_g(k) = \widehat{e}_g(k-1)$ .

### 3.6.5 Cost Function Flexibility

For the design of an model predictive control, the most significant parameters is the design of the cost function, as it not only permits the proper selection of control objectives of the specific application but also provides the flexibility of adding any other constraints to it. This distinctive feature allows controlling various controlling parameters like voltage, current, active and reactive power by utilizing a single cost function. The various controlling parameters that can be added to the single cost functions are presented in Fig. 3.12.

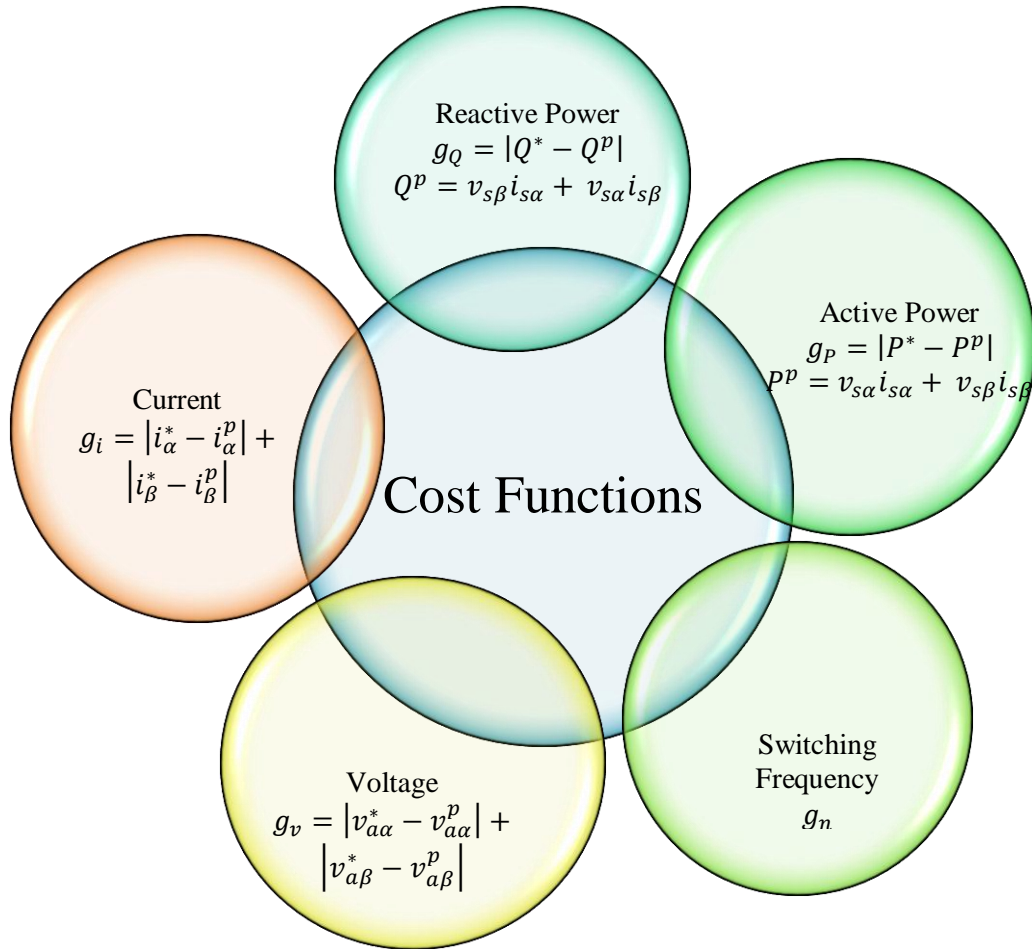


Figure 3.12: Control parameter flexibility of MPC.



From Fig. 3.12, it can be seen that because of the cost function flexibility of the proposed MPC controller, different control parameters with different units can be added to a single cost function. This addition of each term with different magnitudes and units is done by multiplying them with weighting factors. The weighting factors also set priority of one control variable over another control variable in the cost function. However, the choice of these weighting factors is not straight forward [80]. A few exact ways to deal with decide a fix weight factor utilizing experimentation have been researched in the literature [80]. However, a settled weight factor is not powerful to parameter variety and different vulnerabilities of the system. The generalized formulation of adding different control parameters with weight factor can be expressed as

$$g = [x_1^p(K+1) - x_1^*(K+1)] + \lambda_1[x_2^p(K+1) - x_2^*(K+1)] + \dots + \lambda_n[x_n^p(K+1) - x_n^*(K+1)] \quad (3.39)$$

where, the weight factor is presented by  $\lambda$  for each controlling parameters. All possible control actions are evaluated against the control objectives. Using cost function, the control action which yields minimum cost, is stored and applied to the inverter for the next cycle.

### 3.6.6 Cost function Design

The cost function for the proposed on-grid PV inverter has the following composition

$$g = f(i^*(k+1), i^p(k+1) + h(n_{sw})) \quad (3.40)$$

where,  $n_{sw}$  is the number of commutations of the power semiconductor devices, which is included in the cost function in order to evaluate the reduction of average switching frequency. The first term in Eqn. (3.40), i.e.,  $f(i^*, i^p)$ , is dedicated to achieve reference tracking, and it can be expressed as [51, 87]

$$f(i^*(k+1), i^p(k+1)) = |i_\alpha^*(k+1) - i_\alpha^p(k+1)| + |i_\beta^*(k+1) - i_\beta^p(k+1)| \quad (3.41)$$

where,  $i_\alpha$  and  $i_\beta$  are the real and imaginary components of current vector  $i$ , respectively, and  $i_\alpha^*$ ,  $i_\beta^*$  and  $i_\alpha^p$ ,  $i_\beta^p$  are the real and imaginary components of the reference and predictive current vector,  $i^*$ , and  $i^p$ , respectively.

The objective of the second term in (3.40), i.e.,  $h(n_{sw})$ , is to reduce the number of commutation. The term  $h(n_{sw})$  and  $n_{sw}$ , can be expressed as [87]

$$h(n_{sw}) = \lambda n_{sw} \quad (3.42)$$

$$n_{sw}(k+1) = \sum_{x=\{a,b,c\}} |S_{x1}(k+1)_i - S_{x1}(k)_i| + |S_{x2}(k+1)_i - S_{x2}(k)_i| \quad (3.43)$$

where, the possible switching state for the next sample instant  $(k+1)$  is represented by  $S_x(k+1)$ , the applied switching state to the inverter at time  $k$  is indicated by  $S_x(k)$  and  $i$  is the index voltage vectors  $\{v_0 \dots v_7\}$ . The average switching frequency  $f_{sw}$  per semiconductor switch is

calculated by the following Eqn. (3.44) using the total number of switching transitions  $n_{sw}(T)$  over the duration T [87].

$$f_{sw} = n_{sw}(T) / 12 / T \quad (3.44)$$

A switching state that implies fewer commutations of the power semiconductors will be preferred. In this manner, the use of  $h$  will have a direct effect in the switching frequency of the converter. The weighting factors  $\lambda$  handle the relation between terms dedicated to reference tracking, and reduction of switching frequency. A large value of certain  $\lambda$  implies greater priority of switching frequency than the reference tracking.

Therefore, in summary the cost function of the proposed predictive current controller is determined by placing the Eqns. of (3.41) and (3.42) to Eqn. (3.40) as

$$g = |i_{\alpha}^*(k+1) - i_{\alpha}^p(k+1)| + |i_{\beta}^*(k+1) - i_{\beta}^p(k+1)| + \lambda n_{sw} \quad (3.45)$$

### 3.6.7 Algorithm of the Proposed Controller

The algorithm developed for the proposed controller is presented in Fig. 3.13. The algorithm consists of five sections: (i) measurement, (ii) estimation, (iii) prediction, (iv) optimization, and application of the optimal voltage vector,  $V_{opt}$ . The flowchart of the algorithm shown in Fig. 3.13 consists of two loops: inner and outer loop. The inner loop is executed for each possible state of the seven voltage vectors, and the outer loop is executed every sampling time for determining the most optimized switching state. Therefore, the most optimized switching state is applied to the next sampling period. The overall strategy of the control is executed using the following steps.

Step 1: The load current  $i(k)$ , grid voltage  $\widehat{e}_g(k)$ , and dc link voltage  $V_{dc}$  are measured.

Step 2: For the immediate next sampling instant, the future load current  $i^p(k+1)$  and number of switching transitions  $n_{sw}(k+1)$  are predicted for all the possible switching states.

Step 3: The designed cost function  $g$  is estimated for each of the prediction.

Step 4: For the minimized cost function  $g_{opt}$ , the proper switching state is selected.

Step 5: The newly selected switching state  $S(j_{opt})$  is then applied to the next sampling instant.

The equations and the cost function used in the flow chart of Fig. 3.13 are detailed in previous sub-sections and the working strategy of the algorithm is presented in the next sub-section of this chapter.

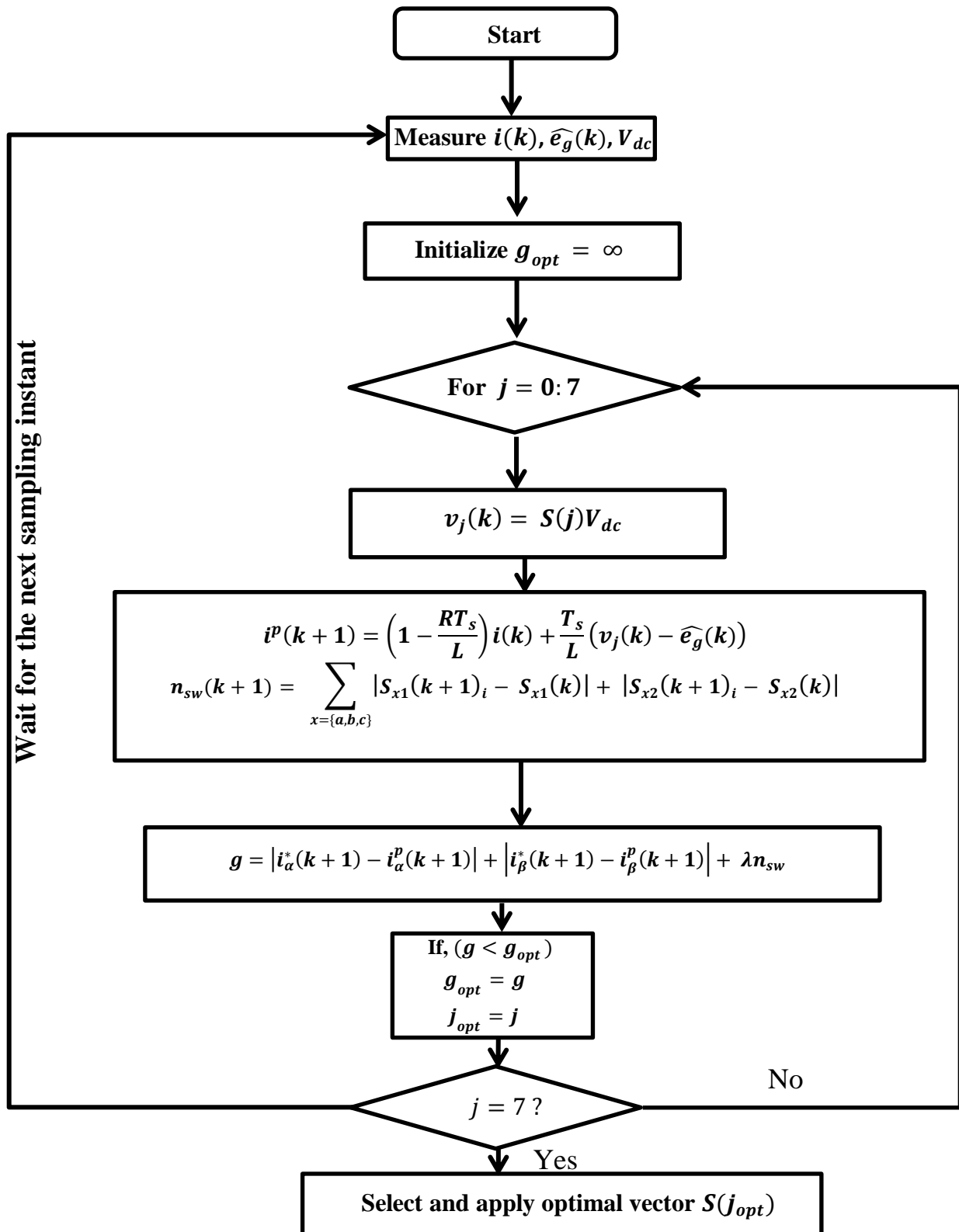


Figure 3.13: Flow chart of the proposed predictive controller.

### 3.6.8 Working Strategy of the Proposed Controller

For demonstrating the working strategy of the proposed controller, a pictorial representation is presented in Figs. 3.14 and 3.15. The three-phase load currents ( $i_\alpha, i_\beta$ ) and their references are presented in the figures after the transformation of  $abc$  frame to  $\alpha\beta$  plane. The future predictive load currents  $i(k+1)$  are evaluated by utilizing the measured current  $i(k)$  for all the available switching voltage vector  $v(k)$ , which is indicated as  $i_p(k+1)$  in the Fig. 3.14. It is seen that the vector  $V_2$  chooses the nearest predictive current vector to the reference. Again, from Fig. 3.15, for the load current ( $i_\alpha$ ), the minimal error is provided by vectors  $V_2$  and  $V_6$  and similarly for the load current ( $i_\beta$ ), the minimal error is provided by the vectors  $V_2$  and  $V_3$ . Therefore, the vectors  $V_2$  is selected as the optimal vector which provides the most optimized cost function. Hence, it can be said that the difference between the predictive and reference vector characterizes the cost function as presented in the figures. Although for current control, it is easier to visualize these errors, for complicated cost function, this representation is too difficult.

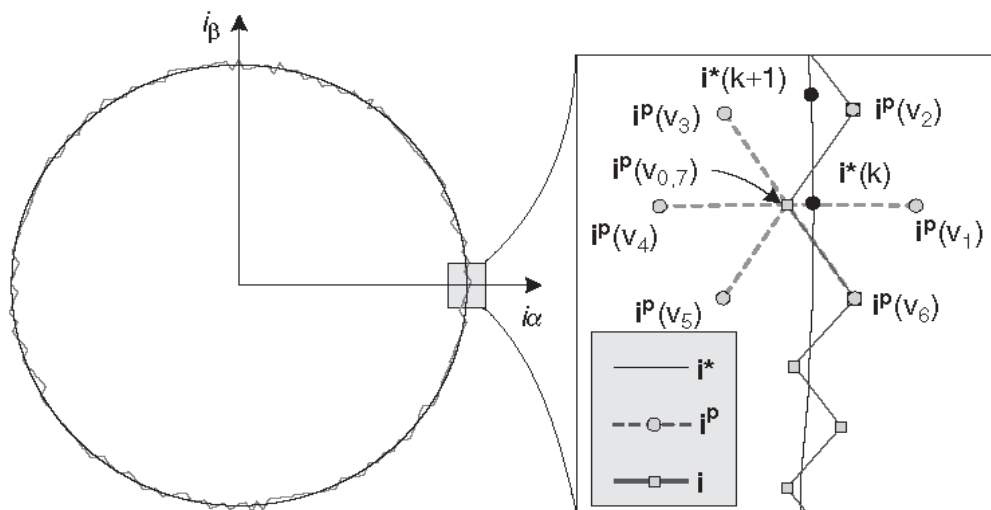


Figure 3.14: The representation of reference and predictive currents in vector plot [51].

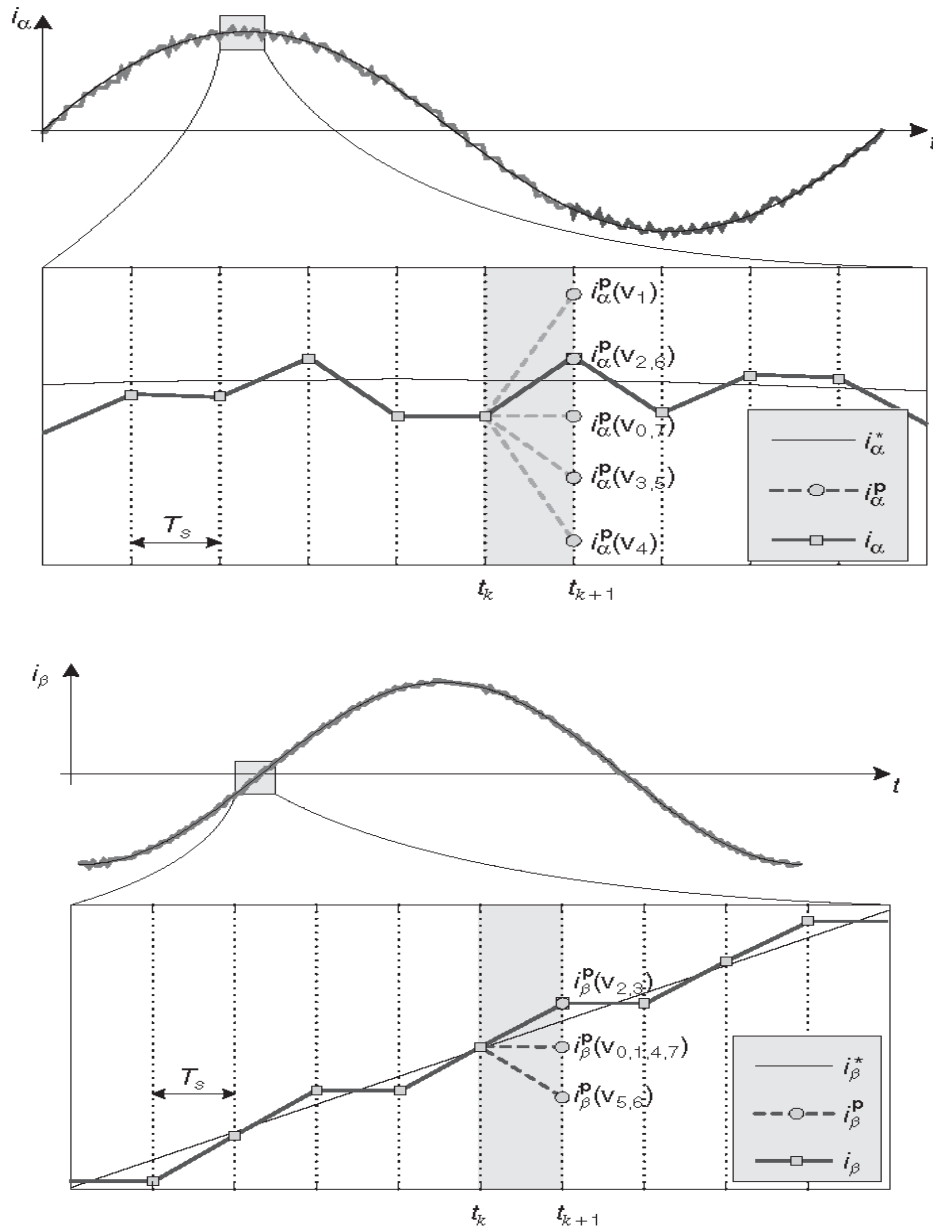


Figure 3.15: Graphical representation of selecting optimal voltage vectors of reference and predictive currents [51].

In a summary, the working strategy can be presented by some numerical values. As mentioned earlier, the defined cost function generates a value for each of the possible voltage vectors, presented in Table 3.4 and the respective voltage vector in  $\alpha\beta$  plane is shown in Fig. 3.16, taken as an example.

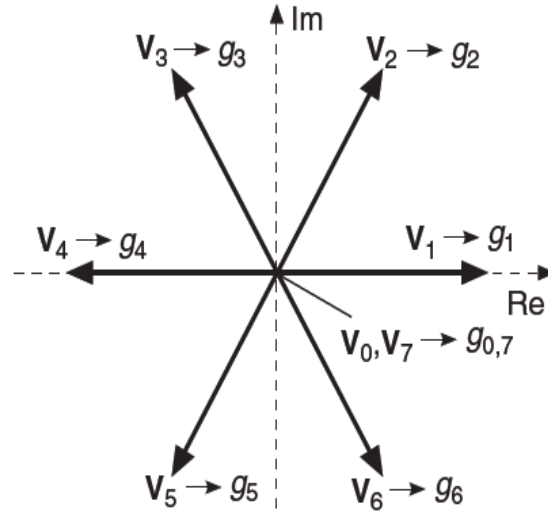


Figure 3.16: Space vector representation of all possible voltage vector of two-level VSI.

From Table 3.4, it can be seen that the different voltage vector provides different cost function values and the lowest value is generated by the voltage vector  $V_2$  as indicated in Table 3.4. Therefore, the selected vector is  $V_2$  and this vector is now applied to the inverter.

Table 3.4: Value of cost function for the eight individual voltage vectors [51]

Voltage Vector	Value of Cost Function
$V_0$	$g_0 = 0.60$
$V_1$	$g_1 = 0.82$
$V_2$	$g_2 = 0.24$
$V_3$	$g_3 = 0.42$
$V_4$	$g_4 = 0.96$
$V_5$	$g_5 = 1.24$
$V_6$	$g_6 = 1.19$
$V_7$	$g_7 = 0.60$

### 3.7 Existing Controllers Modeling for Comparison

The performance of the proposed predictive current controller is compared with the three existing controllers such as proportional integral pulse width modulation (PI-PWM), proportional resonant pulse width modulation (PR-PWM) and proportional resonant selective harmonic elimination pulse width modulation (PR-SHEPWM) for the same parameters as presented in the previous section. The description of the comparison is given one by one as below.

### 3.7.1 PI-PWM controller

The classical PI-PWM controller using PWM modulation technique is the most widely utilized linear controller because of its simplicity and easier implementation. This popular controller also suffers from some serious drawbacks, such as poor THD, poor dynamic response, having no decoupling capacity, more sensitive to the system model etc. To justify the drawbacks and compare it with the performance of proposed controller, the block diagram of a closed loop PI-PWM controller is shown in Fig. 3.17.

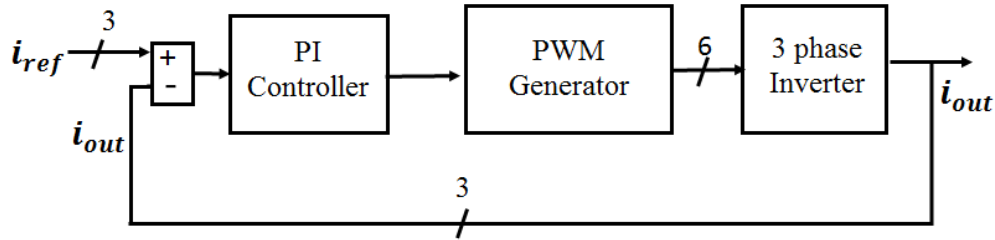


Figure 3.17: Block diagram of the closed loop PI-PWM controller.

### 3.7.2 PR-PWM Controller

The inability of tracking a sinusoidal reference without having a steady-state error of a conventional PI controller makes the controller ill-suited for a dynamically good response system [123]. The downside of this method causes the existence of the harmonic component in the injected current. Therefore, to transform the steady-state error to zero, the attention of the researcher is drawn to a new controller named PR controller, which is capable of producing zero steady-state error at the same fundamental frequency of the grid. This PR controller can be utilized in the closed loop system where the reference is sinusoidal in nature. Using modified state transformation, and frequency-domain approach or internal model control, the transfer function of both single phase and three phase PR controller can be implemented. From a conventional linear PI controller implemented in a positive and negative sequence, the transfer function can be extracted in the synchronous reference frame (SRF) [124].

$$G_{PR}(s) = G_{PI}^+ + G_{PI}^- = k_p + k_I \frac{s}{s+j\omega} + k_p + k_I \frac{s}{s-j\omega} = K_p + \frac{K_I s}{s^2 + \omega^2} \quad (3.46)$$

For selectively reducing the most notable lower order harmonic component, the ideal transfer function of the controller can be modified as [124]

$$G_{PR-h}(s) = \sum_{PR-h=5,7} K_{Ih} \frac{s}{s^2 + (\omega h)^2} \quad (3.47)$$

For a non-ideal case, Eqn. (3.46) can be written as [124]

$$G_{PR}(s) = K_p + K_I \frac{\omega_c s}{s^2 + 2\omega_c s + \omega^2} \quad (3.48)$$

Similarly, as Eqn. (3.47), the non-ideal transfer function for compensating the lower order harmonic component can be written as [125]

$$G_{PR-h}(s) = \sum_{PR-h=5,7} K_{Ih} \frac{w_c s}{s^2 + 2w_c s + (wh)^2} \quad (3.49)$$

where,  $h$  denotes the order of the harmonic and  $K_{Ih}$  represents the individual gain for which the overall controller can provide a larger gain at the resonant frequency. As a result, the steady-state error can be eliminated. The block diagram of this system with harmonic compensator for 5<sup>th</sup> and 7<sup>th</sup> harmonics is shown in Fig. 3.18.

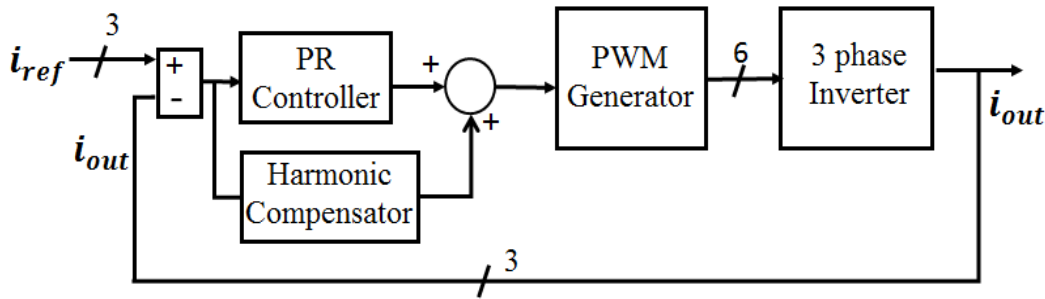


Figure 3.18: Block diagram of the PR-PWM controller with harmonic compensator.

A closed loop PR controller with harmonic compensator using Eqns. (3.48) and (3.49) for non-ideal case is simulated. The parameters of the PR controller are considered as  $K_p = 0.6$ ,  $K_I = 10$  and the cut off frequency  $w_c = 0.05$  rad/s for the fundamental component, while for the compensation of 5<sup>th</sup> and 7<sup>th</sup> harmonics  $K_I$  and  $w_c$  is taken as 200 and 0.05 rad/s, respectively. The frequency response for the compensation of 5<sup>th</sup> and 7<sup>th</sup> harmonics is shown in Fig. 3.19 using bode plot. It can be seen that the existence of the resonant unity (or 0 dB) peaks at the required selected frequencies of 250 and 350 Hz.

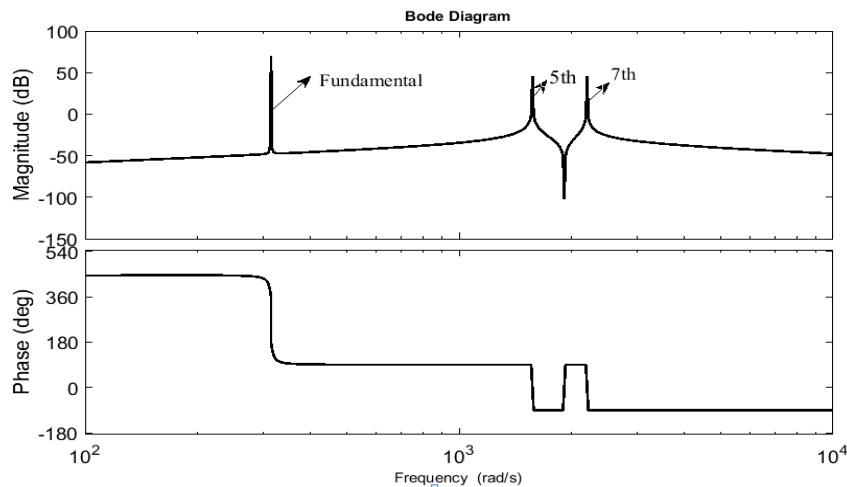


Figure 3.19: Bode plot of the PR controller along with harmonic compensator.



### 3.7.3 PR-SHEPWM Controller

To suppress these specific lower order harmonics, an optimal or programmed technique has been developed in 1964 [126], referred to as selective harmonic elimination (SHE). In this method, the width of each pulse of the inverter output voltage is pre-calculated to reduce the specific harmonics. By utilizing the same order dominant harmonics in the negative cycle, these specific lower order harmonics are suppressed by utilizing a proper switching angle. Therefore, the switching angle of this method is limited to zero and  $\frac{\pi}{2}$ , which can be presented as

$$0 < \alpha_1 < \alpha_2 < \alpha_3 \dots < \alpha_N < \frac{\pi}{2} \quad (3.50)$$

The magnitude of voltage containing the harmonic component can be presented as [126]

$$V_n = \frac{4V_{dc}}{n\pi} \sum_{k=1}^N (-1)^{k+1} \cos(n\alpha_k) \quad (3.51)$$

where, n is the order of the harmonics, N represents the number of switching angles in the quarter wave symmetry,  $V_{dc}$  is the dc link voltage and  $\alpha_k$  indicates the switching angle of  $k^{\text{th}}$  harmonic. The magnitude of  $V_n$  is zero for even harmonics as it is considered as odd quarter-wave symmetry. In this work, elimination of the 5<sup>th</sup> and 7<sup>th</sup> harmonics of the three-phase system is considered, as the 3<sup>rd</sup> harmonics will be balanced out due to the symmetry of the wave. For suppressing the harmonics the non-linear equations found from the Eqn. (3.52) are [126]

$$\left. \begin{aligned} M &= \frac{4}{\pi} \cos(\alpha_1) + \cos(\alpha_2) + \cos(\alpha_3) \\ 0 &= \cos(5\alpha_1) + \cos(5\alpha_2) + \cos(5\alpha_3) \\ 0 &= \cos(7\alpha_1) + \cos(7\alpha_2) + \cos(7\alpha_3) \end{aligned} \right\} \quad (3.52)$$

where, M represents the modulation index. To solve these non-linear equations, various methods are available in the literature. Here, the Newton-Raphson method is utilized and the results are stored in the look-up table. The output current of the inverter is compared with the reference to produce the error and the output is sent to a PR controller to produce the required modulation index which is utilized in the SHE method. Figure 3.20 presents the block diagram of the PR-SHEPWM controller.

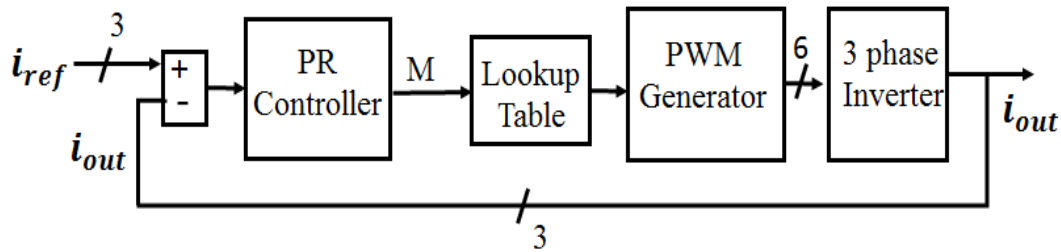


Figure 3.20: Block diagram of the PR-SHEPWM controller for generating gate pulse of VSI.

The same system is tested utilizing the PR-SHEPWM controller. Here, the steady-state error in the load current with respect to the reference current is estimated by the PR controller where the values of  $K_p$  and  $K_i$  are considered as 0 and 10 respectively. The PR controller output is utilized here to estimate the modulation index,  $M$ . The modulation index is used to select the proper switching angles from the lookup table which is found by Eqn. (3.52) for reducing harmonic components.

### 3.8 Load Flow Analysis

To meet the rapidly growing electricity demand, the power sector is in its quickly developing stage. The conventional system has been updated from a passive system to an active system with the incorporation of Distributed Energy Resources (DER) in the Distribution Network (DN). With high infiltration of DER, the system encounters high R/X proportions, an unpredicted variety of source with a persistent variety of burdens [127]. With every one of the difficulties, the power grid is resolved to give better power quality to the purchasers and keep up the security of the system. Subsequently, to investigate the execution of the system, load flow analyses are vital. Load flow is a strategy that gives a straightforward calculation to build up the attributes of the power system under steady state working condition.

Load is static and power dependably flows to the load with the assistance of transmission and distribution lines. Thus, load flow analysis is likewise alluded to as power flow analysis. Load flow analysis decides whether the voltage of the system stays inside within a definite limit under the typical or emergency working condition and whether hardware, for example, transformer and conductors are over-burden. It is crucial to choose the best operation of the existing system and furthermore to design the future development of the system. Several load flow methods are available in the literature. Among them, sweeping method, impedance method, and Newton-Raphson method are quite popular and some other methods by modifying these methods are also available.

The sweeping method is a ladder network based iterative method, where some of the first solvers are evaluated to realize the model for unbalanced three-phase distribution systems. The expressions related to the method are presented by Eqns. (3.53) and (3.54), where  $V_{abc}$  and  $I_{abc}$

presents the phase voltages and currents which are estimated by the function of system model presented by A, B, C, and D parameters [128].

$$[V_{abc}]_n = [A] \cdot [V_{abc}]_n - [B][I_{abc}]_n \quad (3.53)$$

$$[I_{abc}]_n = [C] \cdot [V_{abc}]_n - [D][I_{abc}]_n \quad (3.54)$$

To ameliorate the speed of computation and convergence, several endeavours have been performed in the literature [129-132]. The sweeping are extensively used commercially as this method is quite simple and easily implementable and robust to nonlinear solutions.

Another common method of load flow analysis is the direct impedance method, which is extensively utilized in real-time application because of its ability of forming simplified impedance matrix. The radial or weakly meshed profile of the DN is utilized in this method [130,133]. Matrix inversions and the necessity for the LU decomposition are avoided. This feature provides a greater advantage to this method rather than the others. This method also has the facility of handling the fault conditions. The related expression of this method is given by the Eqn. (3.55), where the impedance matrix is presented by Z, and the other symbols have the usual meanings.

$$[V^{k+1}]_{abc} = [Z^k]_{abc} \cdot [I^k]_{abc} + [V^k]_{abc} \quad (3.55)$$

For non-linear load, the previously described two methods need numerous solvers, while the Newton-Raphson (NR) method needs fewer in numbers. Although it requires the Jacobian matrix formation, it is quite efficient in solving highly meshed systems. In this method, the non-linear equations are linearized by a given initial solution, which are iteratively solved. The related equation of this method is presented in Eqn. (3.56) [134].

$$\begin{bmatrix} \theta^{k+1} \\ |V^{k+1}| \end{bmatrix}_{abc} = \begin{bmatrix} \theta^k \\ |V^k| \end{bmatrix}_{abc} - [J(x^k)]_{abc}^{-1} \cdot \begin{bmatrix} \Delta P(x^k) \\ \Delta Q(x^k) \end{bmatrix}_{abc} \quad (3.56)$$

where, voltage magnitude and angle is indicated by  $|V|$  and  $\theta$ , J is the Jacobian matrix, state variables of vector is  $x$  and the reactive and active power injection is indicated by  $P$  and  $Q$ . In this research work, this NR method is utilized for the load flow analysis. The proposed on-grid PV system utilizing MPC is connected to a test grid for ensuring the penetration of power produced by the system. A test grid is actually a DN model which is capable of replicating the characteristics of a real distribution feeder [135]. In general, the main goal of test feeder is to reproduce a real network comprising specific particularities within a specified region. These test grids are very significant and widely acceptable tools in the research area of power system. The results of research can be easily checked and compared with the others studies by utilizing these test feeders. Several distribution test feeders are existing such as IEEE test grids (3, 13, 34, 37, 123-bus feeders), European test grid, Neutral earth voltage (NEV), Low voltage network (LVN)

test feeder etc. [136]. In this work, IEEE 13 bus test grid is utilized for performing the load flow analysis. The detailed description of the selected test feeder is presented in the next sub-section.

The IEEE 13 bus test feeder is utilized to test the performance of the proposed system. The test feeder shows some fascinating features. The 13 bus test feeder contains shunt capacitor banks, distributed and unbalanced load and in-line transformers. The single line diagram of the test feeder with the proposed designed system is shown in Fig. 3.21. The nominal voltage of the test feeder is 4.16kV and it contains two in-line transformer and shunt capacitor banks. The parametric values of the transformer and shunt capacitor bank are presented in Table 3.5 and 3.6 [137]. The line segment data i.e. the lengths of the line from Node A to Node B are presented in Table 3.7. Table 3.7 also shows a configuration code which is utilized to present the spacing of the model. The parametric values of different distributed and spot loads at different nodes are presented in Table 3.7.

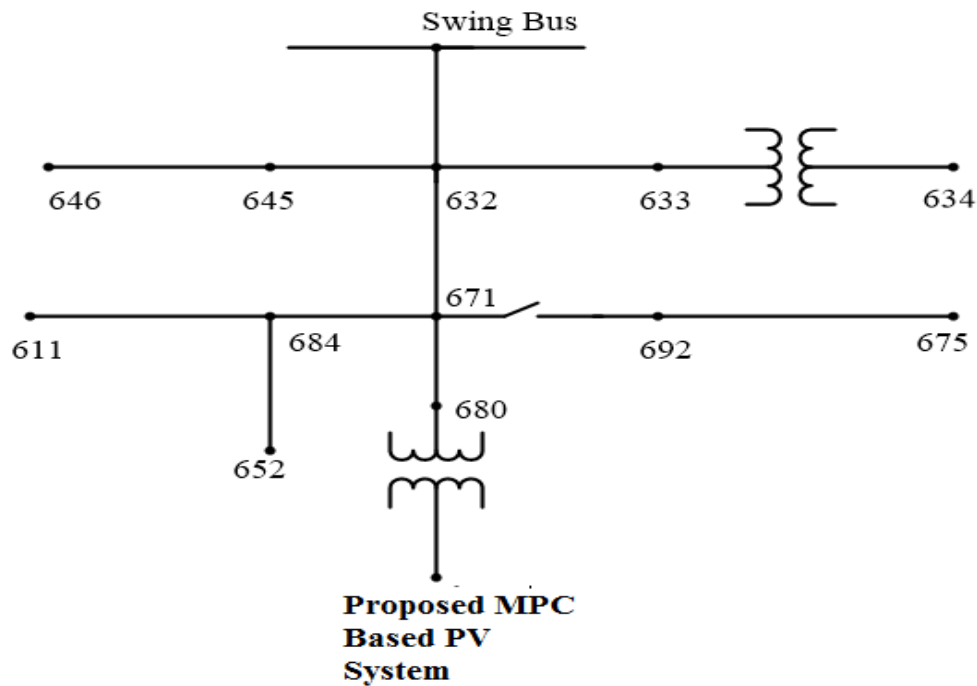


Figure 3.21: Single-line diagram of IEEE 13 bus system.

Table 3.5: Parametric value of in-line transformer.

	kVA	kV-high	kV-low	R - %	X - %
XFM -1	500	4.16 – Gr.W	0.48 – Gr.W	1.1	2
XFM -2	500	4.16 – Gr.W	0.48 – Gr.W	1.1	2

Table 3.6: Parametric value of shunt capacitor.

Node	Ph-A (kVAr)	Ph-B (kVAr)	Ph-C (kVAr)
675	200	200	200
611			100
Total	200	200	300

Table 3.7: Table for the line segment, distributed load and spot load data for the IEEE 13 bus test feeder [137].

Line Segment Data				Distributed Load Data								
Node A	Node B	Length (ft.)	Config.	Node A	Node B	Load Model	Ph-1 (kW)	Ph-1 (kVAr)	Ph-2 (kW)	Ph-2 (kVAr)	Ph-3 (kW)	Ph-3 (kVAr)
632	645	500	603	632	671	Y-PQ	17	10	66	38	117	68
632	633	500	602	<b>Spot Load Data</b>								
633	634	0	XFM-1	Node	Load Model	Ph-1 (kW)	Ph-1 (kVAr)	Ph-2 (kW)	Ph-2 (kVAr)	Ph-3 (kW)	Ph-3 (kVAr)	
645	646	300	603	634	Y-PQ	160	110	120	90	120	90	
650	632	2000	601	645	Y-PQ	0	0	170	125	0	0	
684	652	800	607	646	D-Z	0	0	230	132	0	0	
632	671	2000	601	652	Y-Z	128	86	0	0	0	0	
671	684	300	604	671	D-PQ	385	220	385	220	385	220	
671	680	1000	601	675	Y-PQ	485	190	68	60	290	212	
671	692	0	Switch	692	D-I	0	0	0	0	170	151	
684	611	300	605	611	Y-I	0	0	0	0	170	80	
692	675	500	606		Total	1158	606	973	627	1135	753	

### 3.9 Power loss Analysis

The loss of power occurs due to the switching devices used in the circuit which significantly influence the efficiency of the voltage source inverters. The overall losses in the devices include the addition of conduction, switching and harmonic losses. Collector-emitter voltage and collector-current influence the conduction loss. The reduction of conduction loss requires the decreasing of the collector-emitter voltage during the conduction time, which can only be altered by the manufacturer of the device. Moreover, the temperature of the junction also have an influence on the value of the losses. The mathematical expression for determining the average and instantaneous conduction loss of an IGBT can be expressed as [138-139]

$$P_{con} = \left(\frac{1}{T_0}\right) \int_0^{T_0} (V_{ce0} + I_x(t) * R_{ce}) * I_x(t) * \tau(t) dt \quad (3.57)$$

$$P_{con_{instantaneous}} = (V_{ce0} + I_x(t) * R_{ce}) * I_x(t) * \tau(t) dt \quad (3.58)$$

where,  $V_{ce0}$  is the turn-on / threshold voltage of the IGBT,  $R_{ce}$  is the differential resistance of the IGBT and  $I_x(t)$  represents the arm current through the upper IGBT. The value of  $V_{ce0}$  and  $R_{ce}$  is taken from a manufacturer datasheet at a specified temperature [140]. The mathematical expression of  $I_x(t)$  and  $R_{ce}$  are as follows.

$$I_x(t) = (I_{dc}/3) + (I_{ac}/2) \quad (3.59)$$

$$R_{ce} = \frac{V_{ce2} - V_{ce1}}{I_{ce2} - I_{ce1}} \quad (3.60)$$

The term  $\tau(t)$  is related with the modulation index  $m$  of the controlling method. For PWM only, duty cycle  $\tau(t)$  is present and its expression is

$$\tau(t) = \left(\frac{1}{2}\right) * (1 + m * \sin(2\pi * f_0 * t)) \quad (3.61)$$

where, the output frequency is indicated by  $f_0$ . In case of MPC, there is no need of modulation index. Therefore, in this case this term is neglected.

Again, the second loss i.e. the switching loss occurs during the turn-on and turn-off condition of IGBT. The dc link voltages, the output load current, the transient parameters of the IGBTs influence the switching loss. The switching loss is also dependent on the junction temperature of the device and the gate driver circuit resistance. This loss can be reduced by using various soft switching techniques. The mathematical expressions for determining the average and instantaneous switching losses are as follows [138-139]

$$P_{sw} = \left(\frac{1}{T_0}\right) \int_0^{T_0/2} f_{sw} * (E_{on} + E_{off}) * \left(\frac{V_{dc}}{V_{ccnom}}\right) * \left(\frac{I_x(t)}{I_{ccnom}}\right) dt \quad (3.62)$$

$$P_{sw_{instantaneous}} = f_{sw} * (E_{on} + E_{off}) * \left(\frac{V_{dc}}{V_{ccnom}}\right) * \left(\frac{I_x(t)}{I_{ccnom}}\right) dt \quad (3.63)$$

where, the switching frequency is presented by  $f_{sw}$ ,  $V_{dc}$  is the dc link voltage and  $V_{ccnom}$  and  $I_{ccnom}$  are the voltage across collector-emitter terminal of IGBT and the collector current during the test, respectively. The values of  $V_{ccnom}$  and  $I_{ccnom}$  are taken from the manufacture datasheet. The values of turn-on and turn-off energy  $E_{on}$  and  $E_{off}$ , respectively, are also taken from the datasheet [140].

The presence of harmonic component in the injected grid current also causes power loss which decreases the penetration of power to the grid. The presence of harmonic component is expressed by the term total harmonic distortion (THD). The total harmonic losses due to the harmonic components are determined by the following expression [141].

$$P_{harmonic} = 3R_L I_L^2 = 3 R_L ( I_1^2 + \sum_{n=2}^{\infty} I_n^2 ) = R_L I_1^2 ( 1 + THD_I^2 ) \quad (3.64)$$

where,  $I_1$ ,  $I_n$  and  $THD_I$  are the fundamental current, current due to harmonic component and amount of current THD, respectively, and  $R_L$  is the per phase resistance.

### 3.10 Fault analysis

In the research area of power system, fault analysis is a significant study in which the behavior of the system is tested under any abnormal condition. A fault occurs in a system causing a disturbance with the normal operation of the system. The fault may be caused by several ways such as may be the falling of trees across the lines, heavy flow of winds or heavy storm, severe amount of lightening, breaking of lines because of overloading, sitting of a bird between the two lines, short-circuit among the lines or line to ground, collision of vehicles with the electrical tower or poles etc. [142]. This sudden change or a fault causes a serious disruption in the system. The fault caused by the above mentioned ways can be classified into three categories, such as: (a) Single line to ground fault, (b) Double line to ground fault, and (c) Balanced three phase fault.

Among the categorized faults, the first two caused by only one or two phases of a system and therefore said to as unsymmetrical faults of a system. These unsymmetrical faults are quite common in the system. Again, the last one caused only if all the phases of the system are short-circuited or open-circuited, hence this one is said to be a balanced or symmetrical fault. This symmetrical fault is rare in the system [142]. The pictorial representations of the faults are shown in Fig. 3.22 [142].

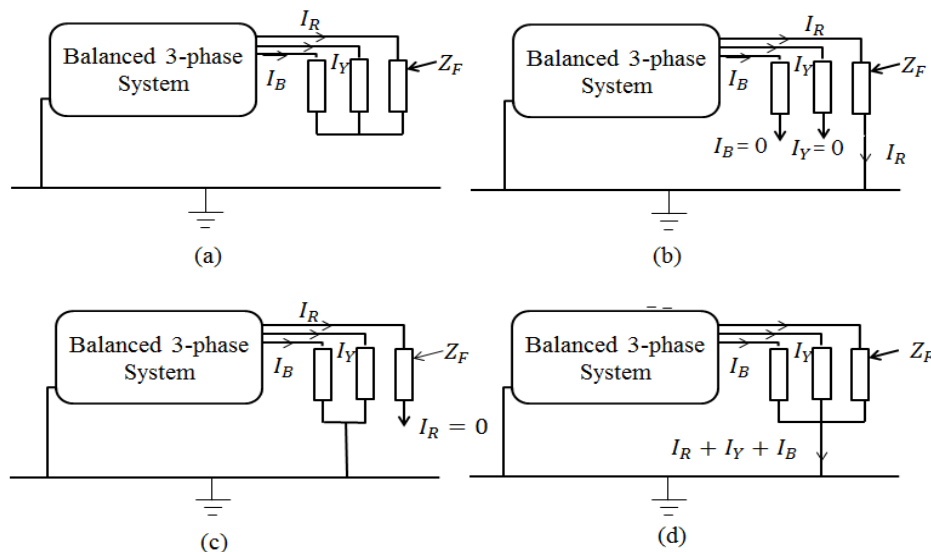


Figure 3.22: Intentional fault injection in the IEEE 13 bus test feeder: (a) a healthy three phase system and several types of fault in the system such as (b) single line to ground fault, (c) Double line to ground fault, and (d) three-phase balanced fault.

In this research work, the proposed system is connected to the IEEE test feeder for ensuring the power penetration through load flow analysis. After that, the performance of the proposed controller based on-grid PV system is further tested by the fault analysis. Unsymmetrical and symmetrical faults are intentionally done in the system and the performance of the system is observed. The result of the analysis is presented in the next chapter.

### **3.11 Conclusion**

The model developed in this research work is presented in detail in this chapter. The design of a three-phase two-level MPC based on-grid PV system includes a PV array, dc/dc converter, proposed controller driven dc/ac inverter, line filter and the grid. The mathematical model of the system is well oriented and presented in this chapter. The integration of the aforementioned components is expected to create a stable system. The proposed system will also be capable of representing itself as an energy efficient control of PV system which will be validated by load flow, and power loss analysis.



## Chapter IV

### Simulation Results

#### 4.1 Introduction

People all over the world firmly believe that the renewable energy sources, especially solar energy will bring a positive impact against the growing demands of electricity. Solar energy also contributes to the overall energy production. However, the energy produced from the solar energy contains harmonic components due to the controlling of the on-grid inverter which makes it less efficient for the system. Therefore, an MPC based energy efficient control is proposed in this research work and the performance of it in terms of tracking accuracy, harmonic analysis, steady-state and dynamic response is presented in this chapter. For validating the controller as an efficient control, load flow, power loss and fault analysis are done and the results are presented in this chapter.

#### 4.2 Performance Analysis of the Proposed Controller

The block diagram of the designed system in the research work consists of PV system, a dc/dc converter, MPC based inverter, R-L line filter and the grid. In this research work, a 39kW PV array is connected to the proposed MPC based inverter through a dc/dc converter to evaluate the effectiveness of the proposed system. The array is designed with 168 modules, each having a maximum power rating of 235W. The whole simulations are carried out by using MATLAB/Simulink tool. The model designed in the MATLAB/Simulink platform is shown in Fig. 4.1. During simulation, the dc link voltage provided by the PV array through a closed loop dc/dc converter is maintained at 850V and the sampling time is considered as  $33\mu s$ . The solver taken during this simulation is ode5 (Dormand-Prince) and fixed step type of it is considered. The parameters values required by the blocks of the model are initialized in a separate m-file and it needs to be executed every-time before the starting of the simulation. The parameters values utilized in the simulation are shown in Table 4.1.

Table 4.1: Parameter values for the simulated systems.

Parameter	Value
Inverter voltage	850V
Reference current	96A
Reference frequency	50Hz
Load resistance	3.44 $\Omega$
Load inductance	70mH
Grid voltage	120V
Grid frequency	50Hz

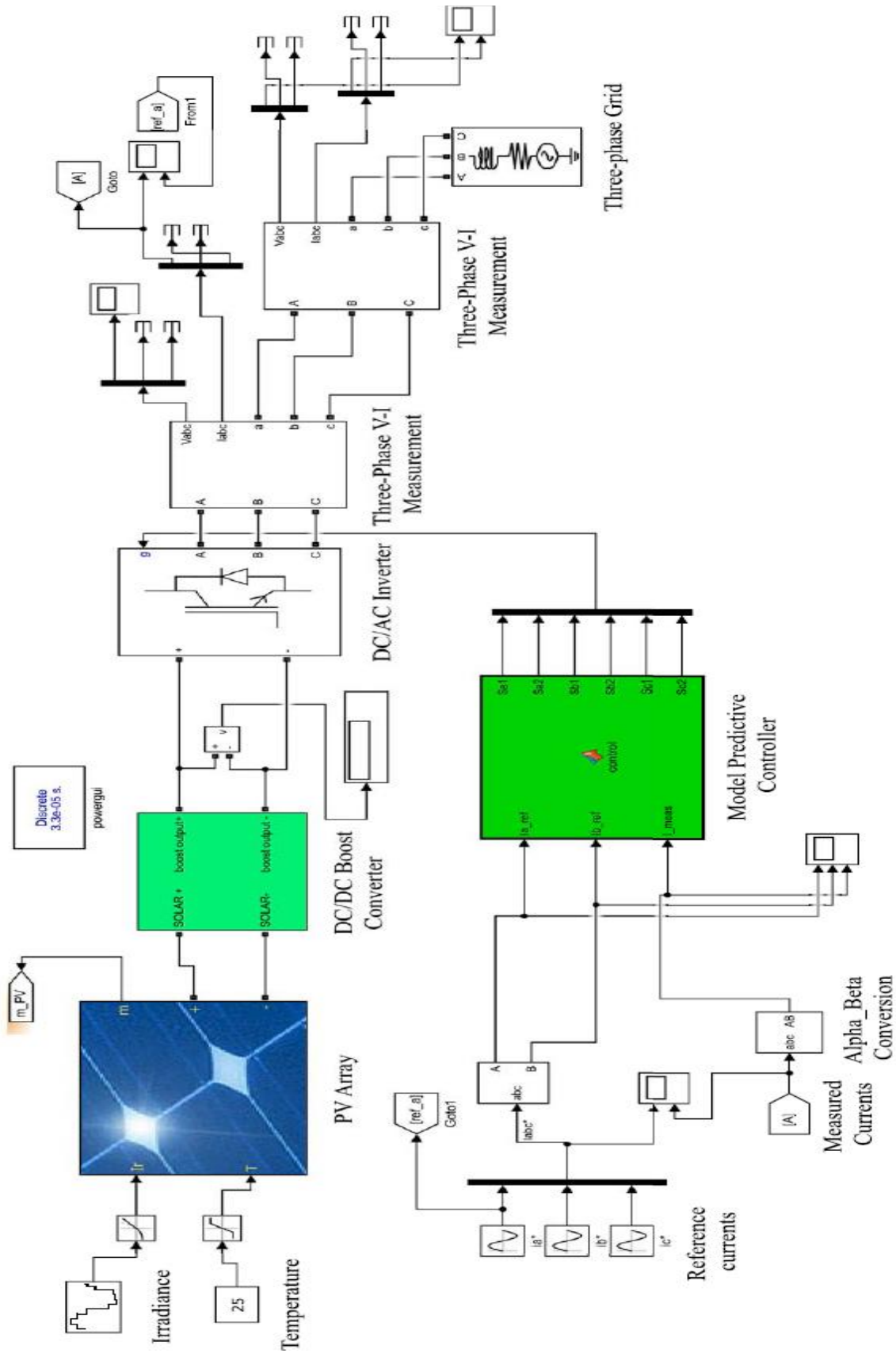


Figure 4.1: MATLAB/SIMULINK representation of the proposed MPC based on-grid PV inverter.

### 4.2.1 Steady-state Analysis

The performance of the proposed controller is analyzed through the steady-state analysis. The algorithm is implemented by the cost function as presented by the Eqn. (3.45). The reference current utilized during the simulation is sinusoidal in nature and having amplitude of 96A with a frequency of 50Hz. Load voltage and load current waveforms from the steady-state analysis of the controller are presented in Figs. 4.2 to 4.5. The phase voltages ( $V_a, V_b, V_c$ ) across the load before LC filter is shown in Fig. 4.2. Figure 4.3 shows the phase voltages ( $V_a, V_b, V_c$ ) across the load after the LC filter.

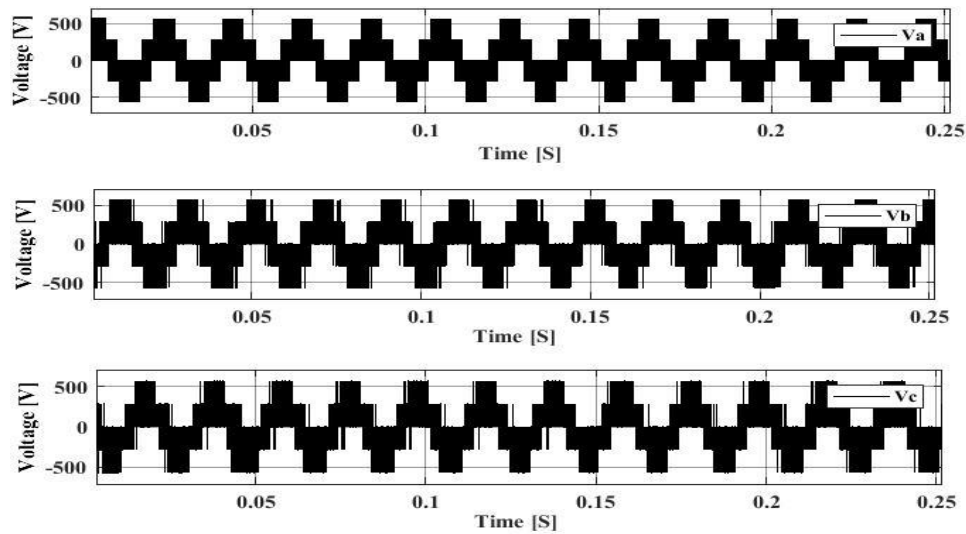


Figure 4.2: Steady-state phase voltage ( $V_a, V_b, V_c$ ) before LC filter using the proposed controller.

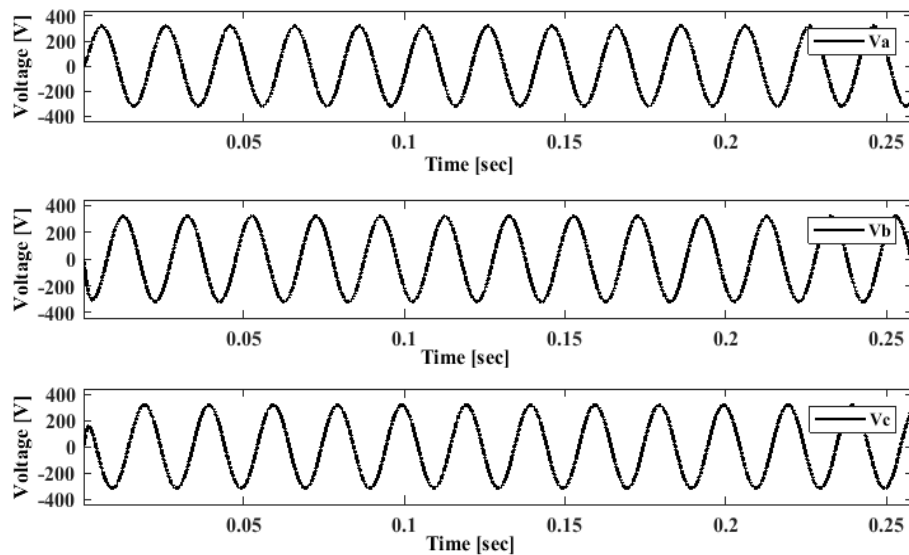


Figure 4.3: Steady-state phase voltage ( $V_a, V_b, V_c$ ) after LC filter using the proposed controller.

The steady-state three-phase load currents ( $I_a, I_b, I_c$ ) using the proposed controller is presented in Fig. 4.4 which indicates a sinusoidal nature load currents with low distortion. The three-phase currents ( $I_a, I_b, I_c$ ) is transformed into two dimensional currents ( $I_\alpha, I_\beta$ ) in  $\alpha\beta$  plane utilizing Clarke's transformation as presented in Eqn. (3.19). Graphical representation of the  $I_\alpha$  and  $I_\beta$  current is shown in Fig. 4.5.

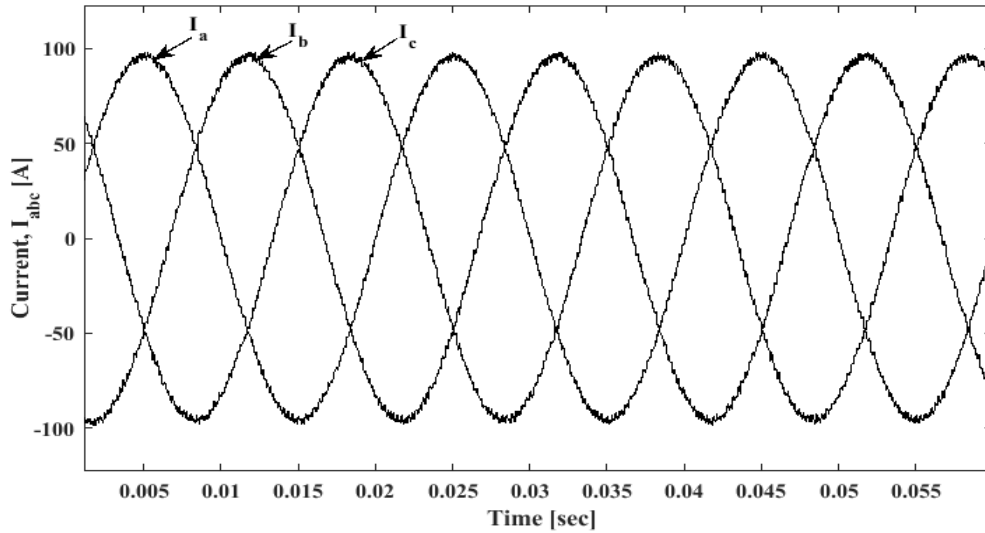


Figure 4.4: Steady-state phase currents ( $I_a, I_b, I_c$ ) using the proposed controller.

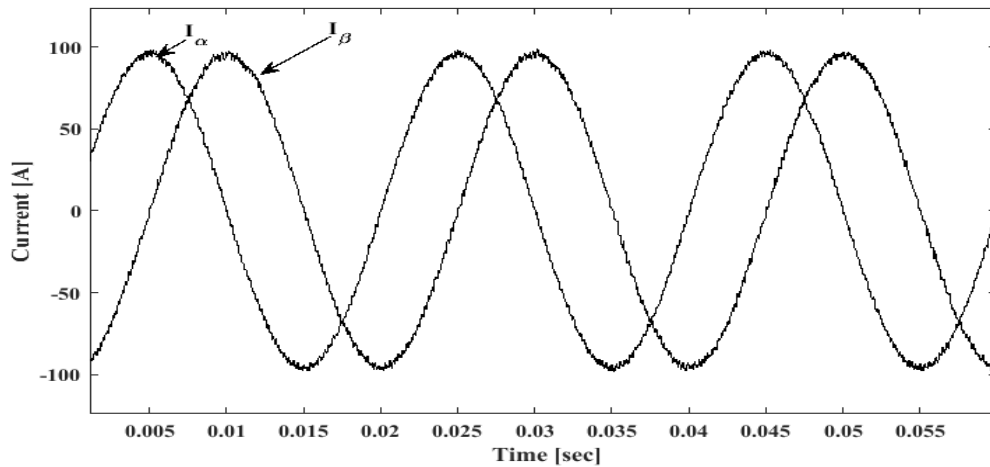


Figure 4.5: Steady-state phase currents ( $I_\alpha, I_\beta$ ) in  $\alpha\beta$  plane using the proposed controller.

### 4.2.2 Current Tracking Accuracy

In order to evaluate the performance of predictive current, reference current tracking accuracy of the controllers is checked. A three phase sinusoidal reference current of 96A and 50Hz frequency is considered. The current waveforms ( $I_\alpha, I_\beta$ ) for transient reference tracking is shown in Fig. 4.6. It can be seen that the controller tracks the reference current accurately at both the transient and steady-state conditions.

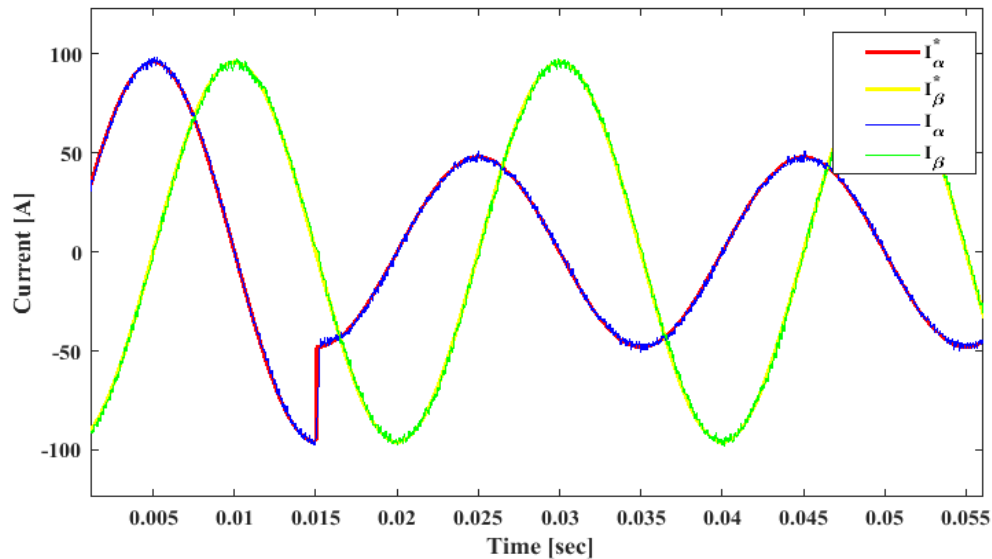


Figure 4.6: The current waveforms ( $I_\alpha, I_\beta$ ) for transient response.

### 4.2.3 Effect of switching frequency term in the cost function

As mentioned earlier, the cost function designed for the proposed controller includes two components. One is for reducing the current tracking error and the other one is for reducing the switching transitions. The two terms are added with a weighting factor  $\lambda$ . Therefore, the value of  $\lambda$  is an important factor for determining an optimized cost function. For determining the effect of switching transitions reduction, the simulation of the whole system is done for  $\lambda = 0$  i.e. neglecting the term of average switching frequency reduction in the cost function. Harmonic analysis is done for the output load current by using FFT analysis and is shown in Fig. 4.7. It is seen that the current without the switching transitions reduction term is 1.82%.

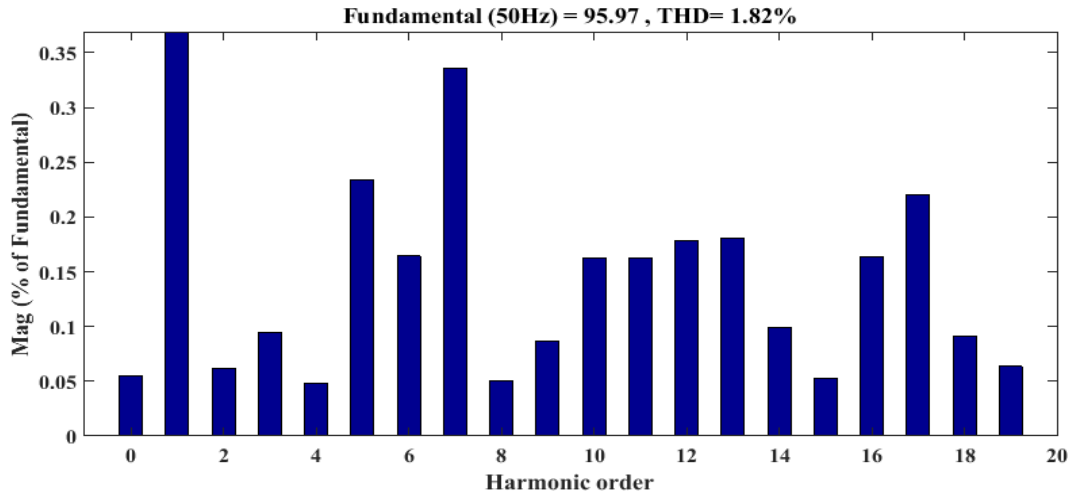


Figure 4.7: Current THD without switching frequency term in the cost function.

Now, the simulation is done with the addition of switching frequency reduction term in the cost function utilizing (3.45). The value of weighting factor  $\lambda$  is varied over a range of 0.001 to 0.7, and the value of switching frequency and the corresponding current THD are calculated and shown in Table 4.2. It is seen that, the switching frequency is 4.46 KHz and the corresponding current THD is 1.82% for  $\lambda = 0$ . If the value of  $\lambda$  increases, the switching frequency decreases, while the current THD increases. For  $\lambda = 0.7$ , the switching frequency is 3.03 KHz which is the lowest one for the observed datasheet as shown in Table 4.2, while the current THD value is 2.38% which is the highest one. The current THD should be lower in order to having lower harmonic loss. The switching frequency should also be lower for a lower switching loss in the semi-conductor device. The switching frequencies, current THDs with the variation of  $\lambda$  are shown in Fig. 4.8.

Table 4.2: Current THD and Losses with the variation of  $\lambda$

Weighting factor, $\lambda$	Average Switching Frequency (kHz)	Conduction Loss (W)	Switching Loss (W)	Current THD (%)
0	4.46	30.62	7.53	1.82
0.01	4.28	29.73	7.51	1.89
0.05	4.20	29.73	7.22	1.87
0.1	4.08	29.70	7.01	1.94
0.2	3.84	29.69	6.65	1.95
0.3	3.70	29.71	6.34	2.06
0.4	3.54	29.72	6.05	2.07
0.5	3.34	29.73	5.79	2.20
0.6	3.27	29.74	5.60	2.28
0.7	3.03	29.77	5.38	2.38

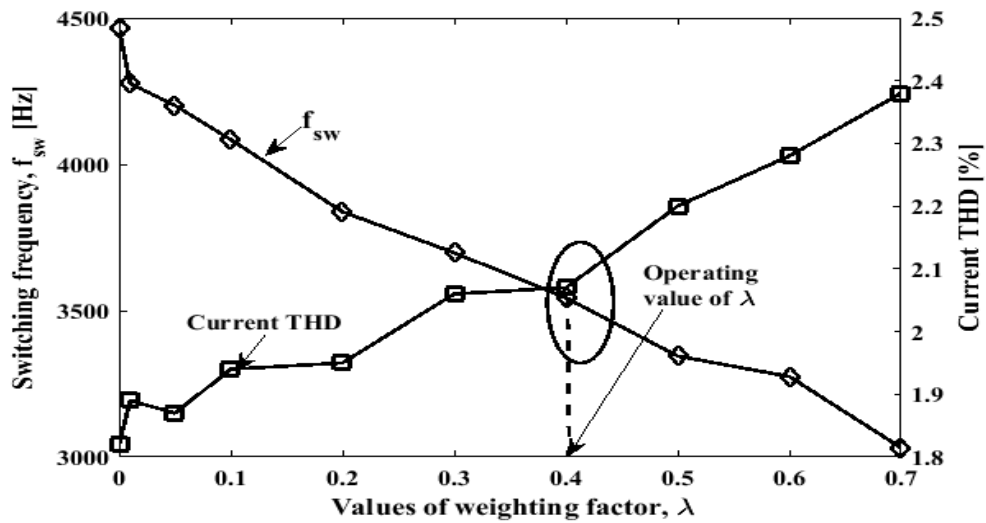


Figure 4.8: Switching frequencies and current THDs with the variation of weighting factor,  $\lambda$ .

From Fig. 4.8, it is seen that, the average switching frequency,  $f_{sw}$  and the current THD curve intersect at  $\lambda = 0.4$ , where the switching frequency is 3.54 KHz and the corresponding current THD is 2.07%. Note that, considering only 0.25% more current THD, the switching frequency is found to be a lower one. Hence, for energy efficient operation of the inverter, it is operated at this trade-off point (i.e.  $\lambda = 0.4$ ) of the average switching frequency and the current THD.

The steady-state current response of the output load current with  $\lambda = 0.4$  for the proposed controller is shown in Fig. 4.9. It is seen that the waveform does not much change from the waveform for  $\lambda = 0$ .

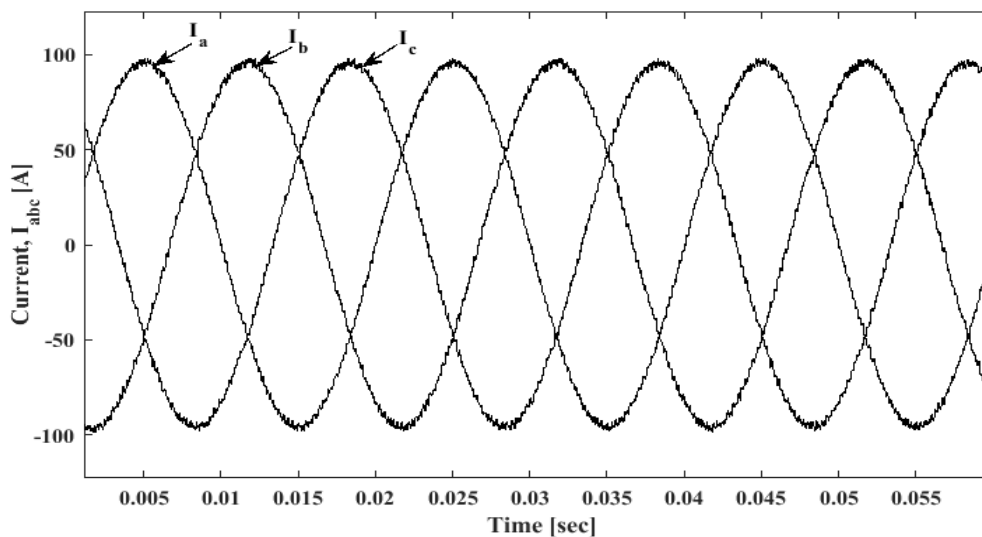


Figure 4.9: Steady-state phase currents ( $I_a, I_b, I_c$ ) using the proposed controller for  $\lambda = 0.4$ .

#### 4.2.4 Power Loss Analysis

Now, for the value of  $\lambda = 0.4$ , the loss analysis is done using the mathematical expression described in sub-section 3.7. The conduction, switching and harmonic losses are calculated for both the conditions of with and without switching transitions term in the cost function and are shown in Figs. 4.10 to 4.12.

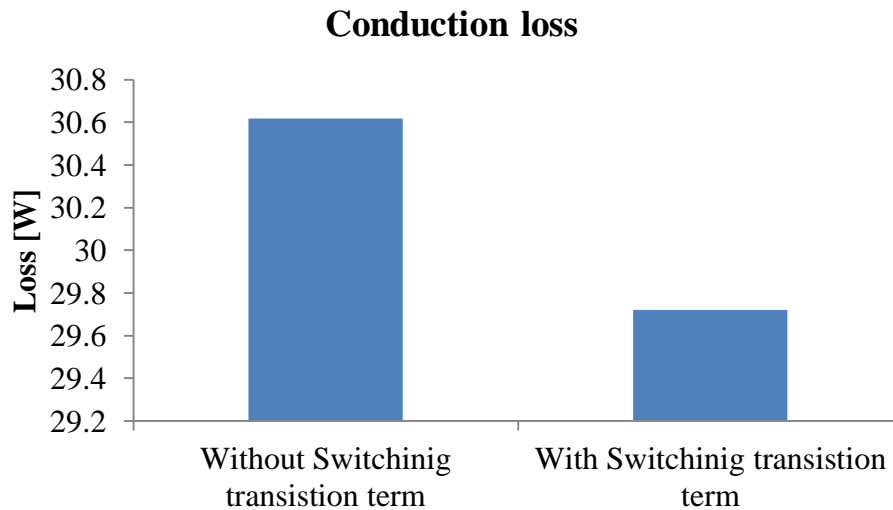


Figure 4.10: Conduction loss with and without switching frequency reduction term in the proposed controller.

From Fig. 4.10, the continuous conduction losses for per phase of a three phase system are 30.62W and 29.72W for the value of  $\lambda = 0$  and  $\lambda = 0.4$ , respectively. Therefore, it can be said that 2.94% (0.8972W) loss is reduced due to the addition of switching transition term in the cost function.

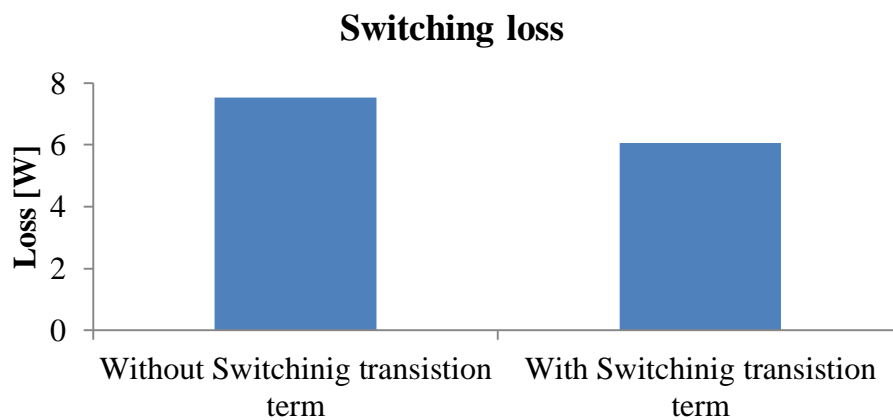


Figure 4.11: Switching loss with and without switching frequency reduction term in the proposed controller.



From Fig. 4.11, the continuous switching losses for per phase of a three phase system are 7.53W and 6.04W for the value of  $\lambda = 0$  and  $\lambda = 0.4$ , respectively. It can be seen that 19.79% (1.49W) loss is reduced due to the addition of switching transition term in the cost function. The harmonic losses are also calculated for the same case and are shown in Fig. 4.12. It is noted that the continuous harmonic losses calculated up to 19<sup>th</sup> harmonics with and without switching transition term in the cost function are 6.79W and 5.25W, respectively. Hence, the proposed system suffers from 22.68% (1.54W) harmonic loss due to trade-off the current THD and switching frequency as shown in Fig. 4.12.

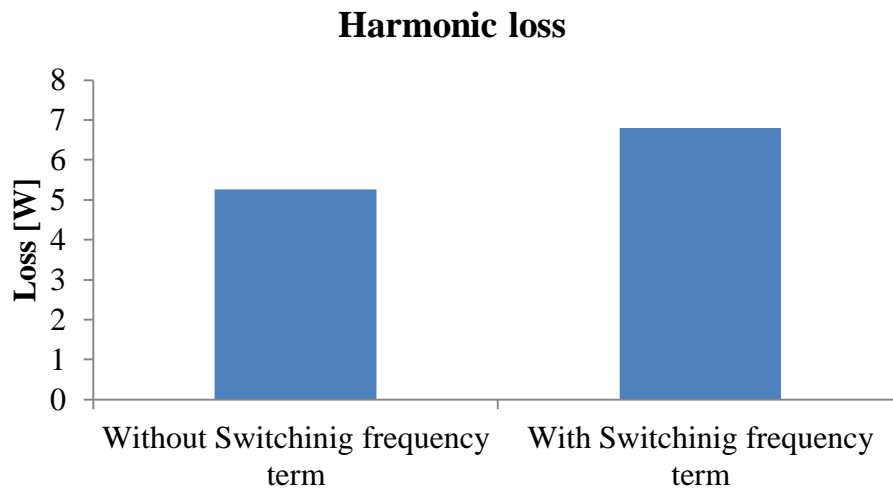


Figure 4.12: Harmonic loss with and without switching frequency term in the proposed controller.

The overall loss per phase with and without switching frequency term is shown in Fig. 4.13.

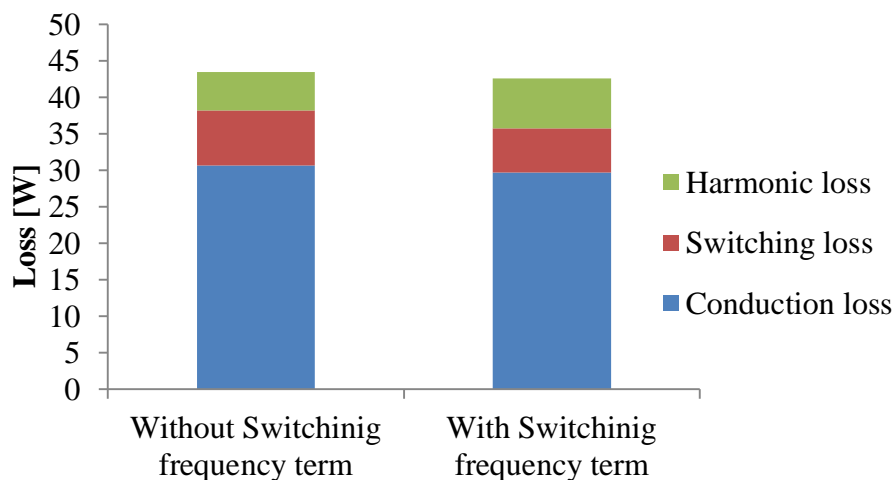


Figure 4.13: The overall loss per phase with and without switching frequency term in the cost function.

From Fig. 4.13, it is seen that the total per phase continuous loss with and without switching frequency reduction term are 42.56W and 43.40W, respectively. Therefore, 1.96% (0.85W) loss is reduced per phase due to the switching frequency reduction. For the three-phase system the total reduced loss is  $(0.83983 \times 3) = 2.51949\text{W}$ , which shows a significant amount of loss reduction due to the incorporation of switching frequency reduction term in the cost function.

#### 4.2.5 Load Flow Analysis

Load flow analysis is done using the IEEE 13 bus system in order to ensure the power penetration to the ac grid. The proposed MPC based PV system is connected to the 680 bus of the IEEE 13 bus system through a step-up transformer as shown in Fig. 4.14. The parameters of the IEEE 13 bus system are presented in the previous chapter, sub-section 3.7. The results of load flow analysis of the system before and after connecting the proposed controller based PV system are shown in Table 4.3. The default active power generation of IEEE 13 bus system is 3518.74kW. From Table 4.3, after connecting the proposed controller based PV system, it can be seen that the penetrated active power generation to the IEEE 13 bus is 32.08kW.

Table 4.3: With and without connecting the proposed PV system to the IEEE 13 bus.

Parameters	Before the connection of Proposed Controller based PV system	After the connection of Proposed Controller based PV system
Total generation	P= 3518.74 kW Q= 1540.14 kvar	P= 3550.82 kW Q = 1514.38 kvar
Total PQ load	P = 3101.90 kW Q= 1880.42 kvar	P = 3103.22 kW Q=1881.25 kvar
Total Zshunt load	P = 363.47kW Q = -479.42 kvar	P = 393.85 kW Q = -486.01kvar
Total losses	P= 53.36 kW Q = 139.14 kvar	P = 53.76kW Q = 119.14kvar

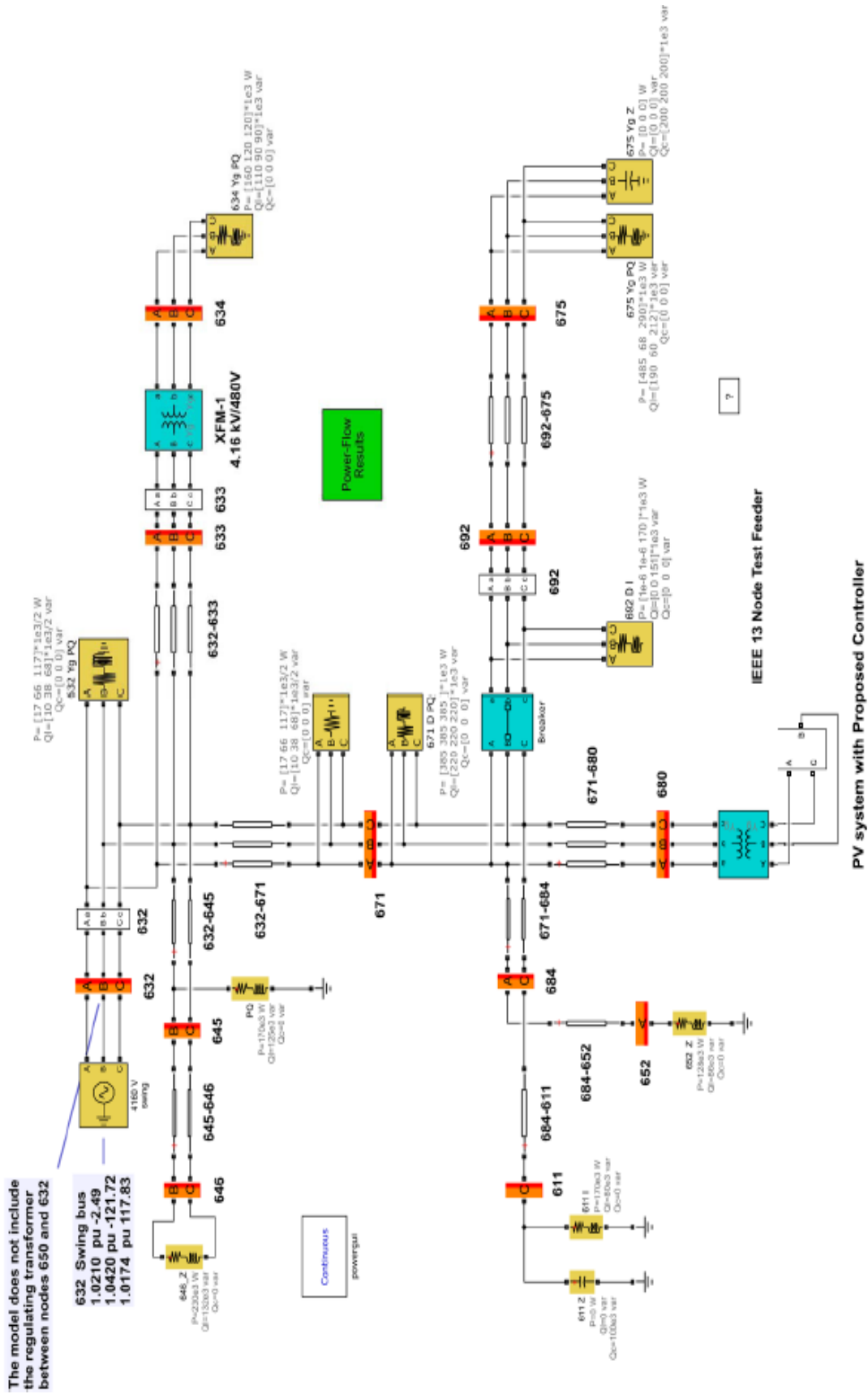


Figure 4.14: IEEE 13 bus system with the proposed controller based PV system for load flow analysis.

### 4.2.5 Fault Handling Capacity Analysis

To analyse the stability of the proposed controller, fault current handling capacity of the controller is tested. While connecting the proposed PV system in the 680 bus of the IEEE 13 bus, intentional fault is done in the bus for testing the performance of the controller. Both symmetrical (LLL) and unsymmetrical (LG, and LLG) faults are created and the voltage and current profile during and after recovering the fault is shown in Figs. 4.15 to 4.17. The three cases are described one by one below.

If an LG fault is occurred from 0.02s to 0.1s in the test system at 680 bus for four cycles, only the faulty phase voltage A has fallen during this time where the other phases are not disturbed as shown in Fig. 4.15. From the Fig. 4.15, it is seen that during the faulty condition, the current in the faulty phase experiences current swell problem which is the sudden increase of current from its rated value. The proposed controller comes at normal condition by recovering fault voltage immediately and takes only 0.06s for recovering the fault current to come back at its normal condition which ensures the fault handling capacity of the controller.

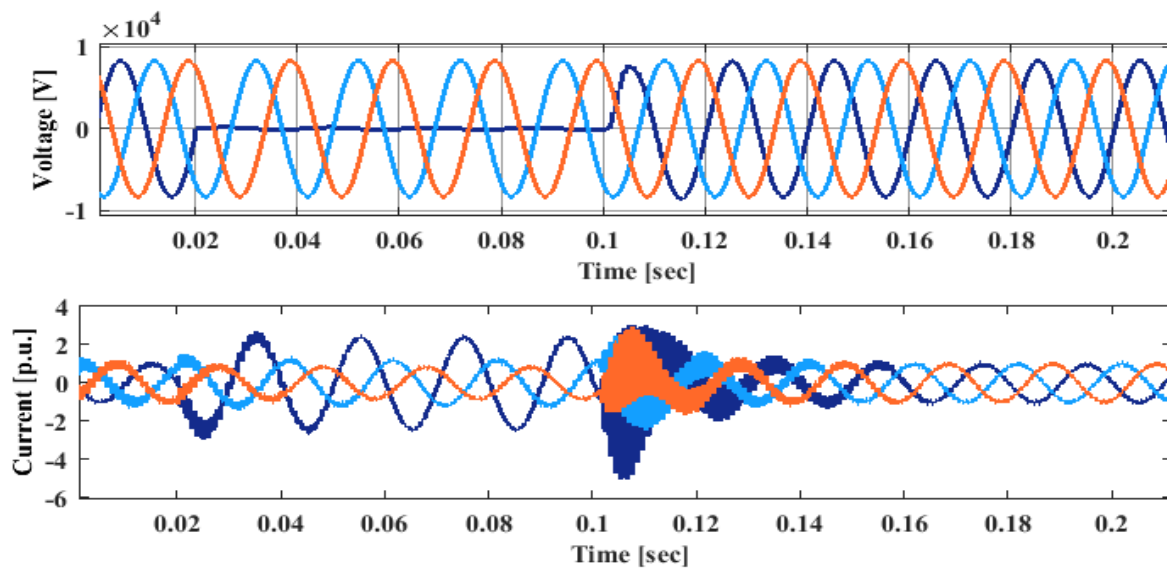


Figure 4.15: Voltage and current profile during and after the LG fault for the proposed controller.

Again, an LLG fault is intentionally created from 0.02s to 0.1s in the system and the associated voltage and current waveform is shown in Fig. 4.16. From Fig. 4.16, it is seen that only the two phase voltages fallen to zero during the fault and the other phase still continues. The current during the fault also experiences the current swell as similar in the LG fault. Here, the voltage during the fault recovery time also experiences voltage swell. The proposed controller takes 0.13s for recovering the fault voltage and takes 0.18s for recovering fault current effect and again come back at the normal condition as shown in Fig. 4.16.

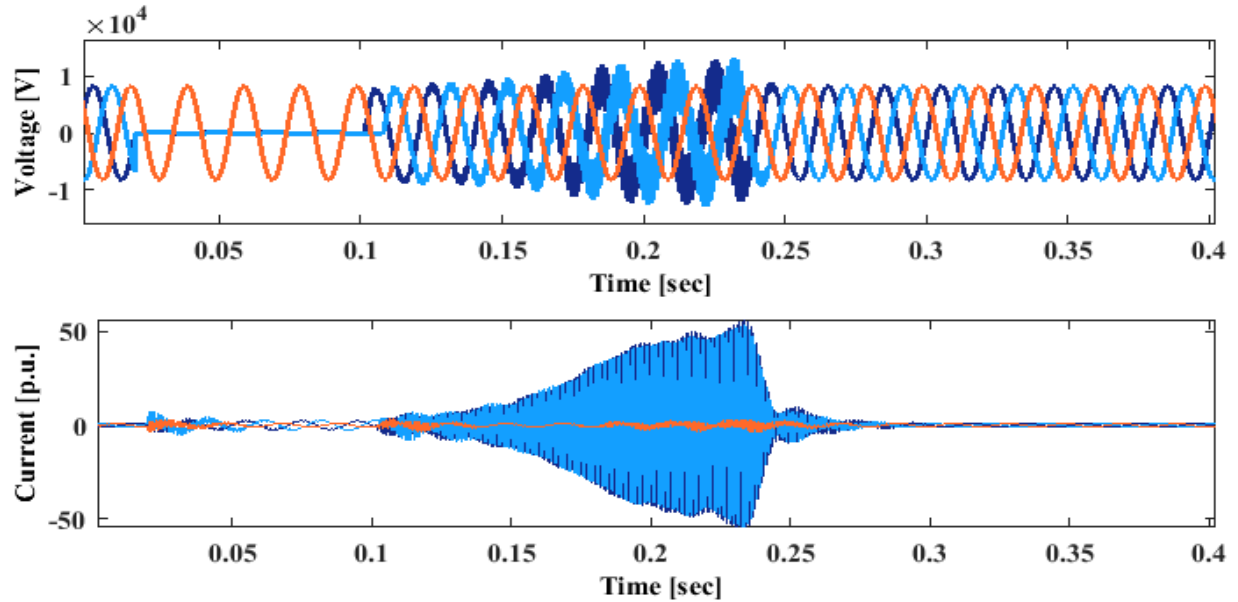


Figure 4.16: Voltage and current profile during and after the LLG fault for the proposed controller.

For testing the behavior of the system under a symmetrical fault, an LLLG fault is intentionally created from 0.02s to 0.03s as shown in Fig. 4.17. The proposed controller in this case takes longer time for recovering the effect of fault voltage and current and takes nearly 0.58s and 0.62s, respectively, to clear the fault. Although it takes longer time, the proposed controller has the ability of handling the rare symmetrical fault in the system.

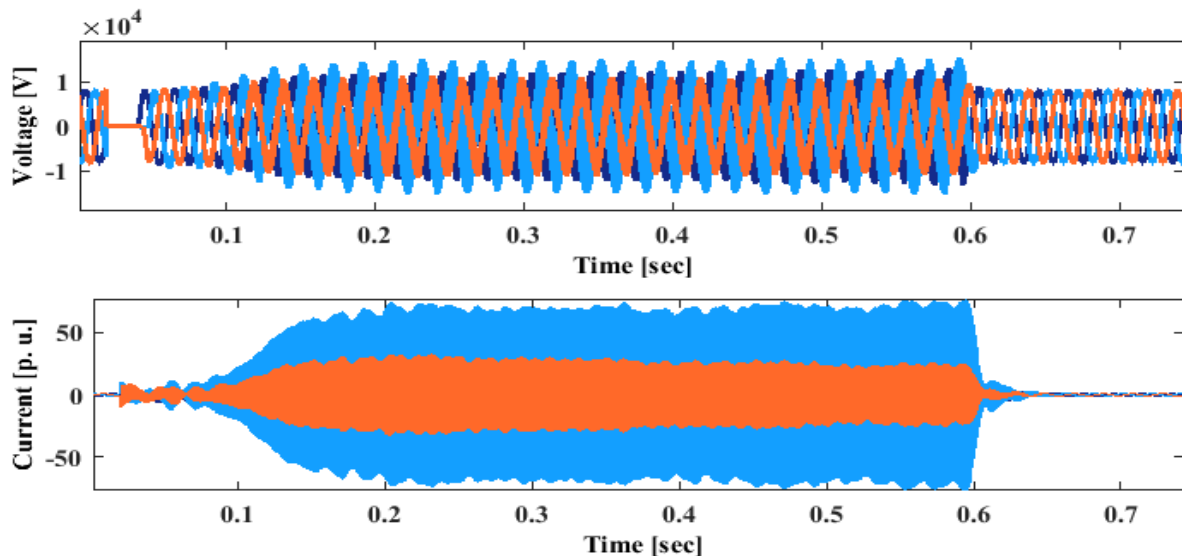


Figure 4.17: Voltage and current profile during and after the LLLG fault for the proposed controller.

After reviewing the aforementioned fault analysis, it can be said that the proposed controller has the ability to operate the inverter under the challenging symmetrical and unsymmetrical fault conditions.

### 4.3 Comparison with the Existing Controllers

The features of the proposed MPC based inverter system is compared with the three existing controllers such as PI-PWM, PR-PWM, and PR-SHEPWM for the same parameters as presented in the previous section. The results of the comparison are given below.

#### 4.3.1 Transient Analysis

In order to test the dynamic performance of the controllers, transient analysis is done. A step reduction is done in the amplitude of the real component of the reference current  $I_\alpha^*$  from 96A to 48A at time 0.015sec, while the imaginary component of the reference current  $I_\beta^*$  is kept constant at 96A for all the aforementioned controllers. The results of the analysis are presented below.

##### 4.3.1.1 PI-PWM Controller

The dynamic responses of the measured load current and voltage in  $abc$  and  $\alpha\beta$  frame for the PI-PWM controller are shown in Figs. 4.18 and 4.19. From Fig. 4.19, it is seen that the controller tracks the change in reference current, but does not provide the decoupled control of load current ( $I_\alpha, I_\beta$ ). This means that a change in one component  $I_\alpha^*$  affects another component while to settle down the change.

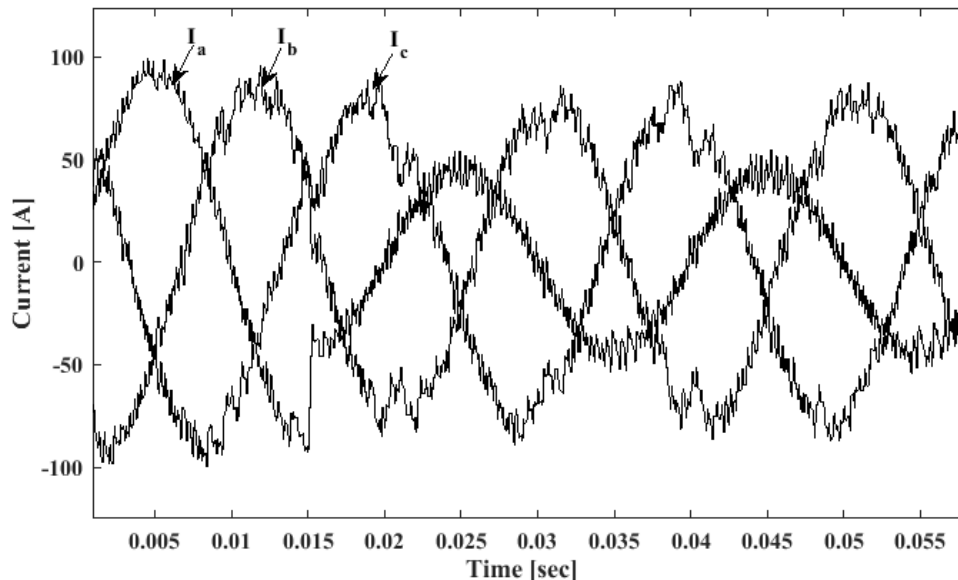


Figure 4.18: Transient phase currents ( $I_a, I_b, I_c$ ) for the PI-PWM controller.

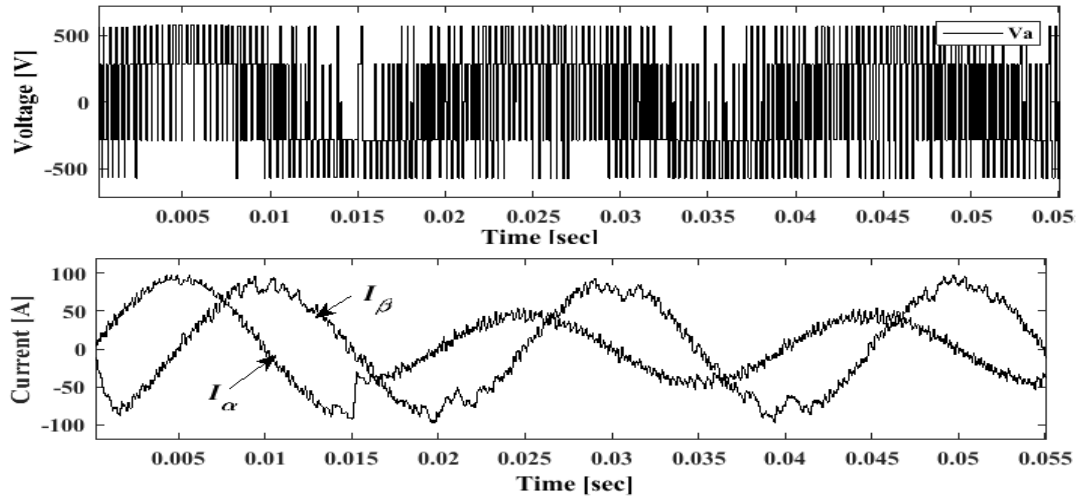


Figure 4.19: Transient phase voltage in phase a, and currents ( $I_\alpha, I_\beta$ ) in  $\alpha\beta$  frame for PI-PWM controller.

#### 4.3.1.2 PR-PWM Controller

For making a comparison of the proposed controller with the existing PR-PWM controller, the response of PR-PWM controller is tested under transient condition. The responses of the measured current and voltage in  $abc$  and  $\alpha\beta$  frame for the PR-PWM controller are shown in Figs. 4.20 and 4.21. It is seen that a step reduction of current from 96A to 48A is done at 0.015s in the real component of the reference current  $I_\alpha^*$  to realize the effect of transient response of the controller. The Fig. 4.20 ensures that the controller is able to respond accurately under the transient condition. Again, from Fig. 4.21, it is seen that the controller tracks the change in reference current, and provides a better transient response than the traditional PI-PWM controller. The controller also provides a decoupled feature but the tracking of change is not instantaneous as the proposed controller.

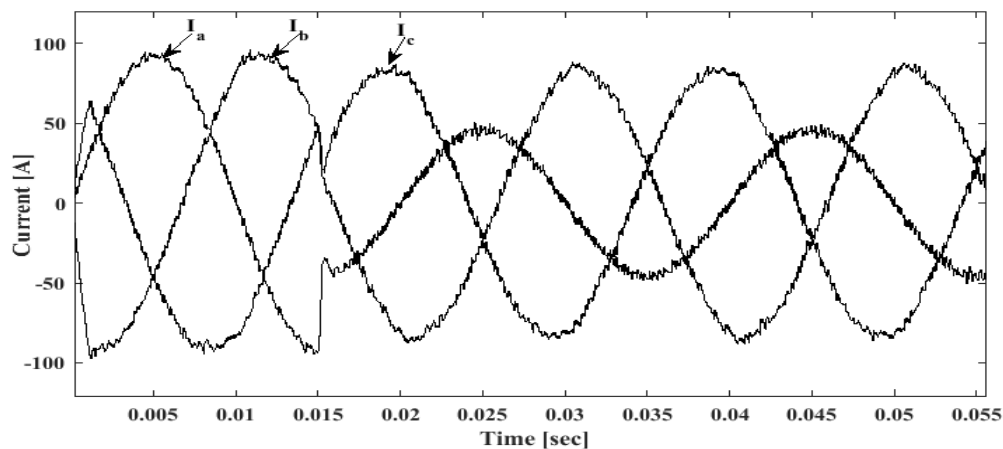


Figure 4.20: Transient phase currents ( $I_a, I_b, I_c$ ) for the PR-PWM controller.

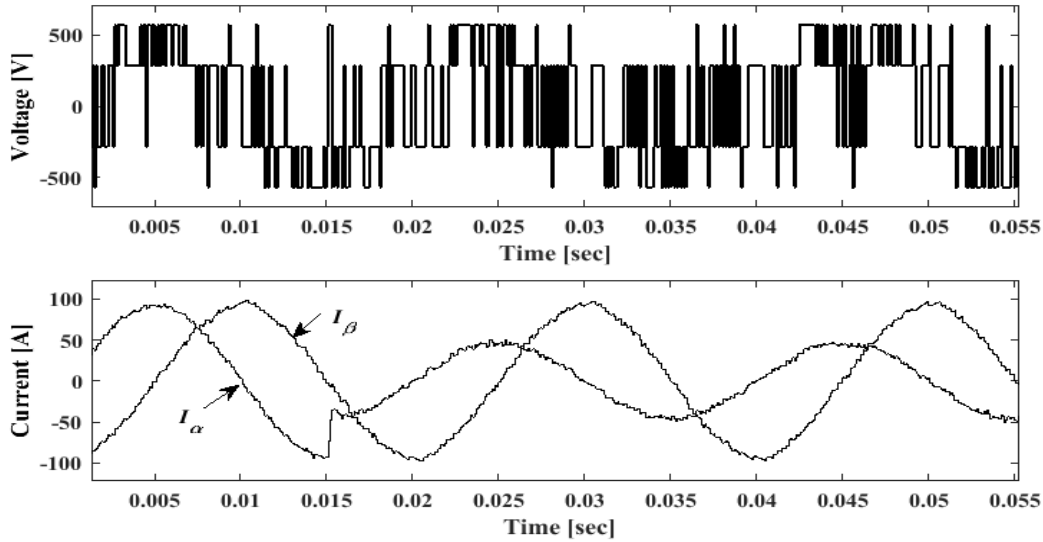


Figure 4.21: Transient phase voltage in phase a, and currents ( $I_\alpha, I_\beta$ ) in  $\alpha\beta$  frame for PR-PWM controller.

#### 4.3.1.3 PR-SHEPWM Controller

For comparing the transient response of the existing PR-SHEPWM controller with the proposed MPC based controller, a step change in the amplitude of reference current  $I_\alpha^*$  (from 96A to 48A) is done again at the same time of 0.015s, while keeping the amplitude of  $I_\beta^*$  fixed. The dynamic responses of the measured current and voltage in  $abc$  and  $\alpha\beta$  frames for the PR-SHEPWM controller are shown in Figs. 4.22 and 4.23. From Fig. 4.22, it is seen that the controller also tracks the change in reference current, but does not provide the decoupled control of load current ( $I_\alpha, I_\beta$ ) as the PI-PWM controller. This means that a change in one component ( $I_\alpha^*$ ) affects another one while to settle down the change, as the PI-PWM controller.

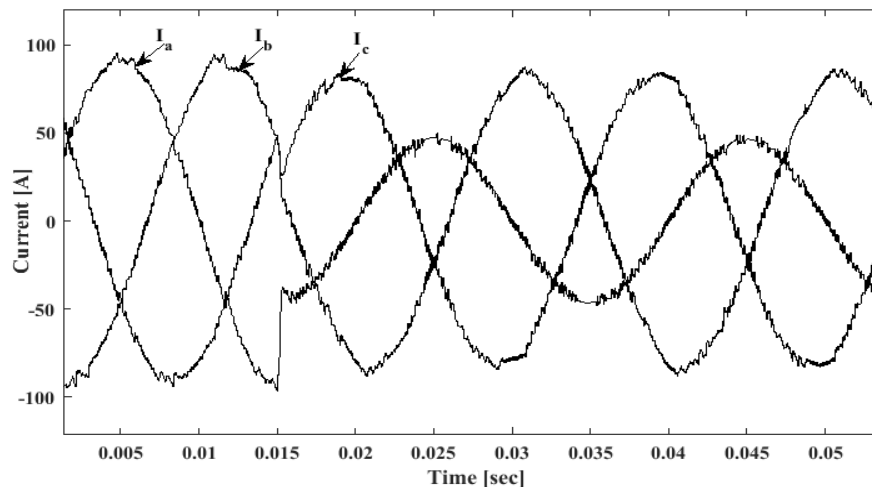


Figure 4.22: Transient phase currents for the PR-SHEPWM controller.



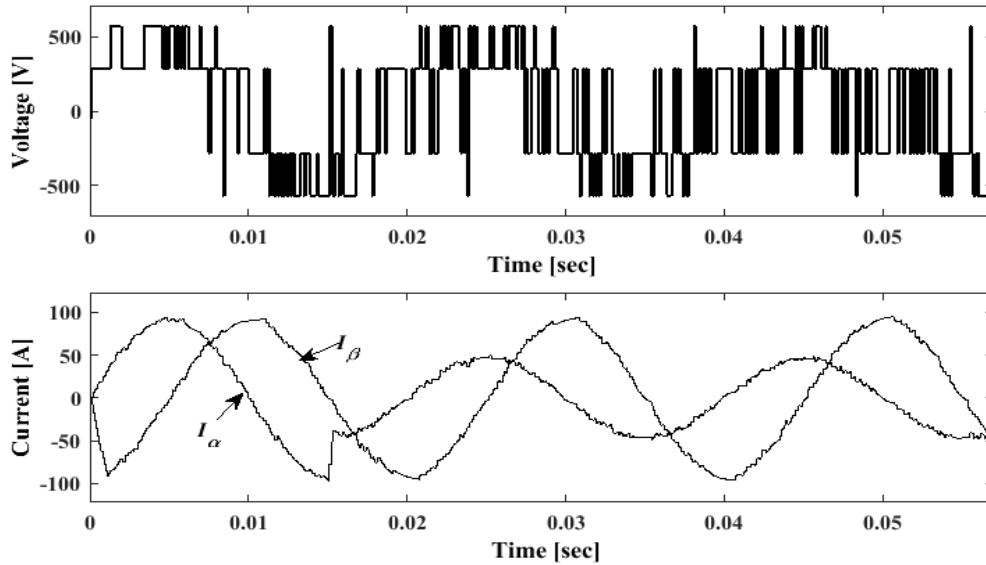


Figure 4.23: Transient phase voltage in phase a, and currents ( $I_\alpha, I_\beta$ ) in  $\alpha\beta$  frame for PR-SHEPWM controller.

#### 4.3.1.4 Proposed MPC based Controller

For realizing the transient behavior of the proposed controller, a step reduction (from 96A to 48A) of the real component ( $I_\alpha^*$ ) of the reference current is done at time 0.015s. The responses of the injected current and voltage in  $abc$  and  $\alpha\beta$  frame for the proposed MPC based controller under transient conditions are shown in Figs. 4.24 and 4.25. A more closed zoom view at the transient position is shown in Fig. 4.26. It is seen that the controller provides decoupled control of load current ( $I_\alpha, I_\beta$ ). This means that a change in one component ( $I_\alpha^*$ ) does not affect the other.

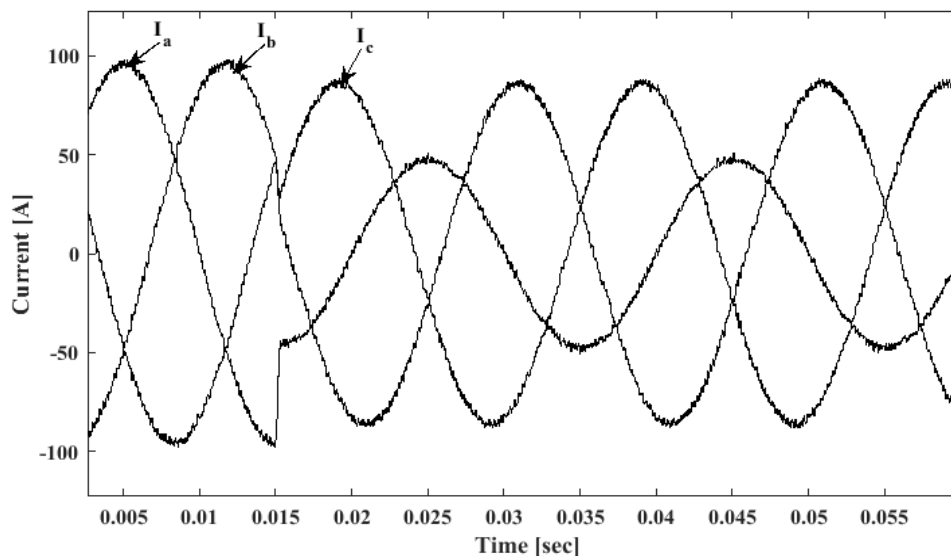


Figure 4.24: Transient phase currents using proposed controller.

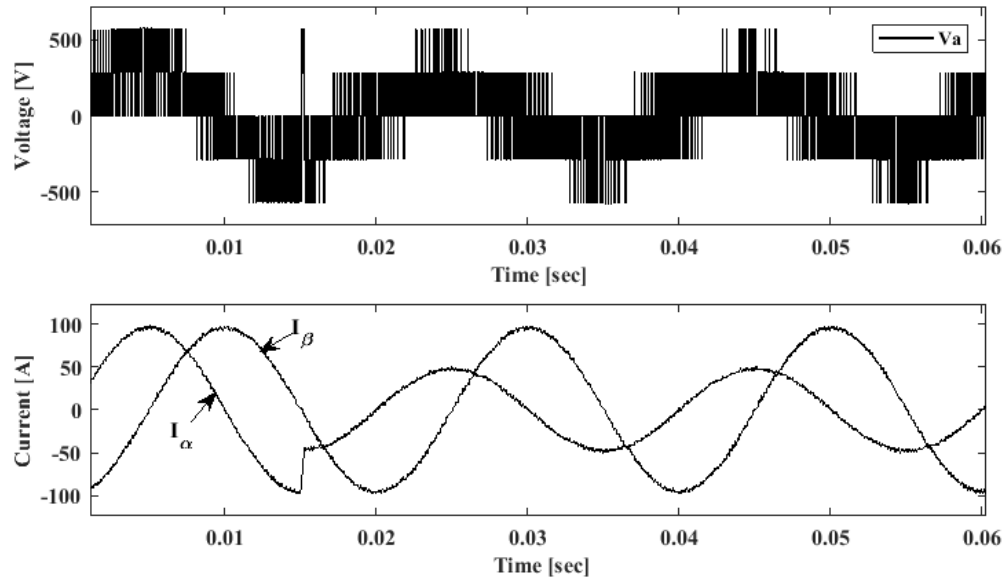


Figure 4.25: Transient phase voltage in phase a, and currents ( $I_\alpha, I_\beta$ ) in  $\alpha\beta$  frame using proposed controller.

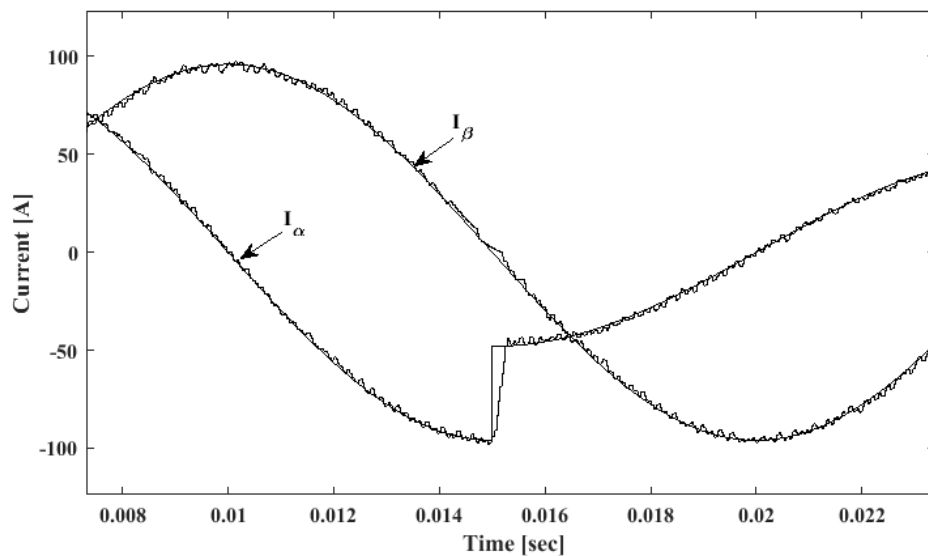


Figure 4.26: Decoupling nature of transient phase currents ( $I_\alpha, I_\beta$ ) in  $\alpha\beta$  plane.

After analyzing the aforementioned transient analysis, it is clearly seen that the proposed MPC based controller provides better transient response than the described three existing controllers.

### 4.3.2 Reference Current Tracking

Appropriate tracking of the reference current is an important feature for any controllers. The reference tracking performance of the proposed controller and the existing PI-PWM, PR-PWM and PR-SHEPWM controllers is presented below.

### 4.3.2.1 PI-PWM Controller

For the PI-PWM controller, the measured phase current waveforms in  $abc$  and  $\alpha\beta$  frames as shown in Fig. 4.27 show that the currents contain harmonic components and become distorted. The reference current tracking accuracy of the controller is poor as shown in Fig. 4.28. Figure 4.29 shows the steady-state current tracking error; the mean absolute current tracking error is 0.3 (30%) for the PI-PWM controller.

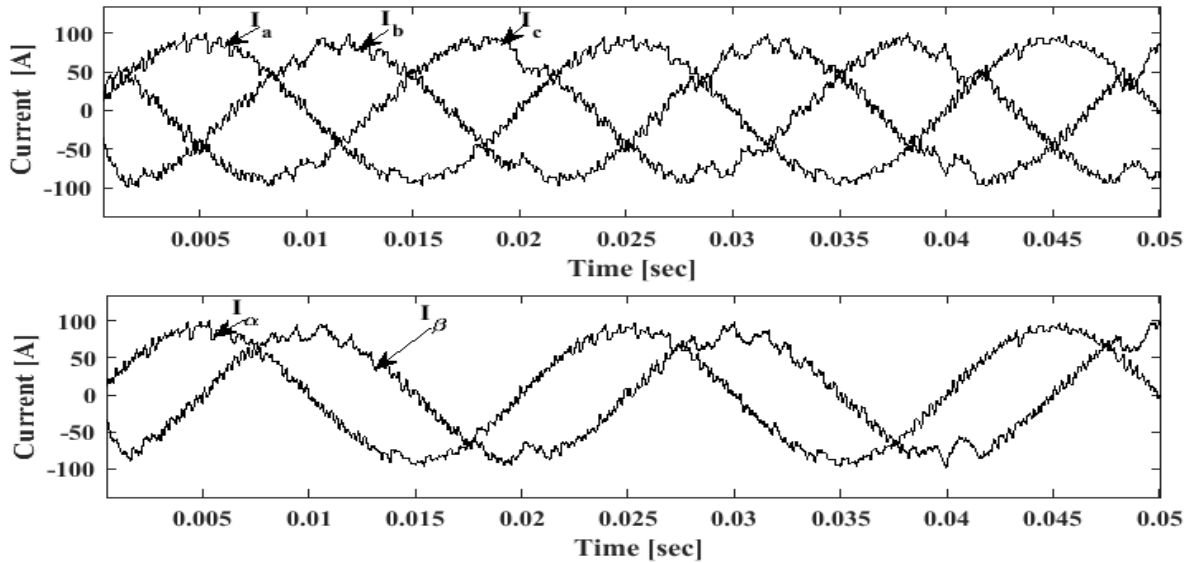


Figure 4.27: Steady-state phase current waveforms in  $abc$  and  $\alpha\beta$  frame for the PI-PWM controller.

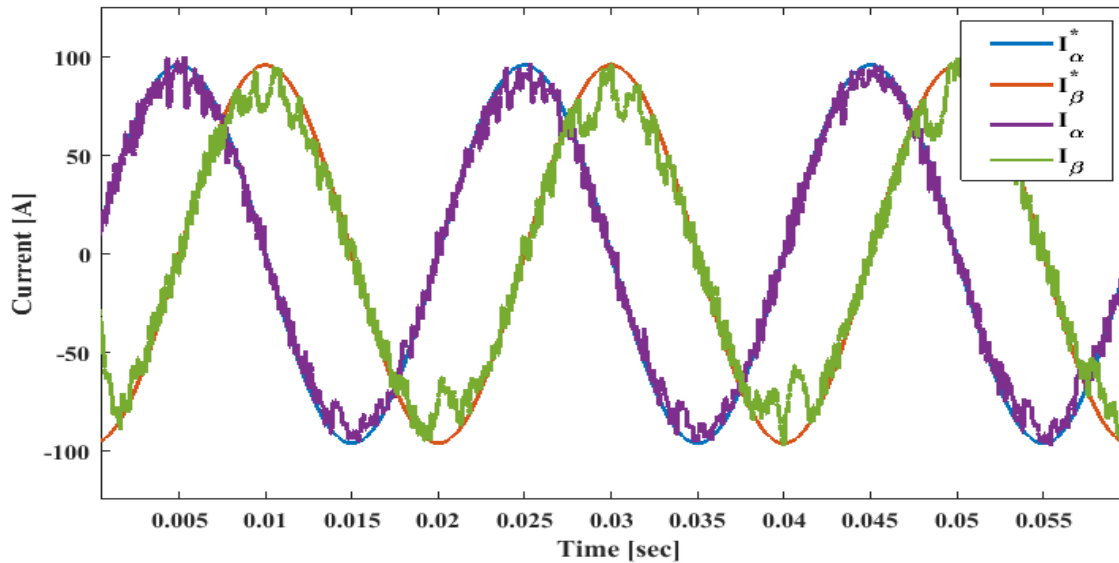


Figure 4.28: Reference current tracking response for PI-PWM control.

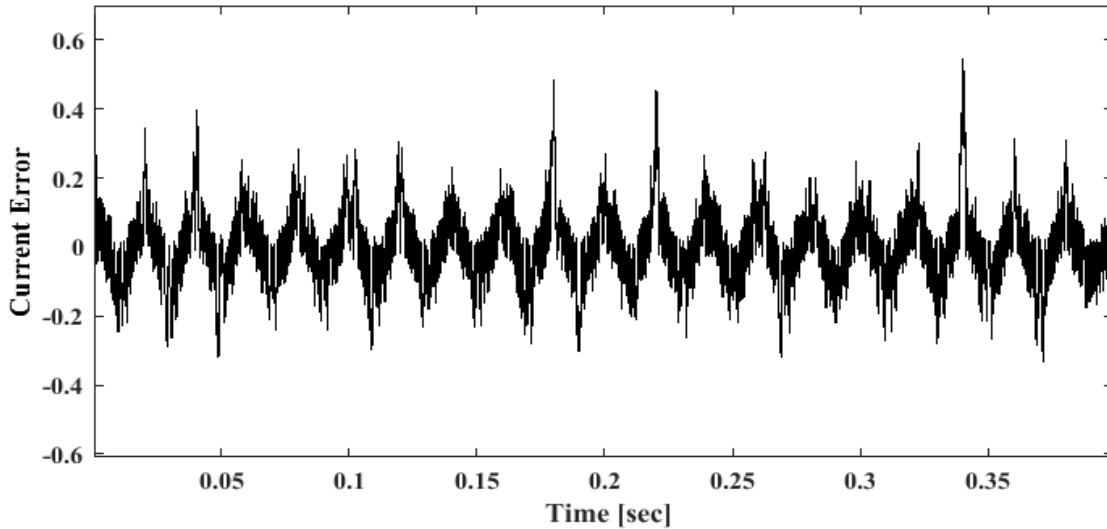


Figure 4.29: Current tracking error for the PI-PWM controller.

From Fig.4.28, it is seen that the output current of the inverter contains severe amount of harmonic component. Therefore, FFT analysis is done to understand the amount of THD of the current as well as the amount of individual harmonic component of the current for the PI-PWM controller, which is shown in Fig. 4.30. The current THD is found to be 7.26% for the PI-PWM controller.

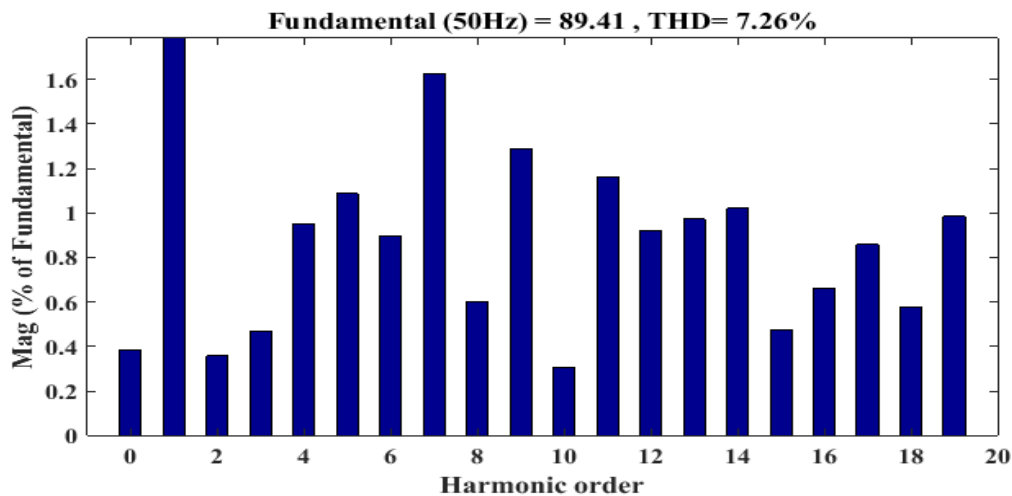


Figure 4.30: Current THD response for the PI-PWM controller.

The total current harmonic distortion is calculated by the following mathematically expression [143-144]

$$I_{THD} = \frac{\sqrt{\sum_{n=2}^{\infty} I_n^2}}{I_1} \times 100\% = \frac{\sqrt{I_2^2 + I_3^2 + \dots + I_n^2}}{I_1} \times 100\% \quad (4.1)$$

where, current THD is indicated by  $I_{THD}$ . These two terms are calculated by the r.m.s. values of current ( $I_1, I_2 \dots i_n$ ).

#### 4.3.2.2 PR-PWM Controller

The three-phase current waveforms produced by the PR-PWM controller are shown in Fig. 4.31, which show that the quality of the inverter output current is better than the PI-PWM controller. The reference tracking accuracy is also better as shown in Fig. 4.32. The mean absolute tracking error for the PR-PWM controller is 0.05 (i.e. 5%) and shown in Fig. 4.33. Therefore, a better indication is observed than the PI-PWM controller.

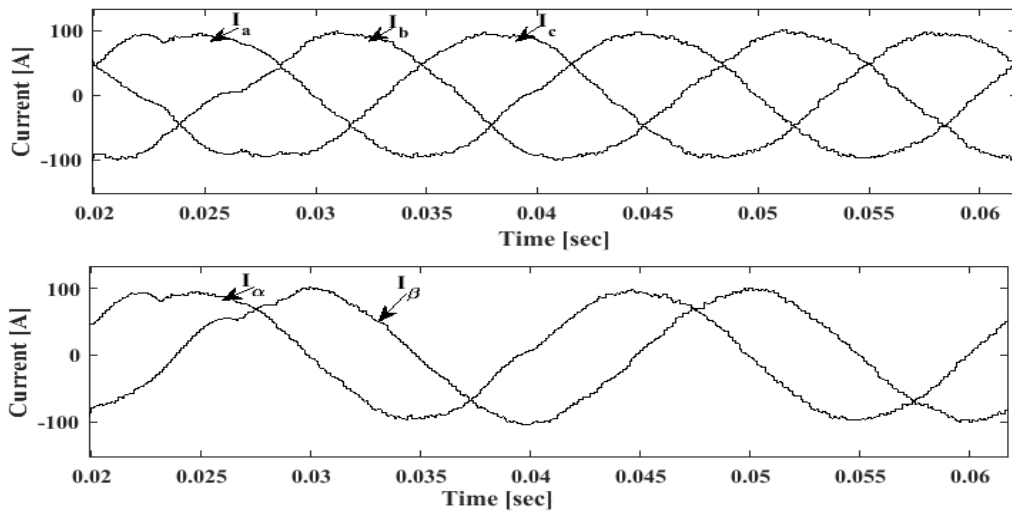


Figure 4.31: Steady state phase current response in  $abc$  and  $\alpha\beta$  frame for the PR-PWM controller.

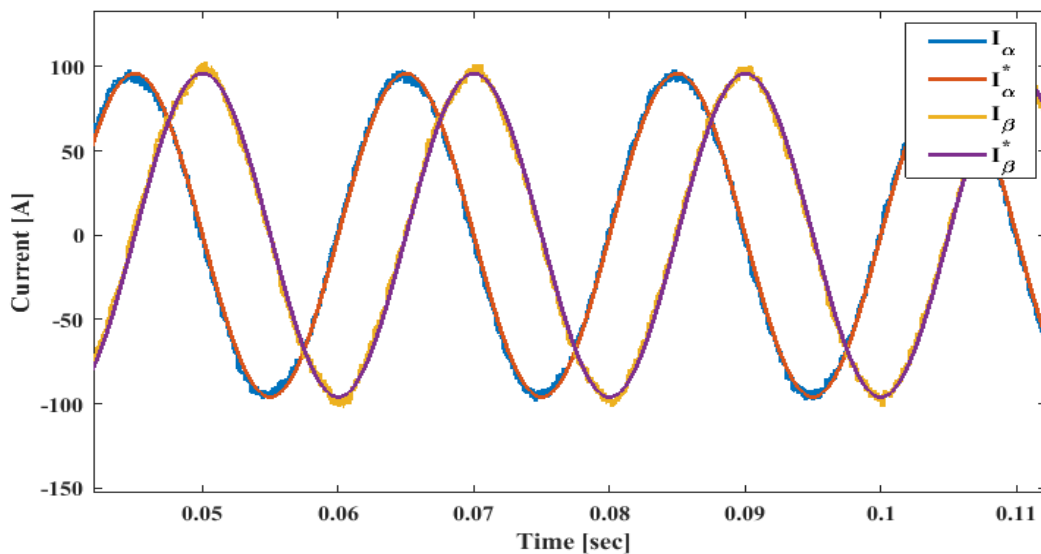


Figure 4.32: Reference current tracking response for PR-PWM control.

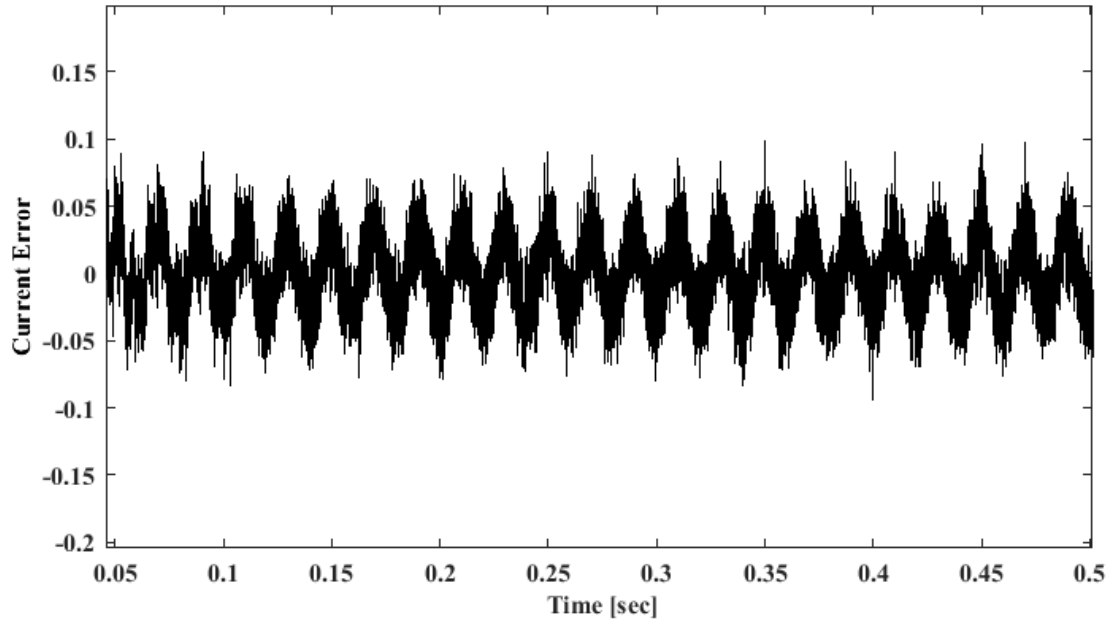


Figure 4.33: Current tracking error response for the PR-PWM controller.

Since the reference current error is better in PR-PWM controller as indicated by the Fig. 4.33, it is expected to have lower current THD for the controller. To ensure it, FFT analysis is done (as shown in Fig. 4.34) and found the value of current THD is 2.81%.

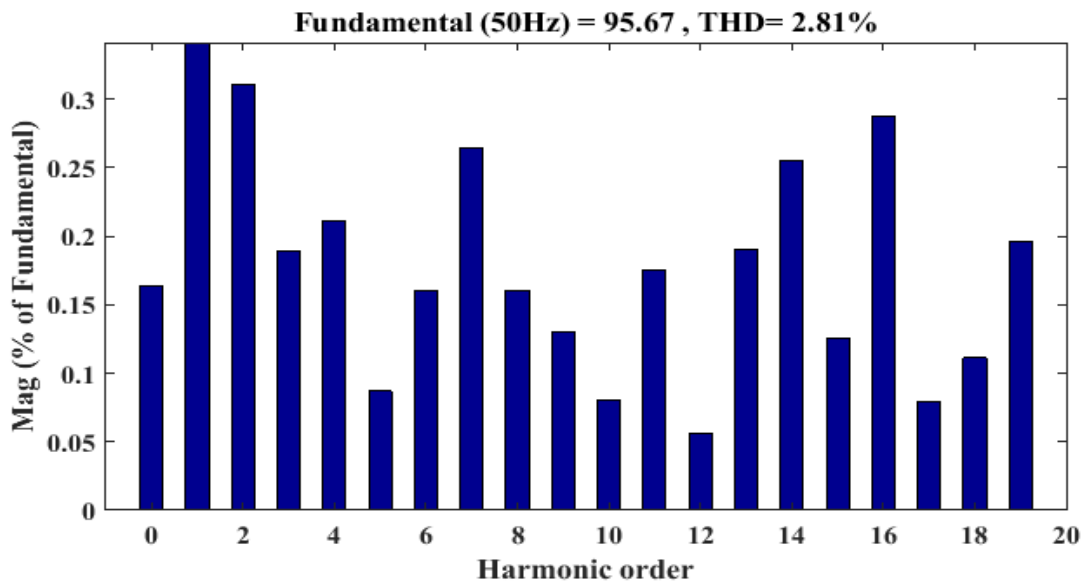


Figure 4.34: Current THD response for the PR-PWM controller.

### 4.3.2.3 PR-SHEPWM Controller

The measured phase current response and reference current tracking for the PR-SHEPWM controller are shown in Fig. 4.35 and 4.36, which show relatively better output from the controller than the conventional PI-PWM controller. However, the controller suffers from higher current distortion than the PR-PWM controller. The current tracking error is 0.065 (i.e. 6.5%), which is also higher than the PR-PWM controller as shown in Fig. 4.37.

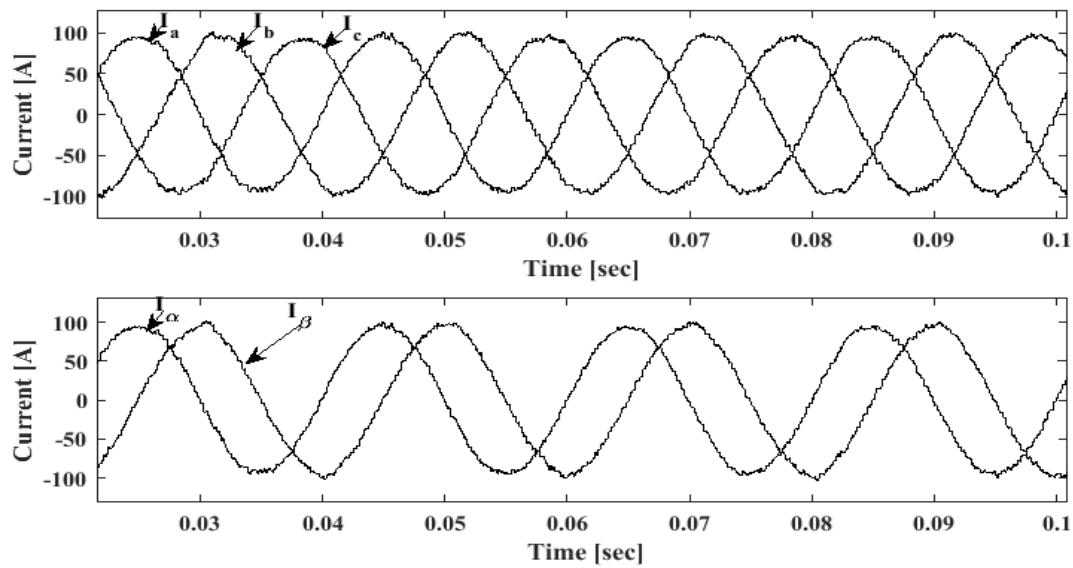


Figure 4.35: Steady state phase current response in  $abc$  and  $\alpha\beta$  frames for the PR-SHEPWM controller.

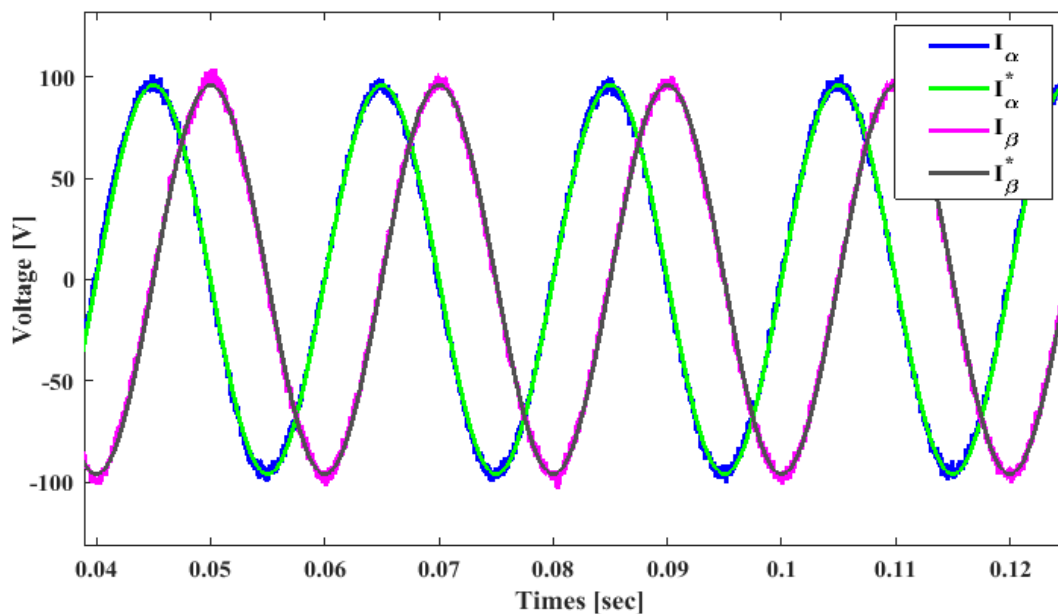


Figure 4.36: Reference current tracking response for PR-SHEPWM control.

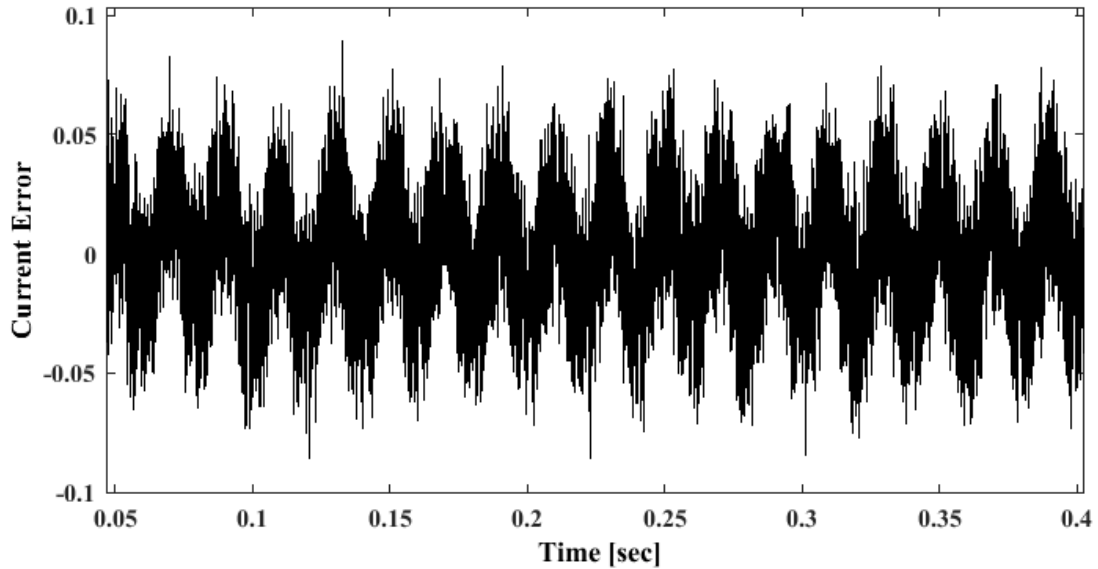


Figure 4.37: Current tracking error response for the PR-SHEPWM controller.

The current THD response for the PR-SHEPWM control is shown in Fig. 4.38. It is clearly seen that the selected 5<sup>th</sup> and 7<sup>th</sup> harmonics are eliminated, however, the other harmonic component, more importantly, 11<sup>th</sup> harmonic, increases the overall THD of the system. This is one of the significant drawbacks of the controller.

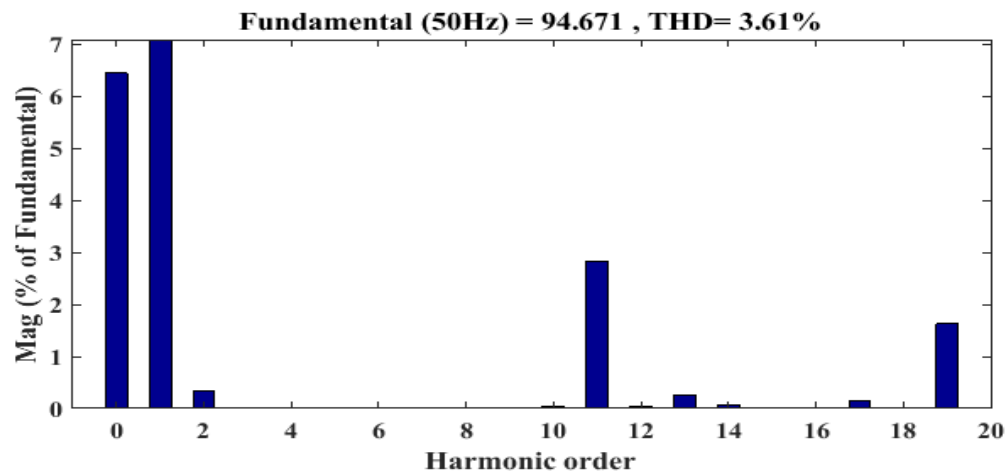


Figure 4.38: Current THD response for the PR-SHEPWM controller.

#### 4.3.2.4 Proposed MPC based Controller

The current tracking accuracy of the MPC at steady-state condition is shown in Figs.4.39. It can be seen that the controller tracks the reference current properly. The mean tracking absolute error at steady-state is 0.025 (i.e. 2.5 %) as shown in Fig. 4.40.



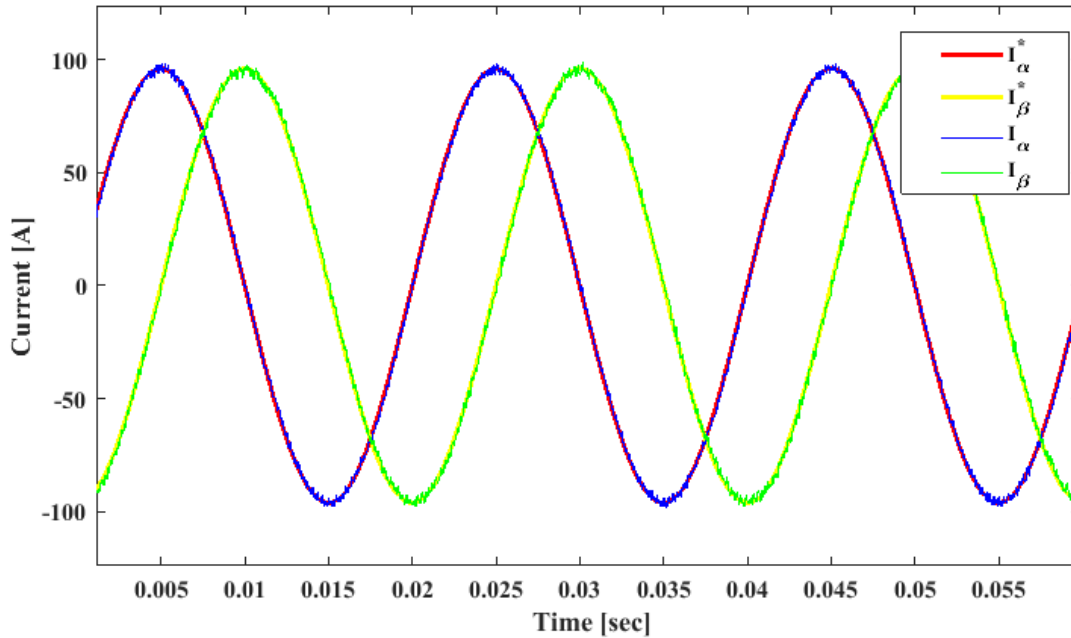


Figure 4.39: The current ( $I_\alpha, I_\beta$ ) tracking performance under steady-state condition.

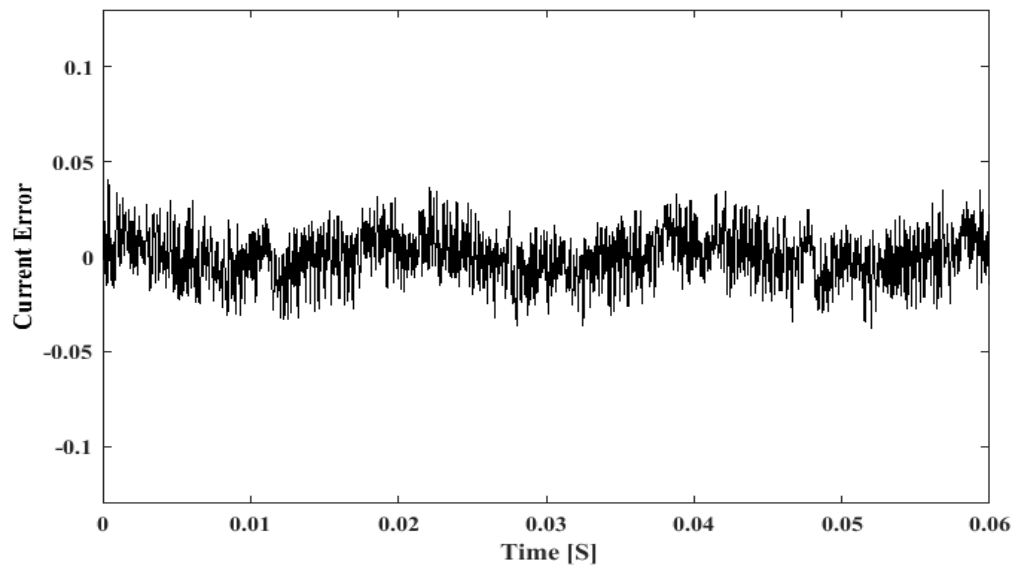


Figure 4.40: Mean tracking absolute error between the reference and measured current.

As mentioned earlier, Fast Fourier Transform (FFT) analysis is carried out for the proposed controller for evaluating the harmonic content in the injected current. The result from the FFT analysis for the controllers is shown in Fig. 4.41. It is seen that the current THD for the proposed controller is 2.07%, which is the lowest one than the other existing controllers.

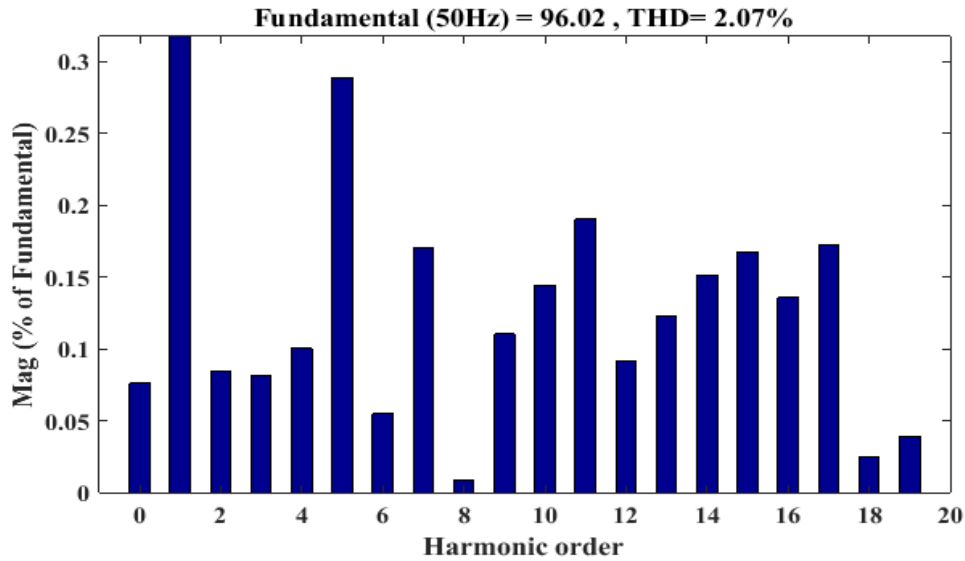


Figure 4.41: Steady-state grid current THD response for the proposed predictive controller.

In summary, if the performance of the described existing controllers are compared to the proposed controller in terms of tracking accuracy, harmonic content in the output injected grid current, the proposed one shows the better performance. The current THD value for the existing controllers and the proposed one is shown in Fig. 4.42 which indicates that the PI-PWM controller has the highest current THD value whereas the proposed controller has the least value. The individual harmonic components exist in the output inverter current/the injected grid current by the controllers is shown in Fig. 4.43 which also shows that the proposed controller performs better than the others.

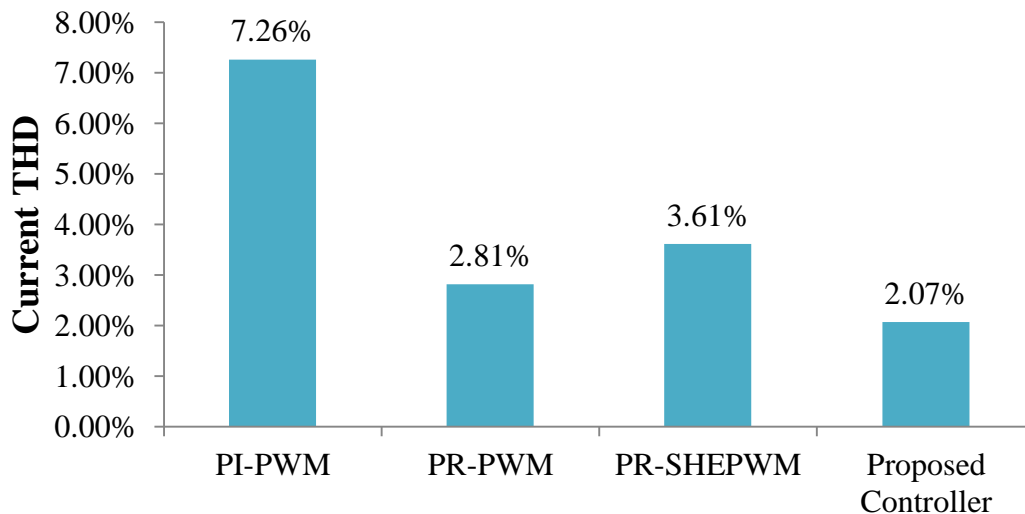


Figure 4.42: Comparison of Current THD values for the PI-PWM, PR-PWM, PR-SHEPWM and the proposed controller.

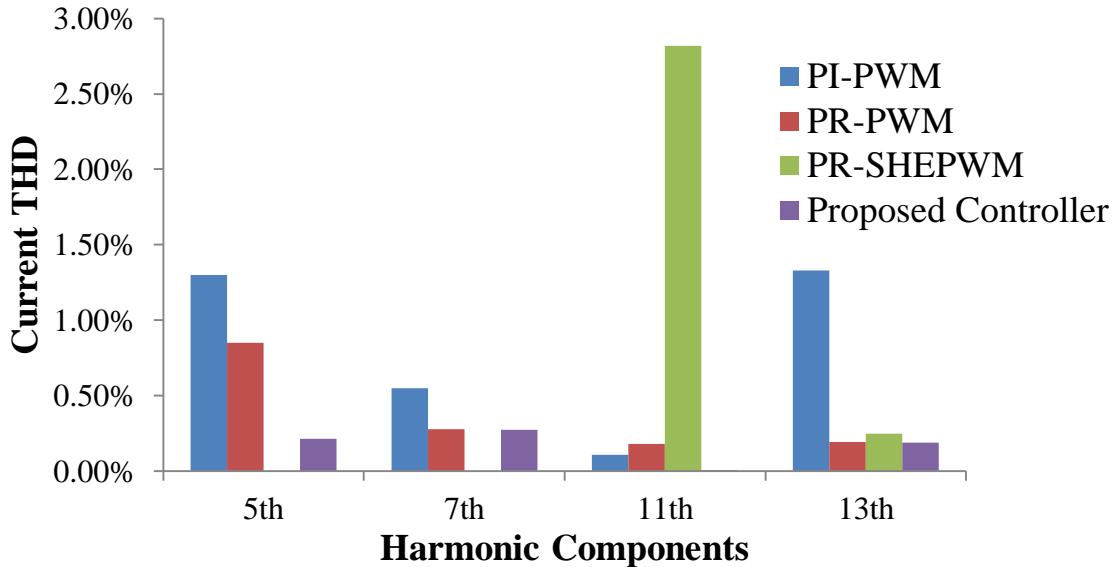


Figure 4.43: Comparison of individual harmonic component THD values for the PI-PWM, PR-PWM, PR-SHEPWM and the proposed controller.

According to the standards of IEEE 929-2000 and European IEC61727 [35-36], the current THD of the injected grid current should be less than 5% and the odd harmonic component from 3<sup>rd</sup> to 9<sup>th</sup> and 11<sup>th</sup> to 19<sup>th</sup> should have THD less than 4% and 2%, respectively. Therefore, the predictive controller meets the standard. The PI-PWM, PR-PWM and PR-SHEPWM controllers shows higher current THD than the proposed controller.

#### 4.3.3. Load flow analysis

For comparing the results obtained from the load flow analysis, the same system is designed using PI-PWM controller. The used parameters in simulation are same for both the PWM and MPC based energy conversion. The penetrated power from a specified PV system (39kW) to the grid for both the MPC and PWM is shown in Table 4.4. It can be seen that the penetrated active power generation to the IEEE 13 bus for the MPC is 32.08kW, whereas the traditional PWM penetrates 28.44kW. Hence, 3.64kW (12.8%) more active power is added to the grid due to the use of proposed MPC. This excess power of 3.64kW is consumed by Zshunt load, as shown in Table 4.4.

Table 4.4: Load flow analysis data for PWM and MPC based controller.

Parameters	PWM	MPC
Total generation	P= 3547.18 kW Q= 1512.11 kvar	P= 3550.82 kW Q = 1514.38 kvar
Total PQ load	P = 3103.23 kW Q= 1881.26 kvar	P = 3103.22 kW Q=1881.25 kvar
Total Zshunt load	P = 390.28kW Q = -488.04 kvar	P = 393.85 kW Q = -486.01kvar
Total losses	P= 53.67 kW Q = 118.89 kvar	P = 53.76kW Q = 119.14kvar

#### 4.3.4 Loss analysis

From the load flow analysis, it is seen that more PV power is penetrated to the ac grid using MPC based proposed controller than the traditional PI-PWM controller. This phenomenon indicates the less power loss due to the proposed controller. Therefore, power loss analysis of both the controllers is done to verify the statement. The parameters used in the analysis are shown in Table 4.5 and the related expressions are presented in chapter III.

Table 4.5: Parameters used for the power loss analysis [140].

Parameters	Value	Parameters	Value
Switching frequency, $f_{sw}$	3.54 kHz	DC link voltage, $V_{dc}$	850 V
Turn-On energy, $E_{on}$	1.4 mJ	Turn-on/Threshold voltage of IGBT, $V_{ce0}$	1.5 V
Turn-off Energy, $E_{off}$	2.0 mJ	Output frequency, $f_o$	50 Hz
Voltage across $V_{ce}$ during Test, $V_{ccnom}$	400 V	Modulation Index, $m$	0.95
Collector Current during Test, $I_{cnom}$	50 A	IGBT differential resistance, $R_{ce}$	0.01467 $\Omega$

Figures 4.44 and 4.45 show the arm current through the upper IGBT using the Eqn. (3.59) for MPC and PWM, respectively. Here, it can be seen that, the arm current differs from the output line current (as shown in Fig. 4.4) as dc current in per branch and ac current in per IGBT are considered. Difference between MPC and PWM currents is that, in PWM, arm current is multiplied with duty cycle, whereas, no modulation index or modulation is required for MPC. From Fig. 4.46, the instantaneous conduction and switching loss of MPC is shown using the Eqns. (3.58) and (3.63), respectively, as presented in chapter III. Figure 4.47 shows the instantaneous conduction and switching losses of IGBT for PI-PWM. Comparing the current and loss curve, it can be said that, MPC yields smooth switching, whereas PWM yields distorted switching. Therefore, the wave shape is also distorted. The average continuous phase losses value for MPC and PWM are listed in Table 4.6.

Table 4.6: Average loss for MPC and PWM controllers.

Name of the Loss	MPC	PWM
Conduction Loss (W)	29.72	47.0031
Switching Loss (W)	6.0741	12.1501

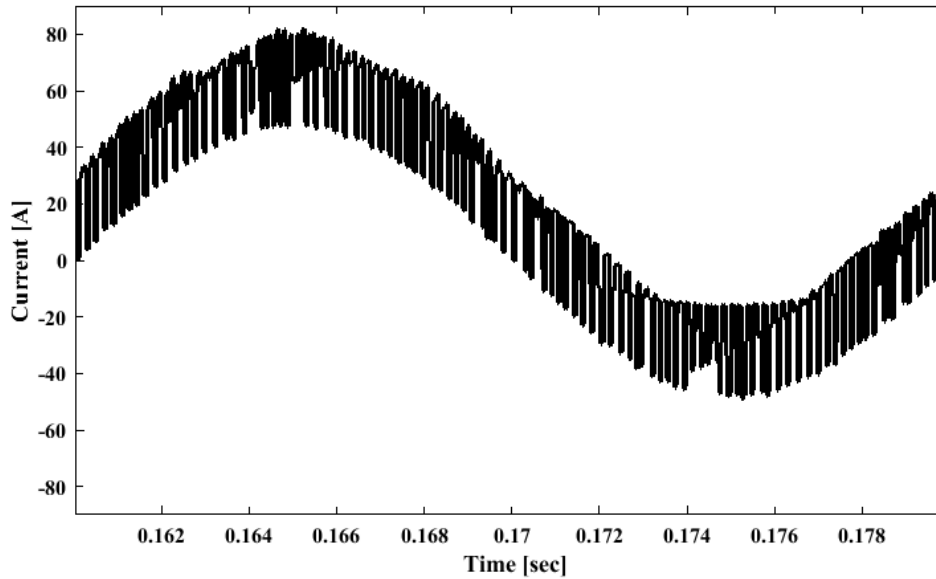


Figure 4.44: Instantaneous arm current in the upper IGBT for MPC.

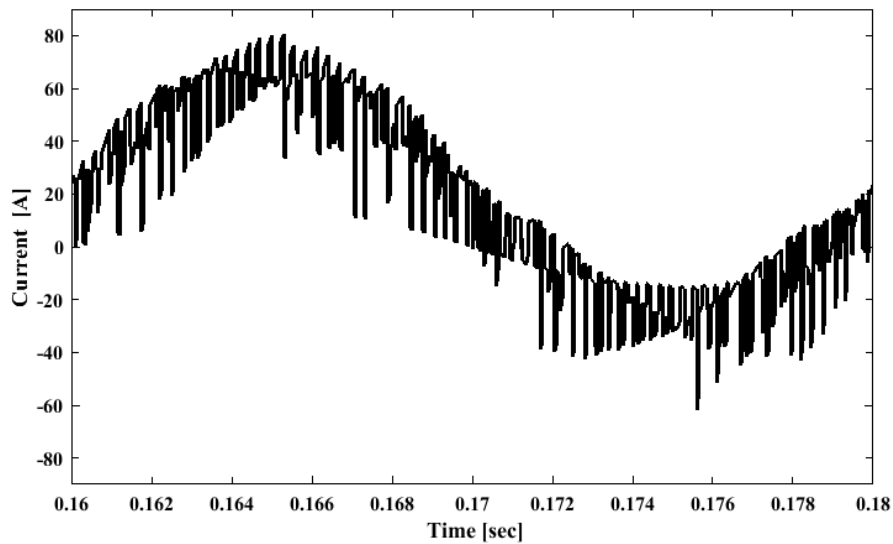


Figure 4.45: Instantaneous arm current in the upper IGBT for PWM.

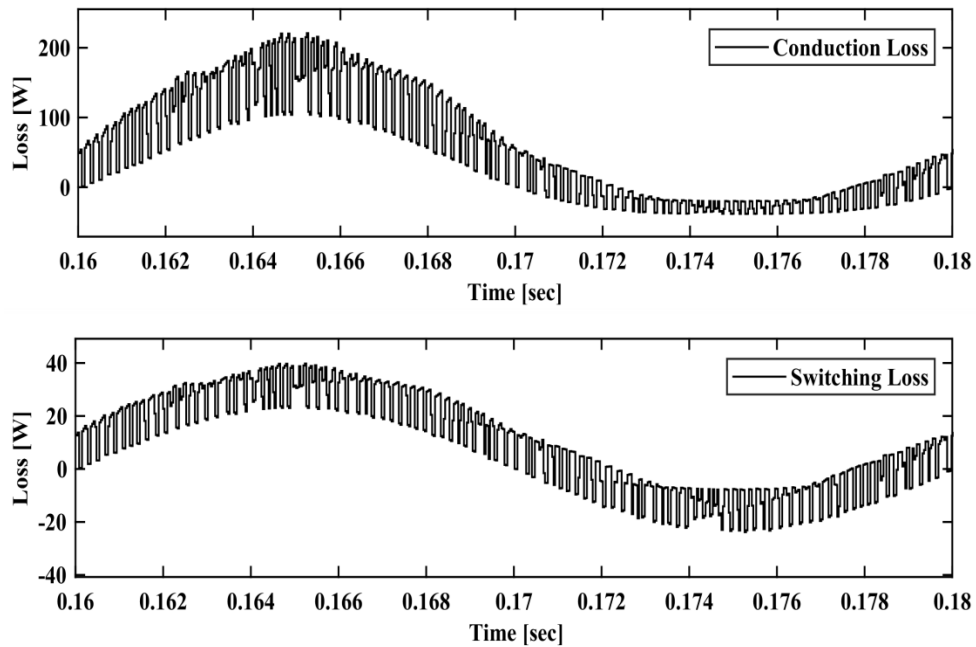


Figure 4.46: Instantaneous conduction and switching losses in MPC.

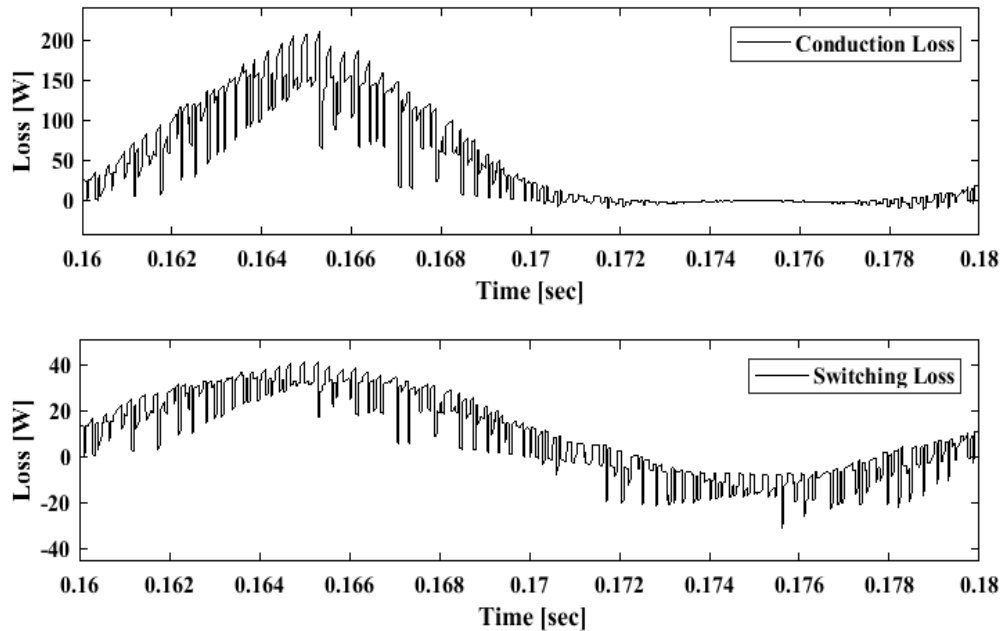


Figure 4.47: Instantaneous conduction and switching losses in PWM.

As mentioned earlier, the chosen reference current is 96A. Now, for further analysis, the reference current is varied from 91 to 100A for both the controller as shown in Fig. 4.48. It is seen that both the conduction and switching loss of MPC are greater than PWM during the variation of reference current.

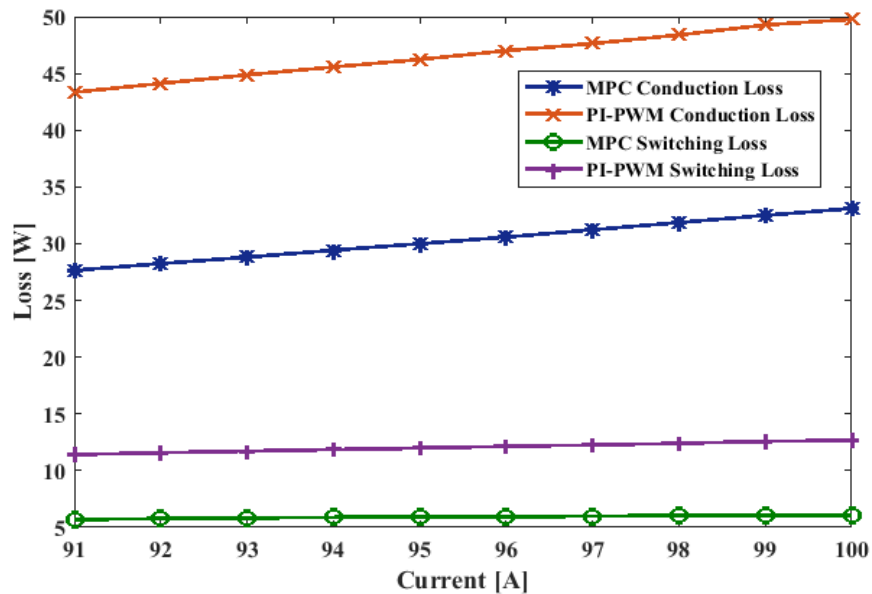


Figure 4.48: Comparison of conduction and switching losses between MPC and PWM.

After determining the switching and conduction losses, another loss due to the harmonic component in the output current i.e. the harmonic loss is calculated using the expression as presented before in chapter III. As mentioned before, for determining the harmonic loss, the r.m.s. value of the output current and its THD percentage due to the harmonic component is required. Using the data found from the FFT analysis as shown in Figs. 4.30 and 4.41, the harmonic loss is calculated for both the PI-PWM and MPC controller.

The per phase continuous harmonic loss for MPC is 6.79W which is 83.59W for PWM. For three-phase, it will be multiplied by 3, hence, for MPC it is 20.38W, and for PWM it is 250.78W. So it can be said that in MPC, 91.87% harmonic loss is reduced. A comparison of conduction, switching, and harmonic losses between MPC and PWM is shown by a bar graph in Fig. 4.49. It is seen that the overall per phase conduction, switching and harmonic losses for MPC is 42.59W, and for PWM, it is 142.75W. Therefore, 70.16% (100.16W) power loss is reduced due to the use of MPC rather than the traditional PWM method. The results found from the analysis ensures the proposed controller as energy efficient one.

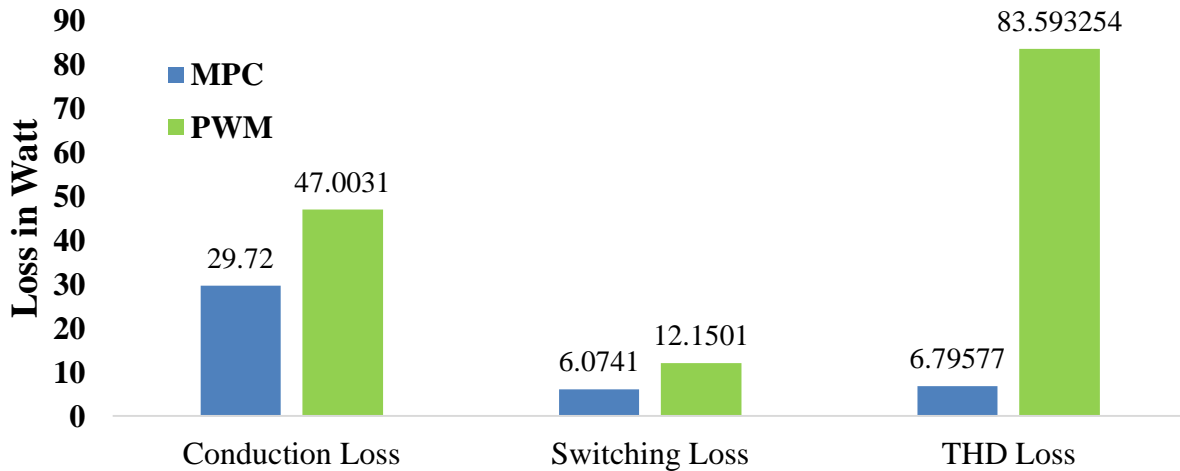


Figure 4.49: Comparison of conduction, switching and harmonic loss for MPC and PWM.

#### 4.4 Conclusion

This chapter presents the performance of the proposed MPC based on-grid PV system in terms of tracking accuracy, harmonic analysis, and steady-state and transient responses. Comparison with the existing controllers, such as PI-PWM, PR-PWM, PR-SHEPWM controllers, are also presented and finally summarized their injected current quality in terms of current THD. The quality of the injected current produced by the proposed controller meets the IEC/IEEE standard. Furthermore, the results of loss, load flow and fault current analyses are presented to ensure the penetration of more power to the ac grid and the fault handling capacity of the proposed controller.



## Chapter V

### Conclusions and Future Prospects

#### 5.1 Conclusion

People all over the world believe that the renewable energy sources (RES) will bring a positive impact on the generation of power and also provide a safe and green earth for the future generation. Among the RES, solar PV can be a significant source of power generation. However, maximum penetration of produced PV power to the grid is still an important issue for modern power system. To overcome the ongoing issue, this research work has focused on the development of MPC based energy efficient on-grid PV inverter system.

The power produced by the PV source is the sole source of harmonic components as its input irradiance and temperature fluctuate from time to time. The harmonic component in the output current causes losses in the system and thus less power is penetrated to the ac grid. To maximize the power penetration, an MPC based on-grid PV inverter system is designed in MATLAB/SIMULINK platform. The proposed MPC selects an optimal control action in every sampling instant for the dc/ac inverter by minimizing a predefined cost function. The cost function is designed for reducing the current tracking error and the average switching frequency. Accurate current tracking will improve the current THD, and lower average switching frequency will reduce the switching loss. The aforementioned two control objectives are combined with a weighting factor in the cost function. The value of the weighting factor is selected by trading-off the average switching frequency and current THD, as they are inversely related.

In this research work, it is found that MPC based controller tracks the reference current accurately with a mean absolute error of 2.5%. The performance of the proposed MPC is observed with and without switching frequency reduction term in the cost function. The current THD, average switching frequency and switching loss are 1.82%, 4.46KHz and 7.53W, respectively, without the switching frequency reduction term in the cost function. After adding the switching frequency reduction term in the cost function, the current THD, switching frequency and the switching loss become 2.07%, 3.54KHz and 6.05W, respectively, with a weighting factor of  $\lambda = 0.4$ . This means that the average switching frequency is reduced by 920 Hz and the corresponding switching loss is reduced by 19.79% (1.49W) per phase, while the current THD is increased by only 0.25%. The overall loss (i.e. summation of conduction, switching and harmonic losses) of the inverter is also calculated. It is shown that the overall losses with and without switching frequency reduction term in the cost function are 42.56 and 43.40W, respectively. Note that, considering only 0.25% more current THD minimizes the

average switching loss as well as reduces the continuous overall losses by 2.52W (for three-phase). Hence, for energy efficient operation, the inverter is operated at the trade-off point of the average switching frequency and the current THD.

To penetrate the produced PV power utilizing the proposed MPC, the total system is connected to an IEEE 13 bus test feeder. Load flow analysis is done and the results are compared with the traditional PWM system. The proposed controller penetrates 3.64kW more power than the traditional PWM controller for a specified capacity of the PV system. The inverter power loss is also compared with the PWM based inverter system. It is shown that the PWM and MPC based controllers provide the continuous overall per phase loss of 142.75W and 42.59W, respectively. This means that a reduction of 70.16% (100.16W) power loss is achieved due to the use of MPC rather than the traditional PWM method, which makes the proposed controller energy efficient. The controller also has the symmetrical and unsymmetrical fault tolerant ability, which is also analysed in the research work.

Furthermore, a comparison in terms of current tracking error, current THD, and steady-state and transient responses has been carried out between the proposed controller and the existing PWM controllers. Three existing controllers, such as PI-PWM, PR-PWM and PR-SHEPWM, are designed with the same parameters utilized in the proposed controller. The mean absolute current tracking errors for the PI-PWM, PR-PWM and PR-SHEPWM controllers are 30%, 5% and 6.5%, respectively, while the error is only 2.5% for the proposed MPC. The current THDs for PI-PWM, PR-PWM and PR-SHEPWM controllers are 7.26%, 2.81%, and 3.61%, respectively, while the proposed controller provides 2.07% which also meets the IEEE/IEC standards. During transient, the proposed controller shows better ability to track the reference current and also provides decoupled current control feature. Therefore, the results of the comprehensive analysis ensure the precedent features of the proposed controller for an on-grid PV inverter system.

So, to conclude, it can be mentioned that all the research objectives are fulfilled by this research work. To enhance the present power generating PV system by reducing current THD and power loss, the designed model can be an optimum solution to establish a greener world for the future generation.

## 5.2 Future Prospects

This work can create the following scopes for future researchers.

- i. The proposed MPC based on-grid PV system is designed and simulated in MATLAB/SIMULINK platform while considering a frequency of 50Hz during the connection of an ac grid. In practical scenario, the inverter suffers from instability due to the frequency mismatch with the grid. Therefore, a phase lock loop (PLL) may be incorporated in that case to avoid the variation of frequency and can be implemented in hardware configuration, which will be a nice future research scope in this area.
- ii. The current THD of the proposed controller still shows some small existence of different dominated harmonic components such as 5<sup>th</sup>, 7<sup>th</sup>, and 11<sup>th</sup>. Selected harmonic elimination technique may be incorporated in future with the proposed controller, which may further improve the performance of the MPC.
- iii. Hybrid power system will be an addition of this research. Wind and hydro based power system will be designed with proper control mechanism and added to the solar PV system for generating more power with more diversity.
- iv. The main drawback of MPC such as variable switching frequency can be overcome by including a modulation block in the proposed control structure.
- v. The stability of the MPC based inverter against large grid impedance variation will be another nice future research scope.

# References

- [1] A. F. Ayad and R. M. Kennel, "Model predictive controller for grid-connected photovoltaic based on quasi-Z-source inverter," in 2013 IEEE International Symposium on Sensorless Control for Electrical Drives and Predictive Control of Electrical Drives and Power Electronics (SLED/PRECEDE), Munich, 2013, pp. 1-6.
- [2] M. B. Shadmand, M. Mosa, R. S. Balog and H. A. Rub, "Maximum power point tracking of grid connected photovoltaic system employing model predictive control," in 2015 IEEE Applied Power Electronics Conference and Exposition (APEC), Charlotte, NC, 2015, pp. 3067-3074.
- [3] A. A. Abushaiba, S. M. M. Eshtaiwi and R. Ahmadi, "A new model predictive based Maximum Power Point Tracking method for photovoltaic applications," in 2016 IEEE International Conference on Electro Information Technology (EIT), Grand Forks, ND, 2016, pp. 0571-0575.
- [4] O. Ellabba, H. Abu-Rub, and Blaabjerg, "Renewable energy resources: Current status, future prospects and their enabling technology," in Renewable and Sustainable Energy Reviews, vol. 39, pp. 748–764, 2014.
- [5] A. Brown, S. Müller, and Z. Dobrotkova, "Renewable energy: Markets and prospects by technology," in IEA information paper, 2011.
- [6] S. R. Bull, "Renewable energy today and tomorrow," in Proceedings of the IEEE, vol. 89, no. 8, pp. 1216-1226, Aug. 2001.
- [7] J. M. C. Geldenhuys, "Model Predictive Control of a Grid-Connected Converter With LCL-Filter", M.S. Thesis, University of Stellenbosch, Private Bag X1, Matieland 7602, South Africa, March 2018.
- [8] "Renewable 2018, Global status report 2018," REN21, Renewable energy policy network for the 21st century [online], 2018. Available: [http://www.ren21.net/wp\\_content/uploads/2018/06/17-8652\\_GSR2018\\_FullReport\\_web\\_-1.pdf](http://www.ren21.net/wp_content/uploads/2018/06/17-8652_GSR2018_FullReport_web_-1.pdf) [Accessed: August, 2018]
- [9] "Global capacity estimate based on International Hydropower Association (IHA)," personal communications with REN21, March-April 2018 and IHA, Hydropower Status Report 2018, (London: May 2018). Available: <http://www.hydropower.org>. [Accessed: August, 2018]
- [10] Global Wind Energy Council (GWEC), "Global Wind Report – Annual Market Update 2017," Brussels, April 2018, pp. 4. Available: <http://files.gwec.net/files/GWR2017.pdf>; [Accessed: September, 2018]

- [11] International Renewable Energy Agency (IRENA), “Innovation Outlook: Advanced Liquid Biofuels,” Abu Dhabi, 2016. Available: [http://www.irena.org/-/media/Files/IRENA/Agency/Publication/2016/IRENA\\_Innovation\\_Outlook\\_Advanced\\_Liquid\\_Biofuels\\_2016.pdf](http://www.irena.org/-/media/Files/IRENA/Agency/Publication/2016/IRENA_Innovation_Outlook_Advanced_Liquid_Biofuels_2016.pdf). [Accessed: September, 2018]
- [12] International Energy Agency (IEA), Geothermal, 2016 Annual Report, Taupo, New Zealand, October 2017. Available: <http://iea-gia.org/wp-content/uploads/2018/01/Annual-Report-2016.pdf>. [Accessed: September, 2018]
- [13] European Commission (EC), “Study on lessons for ocean energy development,” Brussels, April, 2017, p. iii. Available: <https://publications.europa.eu/s/fEDw>. [Accessed: September, 2018]
- [14] IEA PVPS, Snapshot of Global Photovoltaic Markets 2018, op. cit. note 3, pp. 3-4.
- [15] “Global market outlook 2017-2021”, SolarPower Europe, June 2017. Available: [http://www.solar\\_power\\_europe.org/reports/global-market-outlook-2017-2021/](http://www.solar_power_europe.org/reports/global-market-outlook-2017-2021/) [Accessed: September, 2018]
- [16] CleanTechnica Website [online], “Solar panel price continue falling quicker than expected,” February, 2018. Available: <https://cleantechnica.com/2018/02/11/solar-panel-prices-continue-falling-quicker-expected-cleantechnica-exclusive/>. [Accessed: December, 2018].
- [17] H. Malek, “Control of grid-connected photovoltaic systems using fractional order operators,” All Graduate Theses and Dissertations, Utah State University, Logan, Utah, 2014. Available: <https://digitalcommons.usu.edu/etd/2157>
- [18] NREL, “Best research photovoltaic cell efficiencies,” Dec. 2013.
- [19] SREDA Website [online], 2018. Available: [http://www.sreda.gov.bd/index.php/site/re\\_present\\_status](http://www.sreda.gov.bd/index.php/site/re_present_status). [Accessed: December, 2018]
- [20] M. Liserre, R. Teodorescu, and F. Blaabjerg, “Stability of grid-connected PV inverters with large grid impedance variation,” in Proc. 35th IEEE Annual Power Electronics Specialists Conference (PESC 04), vol. 6, pp. 4773–4779, June 2004.
- [21] J. H. R. Enslin and P. J. M. Heskes, “Harmonic interaction between a large number of distributed power inverters and the distribution network,” in Proc. IEEE PESC’03, vol. 4, 2003, pp. 1742–1747.
- [22] R. Teodorescu, F. Blaabjerg, U. Borup, and M. Liserre, “A new control structure for grid-connected LCL PV inverters with zero steady-state error and selective harmonic compensation,” in Proc. 19th Annual IEEE Applied Power Electronics Conference and Exposition, (APEC ’04), vol. 1, pp. 580–586, 2004.
- [23] IEEE, “IEEE standard for interconnecting distributed resources with electric power systems,” Standards Coordinating Committee, IEEE Standards 1547, 2003.

- [24] Characteristics of the Utility Interface for Photovoltaic (PV) Systems, IEC 61727 CDV (Committee Draft for Vote), 2002.
- [25] Limits for Harmonic Current Emission (Equipment Input Current <16 A per Phase), EN 61000-3-2, 1995.
- [26] 2002 National Electrical Code, National Fire Protection Association, Inc., Quincy, MA, 2002.
- [27] B. Verhoeven et al. (1998) Utility aspects of grid connected photovoltaic power systems. International Energy Agency Photovoltaic Power Systems, IEA PVPS T5-01: 1998. [Online]. Available: [www.iea-pvps.org](http://www.iea-pvps.org)
- [28] Y. Xue, L. Chang, S. B. Kjaer, J. Bordonau, and T. Shimizu, "Topologies of single-phase inverters for small distributed power generators: an overview," *IEEE Trans. Power Electron.*, vol. 19, no. 5, pp. 1305–1314, Sep. 2004.
- [29] S. E. Evju, "Fundamentals of grid connected photovoltaic power electronic converter design," Ph.D. dissertation, Department of Electrical Power Engineering, Norwegian University of Science and Technology, Jan. 2007.
- [30] J. P. Benner and L. Kazmerski, "Photovoltaics gaining greater visibility," *IEEE Spectr.*, vol. 29, no. 9, pp. 34–42, Sep. 1999.
- [31] E. Bezzel, H. Lauritzen, and S. Wedel. (2004) The photo electro chemical solar cell. PEC Solar Cell Project, Danish Technological Institute. [Online]. Available: [www.solarcell.dk](http://www.solarcell.dk)
- [32] M. Wuest, P. Toggweiler, and J. Riatsch, "Single cell converter system (SCCS)," in *Proc. 1st IEEE WCPEC*, vol. 1, 1994, pp. 813–815.
- [33] J. Riatsch, H. Stemmler, and R. Schmidt, "Single cell module integrated converter system for photovoltaic energy generation," in *Proc. EPE'97*, vol. 1, Trondheim, Norway, 1997, pp. 71–77.
- [34] F. Blaabjerg, Z. Chen, and S. Kjaer, "Power electronics as efficient interface in dispersed power generation systems," *IEEE Transactions on Power Electronics*, vol. 19, no. 5, pp. 1184–1194, Sept. 2004.
- [35] A. K. Podder, K. Ahmed, N. K. Roy, and P.C. Biswas, "Design and simulation of an independent solar home system with battery backup," in *Proc. IEEE 4th ICAEE*, Dhaka Bangladesh, 28-30 September, 2017, pp. 427-431.
- [36] "Global Market Outlook 2017–2021," SolarPower Europe, 13 June, 2017. [Online]. Available: [http://www.ieapvps.org/file\\_admin/d\\_a\\_m\\_e/public/report/statistics/IEA-PV\\_PS\\_A\\_Snapshot\\_of\\_Global\\_PV\\_1992\\_2016\\_\\_1\\_.pdf](http://www.ieapvps.org/file_admin/d_a_m_e/public/report/statistics/IEA-PV_PS_A_Snapshot_of_Global_PV_1992_2016__1_.pdf) [Accessed: Oct. 08, 2018].
- [37] J. S. Hill, "Global Solar Market Demand Expected To Reach 100 Gigawatts In 2017, Says Solar Power Europe," *Clean Technica*, 24 October, 2017. [Online]. Available:

<https://cleantechnica.com/2017/10/27/global-solar-market-demand-expected-reach-100-gw-2017-solarpower-europe/> [Accessed: Oct. 08, 2018].

- [38] M. Habib, A. A. Ladjici, and E. Bollin, "Finite set MPC control of two level inverter for PV/Battery grid connected system," in Proc. IEEE 6th ICSC, University of Batna 2, Batna, Algeria, May 7-9, 2017, pp. 63-68.
- [39] R. Kennel and D. Schronder, "Predictive control strategy for converters," in Proc. 3rd IFAC Symposium, 1983, pp. 415-422.
- [40] I. M. Syed and K. Raahemifar, "Model predictive control of three phase inverter for PV system", International Journal of Electrical, Computer, Energetic and Communication Engineering, Vol. 9, No. 10, pp. 1048–1053, 2015.
- [41] K. Zhou, K. Low, D. Wang, F. Luo, B. Zhang and Y. Wang, "Zero-phase odd-harmonic repetitive controll for a single-phase PWM inverter", IEEE Transacton on Power Electronics, Vol. 21, No. 1, pp. 193-201, 2006.
- [42] M. Monfared, S. Golestan, and J. M. Guerrero, "Analysis, design, and experimental verification of a synchronous reference frame voltage control for single-phase inverters", IEEE Transacton on Industrial Electronics, Vol. 61, No. 1, pp. 258-269, 2014.
- [43] P. Mattavelli, "A closed-loop selective harmonic compensation for active filters", IEEE Transactions on Industry Applications, Vol. 37, No. 1, pp. 81-89, 2001.
- [44] L. Herman, I. Papic, and B. Blazic, "A proportional-resonant current controller for selective harmonic compensation in a hybrid active power Filter," IEEE Transactions on Power Delivery, Vol. 29, No. 5, pp. 2055-2065, 2014.
- [45] J. Rodriguez et al, "Predictive current control of a voltage source inverter", IEEE Transacton on Industrial Electronics, Vol. 54, No. 1, pp. 495-503, 2007.
- [46] J. Rodriguez et al., "State of the Art of Finite Control Set Model Predictive Control in Power Electronics", IEEE Transanction on Industrial Informatics, Vol. 9, No. 2, pp. 1003–1016, 2013.
- [47] V. N. R. Yaramasu, "Predictive Control of multilevel converters for megawatt wind energy conversion systems," PhD Thesis, Ryerson University, Toronto, Ontario, Canada, 2014.
- [48] S. Kouro et al, "Recent advances and industrial applications of multilevel converters," IEEE Trans. Ind. Electron., Vol. 57, No. 8, pp. 2553–2580, Aug. 2010.
- [49] J. Rodriguez, S. Bernet, B. Wu, J. Pontt, and S. Kouro, "Multilevel voltage-source-converter topologies for industrial medium-voltage drives," IEEE Transaction on Industrial Electronics, Vol. 54, No. 6, pp. 2930–2945, Dec. 2007.

- [50] A. Linder, R. Kanchan, R. Kennel, and P. Stolze, *Model-based predictive control of electric drives*: Cuvillier, 2010.
- [51] J. Rodriguez, and P. Cortes, *Predictive Control of Power Converters and Electrical Drives*, pp. 3–39. Wiley-IEEE Press, 2012. ISBN 9781119963981.
- [52] J. M. Carrasco et al. “Power electronic systems for the grid integration of renewable energy sources: A survey,” *IEEE Transactions on Industrial Electronics*, Vol. 53, No. 4, pp. 1002–1016, June 2006.
- [53] B. Bose, *Power Electronics and Motor Drives: Recent Advances and Trends*. Academic Press, 2006.
- [54] M. Kazmierkowski, R. Krishnan, and F. Blaabjerg, *Control in Power Electronics: Selected Problems*. San Diego, USA, Academic Press, 2002
- [55] I. Takahashi, and T. Noguchi, “A new quick-response and high-efficiency control strategy of an induction motor,” *IEEE Transactions on Industry Applications*, Vol. IA-22, No. 5, pp. 820–827, Sept 1986.
- [56] T. Ohnishi, “Three phase pwm converter/inverter by means of instantaneous active and reactive power control,” in *Proc. IEEE Industrial Electronics, Control and Instrumentation*, 1991, pp. 819–824.
- [57] P. Cortes, M.P.K Kowski, R.M. Kennel, D.E. Quevedo, and J. Rodriguez, “Predictive control in power electronics and drives,” *IEEE Transactions on Industrial Electronics*, Vol. 55, No. 12, pp. 4312–4324, Dec 2008. ISSN 0278-0046.
- [58] J. Pou, J. Zaragoza, S. Ceballos, M. Saeedifard, and D. Boroyevich, “A carrier-based PWM strategy with zero-sequence voltage injection for a three-level neutral-point-clamped converter,” *IEEE Transaction on Power Electronics*, Vol. 27, No. 2, pp. 642–651, Feb. 2012.
- [59] N. Celanovic and D. Boroyevich, “A fast space-vector modulation algorithm for multilevel three-phase converters,” *IEEE Transactions on Industrial Applications*, Vol. 37, No. 2, pp. 637–641, Mar. 2001.
- [60] M. Saeedifard, A. Bakhshai, and G. Joos, “Low switching frequency space vector modulators for high power multi module converters,” *IEEE Transaction on Power Electronics*, Vol. 20, No. 6, pp. 1310–1318, 2005.
- [61] A. Gopinath, A. Mohamed, and M. R. Baiju, “Fractal based space vector PWM for multilevel inverters – a novel approach,” *IEEE Transaction on Industrial Electronics*, Vol. 56, No. 4, pp. 1230–1237, 2009.
- [62] S. Mekhilef and M. Abdul Kadir, “Voltage control of three-stage hybrid multilevel inverter using vector transformation,” *IEEE Transaction on Power Electronics*, Vol. 25, No. 10, pp. 2599–2606, 2010.



- [63] M. Aneesh, A. Gopinath, and M. R. Baiju, "A simple space vector PWM generation scheme for any general  $n$  – level inverter," *IEEE Transaction on Industrial Electronics*, Vol. 56, No. 5, pp. 1649–1656, 2009.
- [64] B. Wu, *High-power converters and AC drives*, 1st ed., ser. Wiley-IEEE Press. John Wiley & Sons, Inc., 2006.
- [65] A. Cataliotti, F. Genduso, A. Raciti, and G. Galluzzo, "Generalized PWM-VSI control algorithm based on a universal duty-cycle expression: Theoretical analysis, simulation results, and experimental validations," *IEEE Transactions on Industrial Electronics*, Vol. 54, No. 3, pp. 1569–1580, 2007.
- [66] O. Dordevic, E. Levi, and M. Jones, "A vector space decomposition based space vector PWM algorithm for a three-level seven-phase voltage source inverter," *IEEE Transactions on Power Electronics*, Vol. 28, No. 2, pp. 637–649, Feb. 2012.
- [67] D. Ahmadi, K. Zou, C. Li, Y. Huang, and J. Wang, "A universal selective harmonic elimination method for high-power inverters," *IEEE Transactions on Power Electronics*, Vol. 26, No. 10, pp. 2743 –2752, Oct. 2011.
- [68] Z. Du, L. Tolbert, J. Chiasson, and B. Ozpineci, "Reduced switching-frequency active harmonic elimination for multilevel converters," *IEEE Transactions on Industrial Electronics*, Vol. 55, No. 4, pp. 1761–1770, 2008.
- [69] M. S. A. Dahidah and V. Agelidis, "Selective harmonic elimination PWM control for cascaded multilevel voltage source converters: A generalized formula," *IEEE Transactions Power Electronics*, Vol. 23, No. 4, pp. 1620–1630, 2008.
- [70] Q. Zeng and L. Chang, "An advanced SVPWM-based predictive current controller for three-phase inverters in distributed generation systems," *IEEE Transactions on Industrial Electronics*, Vol. 55, No. 3, pp. 1235–1246, Mar. 2008.
- [71] K. Astrom and T. Hagglund, *PID Controllers: Theory, Design and Tuning*, 1st ed. Instrument Society of America, 1995.
- [72] F. Blaschke, "The principle of field orientation as applied to the new transvektor closed-loop control system for rotating field machines," 1972.
- [73] S. C. Tan, Y. Lai, and C. Tse, "Indirect sliding mode control of power converters via double integral sliding surface," *IEEE Transactions of Power Electronics*, Vol. 23, No. 2, pp. 600–611, 2008.
- [74] F. Fuchs, J. Dannehl, and F. Fuchs, "Discrete sliding mode current control of grid-connected three-phase PWM converters with LCL filter," in *IEEE Int. Symp. on Ind. Electron. (ISIE)*, 2010, pp. 779–785.
- [75] B. Bose, *Modern power electronics and AC drives*. Prentice-Hall, 2002.

- [76] M. Cirstea, *Neural and Fuzzy Logic Control of Drives and Power Systems*. San Diego, CA: Elsevier, 2002.
- [77] P. Vas, *Artificial-Intelligence-based Electrical Machines and Drives: Application of Fuzzy, Neural, Fuzzy-neural, and Genetic-algorithm-based Techniques*. OUP Oxford, 1999.
- [78] P. Alsina and N. Gehlot, “Neuro-adaptive control of induction motor stator current,” in *IEEE Ind. Electron. Conf. (IECON)*, Vol. 2, 1995, pp. 1434–1439.
- [79] H. Abu-Ru, J. Guzinski, Z. Krzeminski, and H. A. Toliyat, “Predictive current control of voltage source inverters,” *IEEE Transactions on Industrial Electronics*, Vol. 51, No. 3, pp. 585–593, June, 2004.
- [80] M. Habibillah, “Simplified finite-state predictive torque control strategies for induction motor drives,” PhD Dissertation, The University of Sydney, Australia, 2016.
- [81] E. F. Camacho, & C. Bordons, *Model Predictive Control*. NY: Springer-Verlag, 1999.
- [82] P. Cortés, M. Kazmierkowski, R. Kennel, D. Quevedo, and J. Rodríguez, “Predictive control in power electronics and drives,” in *IEEE Transactions on Industrial Electronics*, vol. 55, no. 12, pp. 4312–4324, December, 2008.
- [83] S. Kouro, P. Cortés, R. Vargas, U. Ammann, and J. Rodríguez, “Model predictive control a simple and powerful method to control power converters,” *IEEE Transactions on Industrial Electronics*, vol. 56, no. 6, pp. 1826–1838, June, 2009.
- [84] M. B. Shadmand, “Model predictive control techniques with application to photovoltaic, DC microgrid and a multi-sourced hybrid energy system,” PhD Thesis, Texas A&M University, December, 2015.
- [85] J. Rodríguez, J. Pontt, C. Silva, P. Cortés, S. Rees, and U. Ammann, “Predictive direct torque control of an induction machine,” in *Proc. Power Electron. Motion Control Conf.*, Riga, Latvia, Sep. 2–4, 2004.
- [86] J. Rodríguez et al, “Predictive control of three-phase inverter,” *Electronics Letters*, vol. 40, no. 9, pp. 561–563, 2004.
- [87] G. Perantzakis, F. Xepapas, S. Papathanassiou, and S. Manias, “A predictive current control technique for three-level NPC voltage source inverters,” *IEEE Power Electronics Specialists Conference*, Jun. 2005, pp. 1241–1246.
- [88] R. Vargas, P. Cortés, U. Ammann, J. Rodríguez, and J. Pontt, “Predictive control of a three-phase neutral-point-clamped inverter,” *IEEE Transactions on Industrial Electronics*, Vol. 54, No. 5, pp. 2697–2705, Oct. 2007.
- [89] G. Perantzakis, F. Xepapas, and S. Manias, “Efficient predictive current control technique for multilevel voltage source inverters,” in *European Conference on Power Electronics and Applications*, Sep. 2005.

- [90] C.E. Garcia, D.M. Prett, and M. Morari, “Model predictive control: theory and practice survey,” *Automatica*, vol. 25, no. 3, pp. 335–348, 1989.
- [91] M.P. Kazmierkowski, and L. Malesani, “Current control techniques for three-phase voltage-source PWM converters: a survey,” *IEEE Transactions on industrial electronics*, Vol. 45, No. 5, pp. 691–703, 1998.
- [92] J. H. Lee, “Model predictive control: review of the three decades of development,” *Int. J. Control Automat. Syst.*, Vol. 9, No. 3, pp. 415–424, 2011.
- [93] M. Morariand, and J. H. Lee, “Model predictive control: Past, present and future,” *Comput. Chem. Eng.*, Vol. 23, No. 4–5, pp. 667–682, May 1999.
- [94] A. Linder, R. Kanchan, R. Kennel, and P. Stolze, *Model-Based Predictive Control of Electric Drives*. Göttingen, Germany: Cuvillier Verlag, 2010.
- [95] S. Kouro, P. Cortes, R. Vargas, U. Ammann, and J. Rodríguez, “Model predictive control—A simple and powerful method to control power converters,” *IEEE Trans. Ind. Electron.*, Vol. 56, No. 6, pp. 1826–1838, 2009.
- [96] L.A. Maccari, V.F. Montagner, and D.M. Lima, “Model predictive current controller applied to grid-connected LCL-filters” in *Proc. 12th IEEE International Conference on Industry Applications (INDUSCON)*, pp. 1–6. Nov 2016.
- [97] J. Scoltock, T. Geyer, and U.K. Madawala, “A Model Predictive Direct Current Control strategy with predictive references for MV grid-connected converters with LCL-filters,” *IEEE Transactions on Power Electronics*, vol. 30, no. 10, pp. 5926–5937, Oct 2015.
- [98] J. Scoltock, T. Geyer, and U. Madawala, “Model Predictive Direct Power Control for a grid-connected converter with an LCL-filter,” in *Proc. IEEE International Conference on Industrial Technology (ICIT)*, pp. 588–593. Feb 2013.
- [99] D.K. Yoo, L. Wang, E. Rogers, and W. Paszke, “Model predictive control of three phase voltage source converters with an LCL-filter,” in *Proc. IEEE 23rd International Symposium on Industrial Electronics (ISIE)*, pp. 562–567. June 2014.
- [100] F. Faraji, S. M. G. Mousavi, A. Hajirayat, A. Akbar, M. Birjandi, and K. Al-Haddad, “Single stage single-phase three-level neutral pont clamped transformerless grid-connected photovoltaic inverters: topology review”, *Renewable and Sustainable Energy Reviews*, Vol. 80, pp. 197–214, 2017.
- [101] G. Papafotiou, J. Kley, K. G. Papadopoulos, P. Bohren, and M. Morari, “Model predictive direct torque control-part 2: Implementation and experimental evaluation” *IEEE Transactions on Industrial Electronics*, Vol. 56, No. 6, pp.1906–1915, 2009.
- [102] T. Geyer, “A comparison of control and modulation schemes for medium-voltage drives: Emerging predictive control concepts versus PWM-based schemes,” *IEEE Transactions on Industry Applications*, Vol. 47, No. 3, pp. 1380–1389, 2011.

- [103] T. Geyer, "Model predictive direct current control: Formulation of the stator current bounds and the concept of the switching horizon," in Proc. IEEE Industry Applications Magazine, Vol. 18, No. 2, pp. 47–59, 2012.
- [104] F. He, Z. Zhao, T. Lu and L. Yuan, "Predictive DC voltage control for three-phase grid-connected PV inverters based on energy balance modeling," The 2nd International Symposium on Power Electronics for Distributed Generation Systems, Hefei, 2010, pp. 516-519.
- [105] W. Jianhua, Z. Jing, L. Longfei, T. Cong and Y. Le, "Predictive control based on analytic model for PV grid-connected inverters," 2012 24th Chinese Control and Decision Conference (CCDC), Taiyuan, 2012, pp. 4295-4299.
- [106] J. Nan, D. Xuanxuan, C. Guangzhao, D. Zhifeng and K. Dongyi, "Model-predictive direct power control of grid-connected inverters for PV systems," in Proc. International Conference on Renewable Power Generation (RPG 2015), Beijing, 2015, pp. 1-5.
- [107] J. Nan, H. Shiyang, C. Guangzhao, J. Suxia and K. Dongyi, "Model-predictive current control of grid-connected inverters for PV systems," in Proc. International Conference on Renewable Power Generation (RPG 2015), Beijing, 2015, pp. 1-5.
- [108] L. Shang, P. Li and Z. Li, "Low Voltage Ride Through Control Method of Photovoltaic Grid-connected Inverter Based on Model Current Predictive Control," 2018 Chinese Control and Decision Conference (CCDC), Shenyang, 2018, pp. 5209-5214.
- [109] N. Asim, K. Sopian, S. Ahmadi, K. Saeedfar, M.A. Alghoul and O. Saadatian , "A review on the role of materials science in solar cells," Renewable Sustainable Energy Rev, Vol. 16, No. 8, pp. 5834-5847, 2012.
- [110] P. Takun, S. Kaitwanidvilai, and C. Jettanasen, "Maximum power point tracking using fuzzy logic control for photovoltaic systems," in Proc. IMECS, Vol. 2, Hong-Kong, 2011, pp. 1-5.
- [111] A. Amir, A. Amir, J. Selvaraj, and N.A. Rahim, "Study of the MPP tracking algorithms: focusing the numerical method techniques," Renewable Sustainable Energy Rev. Vol. 62, pp. 350-371, 2016.
- [112] R. Rajesh, and M.C. Mabel, "A comprehensive review of photovoltaic systems," Renewable Sustainable Energy Rev, Vol.51, pp. 231-248, 2015.
- [113] M.G. Villalva, J.R. Gazoli, and E.R. Filho, "Comprehensive approach to modeling and simulation of photovoltaic arrays," IEEE Transactions on Power Electronics, Vol. 24, No.5, pp. 1198-1208, 2009.
- [114] K. Ishaque, Z. Salam, and A. Syafaruddin, "A comprehensive MATLAB Simulink PV system simulator with partial shading capability based on two-diode model," Solar Energy. Vol. 85, No. 9, pp. 2217-2227, 2011.

- [115] A.R. Reisi, M.H. Moradi, and S. Jamasb, "Classification and comparison of maximum power point tracking techniques for photovoltaic system: A review," *Renewable Sustainable Energy Rev.*, Vol.19, pp. 433-443, 2013.
- [116] C. Hua, and J. Lin, "An on-line MPPT algorithm for rapidly changing illuminations of solar arrays," *Renewable Energy*, Vol. 28, No. 7, pp. 1129-1142, 2003.
- [117] A. Q. Malik, L. Chee, T. K. Sheng and M. Blundell, "Influence of temperature on the performance of photovoltaic polycrystalline silicon module in the bruneian climate," *ASEAN Journal on Science Technology for Development*, vol. 26, no. 2, pp.61-67, 2010.
- [118] P. Bhatnagar, and R.K. Nema, "Maximum power point tracking control techniques: state-of-the-art in photovoltaic applications," *Renewable Sustainable Energy Rev*, Vol. 23, pp. 224-241, 2013.
- [119] The Solarhub webpage [online], Available: [http://www.solarhub.com/solarhub\\_products/2783-LPC235SM-02-Samsung-SDI](http://www.solarhub.com/solarhub_products/2783-LPC235SM-02-Samsung-SDI), [Accessed: 28 May 2017].
- [120] The NREL website [Online]. Available: <http://www.nrel.gov/>, [Accessed on 28 May 2017].
- [121] I. M. Syed, K. Raahemifar, "MPC of single phase Inverter for PV system," *International Journal of Energy and Power Engineering*, Vol. 08, no. 11, pp. 1730-1735, 2014.
- [122] S. Buso and P. Mattavelli, *Digital Control in Power Electronics*, ser. 978-1598291124. Denver: Morgan and Claypool Publishers, 2006.
- [123] L. Herman, I. Papic, and B. Blazic, "A proportional-resonant current controller for selective harmonic compensation in a hybrid active power filter," *IEEE Transactions on Power Delivery*, Vol. 29, No. 5, pp. 2055-2065, October 2014.
- [124] R. Teodorescu, F. Blaabjerg, U. Borup, and M. Liserre, "A new control structure for grid connected LCL PV inverters with zero steady-state error and selective harmonic compensation," in *Proc. 9th Annual IEEE APEC*, Anaheim, CA, USA, 2004, pp. 580-586.
- [125] H. Aggarawal et al, "Model predictive control based selective harmonic mitigation technique for multilevel cascaded H-bridge converters," in *Proc. IECON 2011- 37th Annual Conference of the IEEE Industrial Electronics Society*, Melbourne, VIC, 2011, pp. 4427-4432.
- [126] F. G. Turnbull, "Selected harmonic reduction in static dc-ac inverters," *IEEE Transaction Communication Electronics*, Vol. CE-83, no. 73, pp. 374-378, July, 1964.
- [127] B. Muruganantham, R. Gnanadass and N. P. Padhy, "Performance analysis and comparison of load flow methods in a practical distribution system," *2016 National Power Systems Conference (NPSC)*, Bhubaneswar, 2016, pp. 1-6.

- [128] R. G. Wasley and M. A. Shlash, "Steady-state phase-variable model of the synchronous machine for use in 3-phase load-flow studies," in Proc. of the Institute of Electrical Engineers, Vol. 121, No. 10, pp.1155-1164, 1974.
- [129] D. Shirmohammadi, H. W. Hong, A. Semlyen, and G. X. Luo, "A compensation-based power flow method for weakly meshed distribution and transmission networks," IEEE Transactions on Power Systems, Vol. 3, No. 2, pp. 753-762, 1988.
- [130] S. Ghosh, and D. Das, "Method for load-flow solution of radial distribution networks," in IEE Proceedings Generation, Transmission and Distribution, Vol. 146, No. 6, pp. 641-648, 1999.
- [131] Y. Zhu, and K. Tomsovic, "Adaptive power flow method for distribution systems with dispersed generation," IEEE Transactions on Power Delivery, Vol. 17, No. 3, pp. 822-827, 2002.
- [132] G. W. Chang, S. Y. Chu, and H. L. Wang, "An improved backward/forward sweep load flow algorithm for radial distribution systems," IEEE Transactions on Power Systems, Vol. 22, No. 2, pp. 882-884, 2007
- [133] S. K. Goswami, and S. K. Basu, "Direct solution of distribution systems," in IEEE Proceedings C - Generation, Transmission and Distribution, Vol. 138, No. 1, pp. 78-88, 1991.
- [134] A. Wood and B. Wollenberg, "Power generation operation and control," Second Edition, John Wiley & Sons, Inc., 1996.
- [135] F. E. P. Marcos, C. M. Domingo, T. G. S. Roman, et al., "A review of power distribution test feeders in the United States and the need for synthetic representative networks," Energies, Vol. 10, No. 11, 2017, pp. 1 –14.
- [136] IEEE PES Distribution System Analysis Subcommittee's Distribution Test Feeder Working Group, Available at: <https://ewh.ieee.org/soc/pes/dsacom/testfeeders/>
- [137] IEEE Distribution Planning Working Group Report, "Radial distribution test feeders," IEEE Transactions on Power Systems, Vol. 6, No.3, pp 975-985, August, 1991.
- [138] Y. Zhang, H. Wang, Z. Wang, Y. Yang and F. Blaabjerg, "Simplified Thermal Modeling for IGBT Modules With Periodic Power Loss Profiles in Modular Multilevel Converters," IEEE Transactions on Industrial Electronics, Vol. 66, No. 3, pp. 2323-2332, March 2019.
- [139] M. H. Bierhoff and F. W. Fuchs, "Semiconductor losses in voltage source and current source IGBT converters based on analytical derivation," 2004 IEEE 35th Annual Power Electronics Specialists Conference (IEEE Cat. No.04CH37551), Aachen, Germany, 2004, pp. 2836-2842.

- [140] On semiconductor, "IGBT," NJTG50N60FWG datasheet, December, 2012. Available : <https://www.onsemi.com/pub/Collateral/NGTG50N60FW-D.PDF>
- [141] M. J. Ghorbani, H. Mokhtari, "Impact of harmonics on power quality and losses in power distribution systems," International Journal of Electrical and Computer Engineering (IJECE) ,Vol. 5, No. 1, pp. 166-174, February 2015.
- [142] N.D. Tleis, "Power systems modeling and fault analysis: theory and practice," Newnes, Elsevier Publishing Ltd., Jordan Hill, Oxford, UK, 2008.
- [143] S. Sumathi, L. A. Kumar, and P. Surekha, Harmonic reduction techniques in renewable energy systems, Springer, 2015.
- [144] N. Shah, "Harmonics in power systems causes, effect and control," Siemens, USA, 2013, pp. 1-24.

## Publications

### Journal Papers

1. **Amit Kumer Podder**, Naruttam Kumar Roy, and Hemanshu Roy Pota, “MPPT methods for solar PV systems: a critical review based on tracking nature,” IET Renewable Power Generation, 2018 [Accepted with major revision].
2. **Amit Kumer Podder**, Md. Rakibul Hasan, Naruttam Kumar Roy, and Md. Mostafizur Rahman Komol, “Economic Analysis of a grid connected PV systems : a case study in Khulna,” European Journal of Engineering Research and Science, EJERS, vol. 3, issue 7, pp. 16-21, July, 2018.

### Conference Papers

1. **Amit Kumer Podder**, Md. Habibullah, Naruttam Kumar Roy, “Current THD Analysis of Model Predictive Control based Grid-Connected PV Inverter”, 2019 International Conference on Electrical, Computer and Communication Engineering (ECCE), 7-9 February, 2019, IEEE, Cox's Bazar, Bangladesh. [Accepted]
2. **Amit Kumer Podder**, and Md. Habibullah, “Model predictive based energy efficient control of grid-connected PV systems,” 10<sup>th</sup> International Conference on Electrical and Computer Engineering (ICECE 2018), IEEE, BUET, Dhaka, 20-22 Dec. 2018.
3. **Amit Kumer Podder**, Kawser Ahmed, Naruttam Kumar Roy, and Md. Habibullah, "Design and Simulation of a Photovoltaic and Fuel Cell Based Micro-grid System", 2019 International Conference on Energy and Power Engineering (ICEPE), 14-16 March, 2019, IEEE, Dhaka, Bangladesh [Accepted].
4. **Amit Kumer Podder**, Kawser Ahmed, Naruttam Kumar Roy and Protik Chandra Biswas, “Design and simulation of an independent solar home system with battery backup”, Proceedings of the 2017 4th International Conference on Advances in Electrical Engineering (ICAEE), IEEE, Dhaka, Bangladesh, 28-30 September, 2017